2003-09

A decision support system for the optimal design of base-motion isolators

Hernandez, Manuel A.

Monterey, California. Naval Postgraduate School

NAVAL
POSTGRADUATE
SCHOOL

MONTEREY, CALIFORNIA

THESIS

A DECISION SUPPORT SYSTEM FOR THE OPTIMAL DESIGN OF BASE-MOTION ISOLATORS

by

Manuel A. Hernandez

September 2003

Thesis Advisor:	Joshua Gordis
Thesis Advisor:	Dan Boger

Approved for public release; distribution is unlimited.

THIS PAGE INTENTIONALLY LEFT BLANK

REPORT DOCUMENTATION PAGE			Form Approved OMB No. 0704-0188
Public reporting burden for this collection of information is estimated to average 1 hour per response, including the time for reviewing instruction, searching existing data sources, gathering and maintaining the data needed, and completing and reviewing the collection of information. Send comments regarding this burden estimate or any other aspect of this collection of information, including suggestions for reducing this burden, to Washington headquarters Services, Directorate for Information Operations and Reports, 1215 Jefferson Davis Highway, Suite 1204, Arlington, VA 22202-4302, and to the Office of Management and Budget, Paperwork Reduction Project (0704-0188) Washington DC 20503.			
1. AGENCY USE ONLY *(Leave blank)*	**2. REPORT DATE** September 2003	**3. REPORT TYPE AND DATES COVERED** Master's Thesis	
4. TITLE AND SUBTITLE: **A Decision Support System for the Optimal Design of Base-Motion Isolators**			**5. FUNDING NUMBERS**
6. AUTHOR: Hernandez, Manuel A			
7. PERFORMING ORGANIZATION NAME(S) AND ADDRESS(ES) Naval Postgraduate School Monterey, CA 93943-5000			**8. PERFORMING ORGANIZATION REPORT NUMBER**
9. SPONSORING /MONITORING AGENCY NAME(S) AND ADDRESS(ES) N/A			**10. SPONSORING/MONITORING AGENCY REPORT NUMBER**
11. SUPPLEMENTARY NOTES The views expressed in this thesis are those of the author and do not reflect the official policy or position of the Department of Defense or the U.S. Government.			
12a. DISTRIBUTION / AVAILABILITY STATEMENT Distribution Statement (mix case letters)			**12b. DISTRIBUTION CODE**

13. ABSTRACT (maximum 200 words)

Transient analysis of large structural systems is a computationally demanding process, which in the past has prevented dynamic redesign and optimization. Large structures, such as buildings or ships, subjected to random base motions use isolators to minimize strain energies, which may cause damage or structural failure.

This research focuses on the optimization of isolator parameters in order for structural systems to withstand potentially catastrophic transient vibrations. Many non-linear hysteretic, viscoelastic, and sliding friction isolators were numerically modeled using the scientific programming language, MATLAB. The existing programs used to solve the Voltera integral formulation for Transient Structural Synthesis (TSS) and the Recursive Block-by-Block (RBB) algorithm were investigated and enhanced to yield greater accuracy and increased computational speed. The final product is a user-friendly Decision Support System (DSS) for use with both civil and military applications. Based on different types of base motions and the inherent dynamics of the structure, this DSS is capable of optimizing isolator parameters to meet a user specific objective.

14. SUBJECT TERMS Structural dynamics, structural isolation, nonlinear transient analysis, structural synthesis, decision support system, recursive block-by-block, convolution, Wen, hysteresis, earthquake			**15. NUMBER OF PAGES** 105
			16. PRICE CODE
17. SECURITY CLASSIFICATION OF REPORT Unclassified	**18. SECURITY CLASSIFICATION OF THIS PAGE** Unclassified	**19. SECURITY CLASSIFICATION OF ABSTRACT** Unclassified	**20. LIMITATION OF ABSTRACT** UL

NSN 7540-01-280-5500 Standard Form 298 (Rev. 2-89)
Prescribed by ANSI Std. 239-18

THIS PAGE INTENTIONALLY LEFT BLANK

Approved for public release; distribution is unlimited.

A DECISION SUPPORT SYSTEM FOR THE OPTIMAL DESIGN OF BASE-MOTION ISOLATORS

Manuel A. Hernandez, P.E.
Lieutenant, United States Navy
B.S.M.E., Florida International University, 1996

Submitted in partial fulfillment of the
requirements for the degree of

MASTER OF SCIENCE IN MECHANICAL ENGINEERING
MASTER OF SCIENCE IN INFORMATION TECHNOLOGY MANAGEMENT

from the

NAVAL POSTGRADUATE SCHOOL

September 2003

Author: Manuel A. Hernandez, P.E.

Approved by: Dr. Joshua Gordis
Thesis Advisor

Dr. Dan Boger
Thesis Advisor

Anthony J. Healey
Chairman, Department of Mechanical Engineering

Dr. Dan Boger
Chairman, Department of Information Sciences

THIS PAGE INTENTIONALLY LEFT BLANK

ABSTRACT

Transient analysis of large structural systems is a computationally demanding process, which in the past has prevented dynamic redesign and optimization. Large structures, such as buildings or ships subjected to random base motions, use isolators to minimize strain energies, which may cause damage or structural failure.

This research focuses on the optimization of isolator parameters in order for structural systems to withstand potentially catastrophic transient vibrations. Many non-linear hysteretic, viscoelastic, and sliding friction isolators were numerically modeled using the scientific programming language, MATLAB. The existing programs used to solve the Voltera integral formulation for Transient Structural Synthesis (TSS) and the Recursive Block-by-Block (RBB) algorithm were investigated and enhanced to yield greater accuracy and increased computational speed. The final product is a user-friendly Decision Support System (DSS) for use with both civil and military applications. Based on different types of base motions and the inherent dynamics of the structure, this DSS is capable of optimizing isolator parameters to meet a user specific objective.

THIS PAGE INTENTIONALLY LEFT BLANK

TABLE OF CONTENTS

I. INTRODUCTION 1

II. BACKGROUND 3
- A. EARTHQUAKES 3
  - 1. Fault Lines 4
  - 2. Seismic Waves 6
- B. BASE MOTION ISOLATION 7
  - 1. Elastomeric and Hysteretic Isolators 8
  - 2. Sliding Isolators with Restoring Force Mechanisms 10
  - 3. Viscoelastic Isolators 11
- C. RELEVANT RESEARCH 11
  - 1. Governing Equations of Motion 12
  - 2. Voltera Integral Equation 13
  - 3. Transient Structural Synthesis 14
  - 4. Recursive Block-by-Block Algorithm 15
- D. OPTIMIZATION – NONLINEAR PROGRAMMING 15
  - 1. One-Variable Optimization Problems 17
  - 2. Multi-Variable Optimization Problems 18
  - 3. Constrained Optimization 19
- E. DECISION SUPPORT SYSTEMS 20

III. INVESTIGATION AND ENHANCEMENTS 21
- A. CORRECTIONS TO EXISTING NUMERICAL ISOLATOR MODELS 21
  - 1. Wen Model Validation 25
- B. SLIDING NUMERICAL ISOLATOR MODELS 26
  - 1. Flat Sliding Surface with Restoring Device 26
  - 2. Spherical Sliding Surface 27
  - 3. Conical Sliding Surface 27
- C. CONVOLUTION-DRIVEN NUMERICAL INTEGRATION 28
  - 1. Trapezoid Rule – Error Oh^3 29
  - 2. Simpson's Rule – Error Oh^5 30
  - 3. Weddle's Rule – Error Oh^9 30
- D. PROGRAM OPTIMIZATION FOR SPEED 33
- E. OASIS (GUI) 35

IV. PROGRAM VERIFICATION 39
- A. WORKING MODEL 2-D 39
  - 1. 2DOF System 39
  - 2. 7DOF System 40
- B. SINGLE BAY – FOUR STORY BUILDING FRAME 41
  - 1. Four Story Building Frame 41

V. SAMPLE OPTIMIZATION PROBLEMS....43
A. SINGLE BAY FOUR-STORY BULDING....43
1. Parallel Spring and Damper....43
2. Flat Slider with Restoring Spring....46
3. Spherical Slider....49
4. Bilinear – No Strain Hardening....52
5. Maxwell....56
6. Wen – Sine Base Motion....59
7. Wen – Kobe Japan 1995 NS....63
B. FIFTEEN BAY THIRTY-STORY BULDING....71
1. Wen – Sine Base Motion....71
2. Wen – Kobe Japan 1995 US Base Motion....76
VI. CONCLUSION....81
VII. RECOMMENDATIONS....83
LIST OF REFERENCES....85
INITIAL DISTRIBUTION LIST....87

LIST OF FIGURES

Figure 1. Plate-Boundary Diagram (From Ref. 1) 4
Figure 2. Normal Fault (From Ref. 6) 5
Figure 3. Reverse Fault (From Ref. 6) 5
Figure 4. Strike-Slip Fault (From Ref. 6) 6
Figure 5. Body Wave Propagation (From Ref. 6) 7
Figure 6. Idealized Hysteretic Force-Displacement Relation of a LRB (From Ref. 7) 8
Figure 7. Bilinear Hysteretic Numerical Model of a LBR 9
Figure 8. Wen Hysteretic Numerial Model of a LRB 10
Figure 9. Idealized Force Displacement Loops of Sliding Bearings (From Ref. 7)....10
Figure 10. Forced, 2-DOF Undamped System....13
Figure 11. Iterative method used to solve for the isolator forces 15
Figure 12. Multiple Solutions to a NLP Problem (From Ref. 10)....16
Figure 13. Different Combinations of Objectives with Constraints (From Ref. 10)....17
Figure 14. Golden Section Interval Refinement (From Ref. 11)....18
Figure 15. Force Discontinuities in with the Bilinear Model (Force vs. Disp) 23
Figure 16. Force Discontinuities with the Maxwell Model (Force vs. Time)....23
Figure 17. Force Discontinuities with the Maxwell Model (Force vs. Disp)....24
Figure 18. Blocked Data Flow for an Isolator Model that Requires Retained Values....24
Figure 19. Hysteresis Loops for Different Wen Parameters 25
Figure 20. Hysteresis of: (a) Torsional Device; (b) LRB from Ref [13]....26
Figure 21. Conical Sliding Surface Numerical Model (Force vs. Disp) 28
Figure 22. Example of a Recursive Block-by-Block Process 31
Figure 23. Example of a Recursive Block-by-Block Process with Simpson's Rule....32
Figure 24. Accuracy Improvement for a 2-DOF SMD System 32
Figure 25. Differential Integration Error for 2-DOF SMD System 33
Figure 26. Main GUI Module....35
Figure 27. Transient Structural Synthesis Module 36
Figure 28. Isolator Options and Constraints....36
Figure 29. Optimization Module with Advanced FMINCON Options....37
Figure 30. 2DOF Validation Model – Response for Mass #2 40
Figure 31. 7DOF Validation Model – Response for Mass #2 41
Figure 32. Lateral Hysteresis of Corner Node , 16 blocks 42
Figure 33. Hysteresis of Corner Node (From Ref. 8)....42
Figure 34. Parallel Spring – Damper: Force vs. Displacement – Starting Values 44
Figure 35. Parallel Spring – Damper: Force vs. Displacement – Optimal Values....44
Figure 36. Parallel Spring – Damper: Displacement of node #20– Before Optimization 45
Figure 37. Parallel Spring – Damper: Displacement of node #20– After Optimization ...45
Figure 38. Flat Slider with Restoring Spring: – Before Optimization 47
Figure 39. Flat Slider with Restoring Spring: – After Optimization....47

Figure 40. Flat Slider with Restoring Spring: Lateral Acceleration of node #20 – Before Optimization....48
Figure 41. Flat Slider with Restoring Spring: Lateral Displacement of node #20 – After Optimization....48
Figure 42. Spherical Slider: Force vs. Displacement – Before Optimization....50
Figure 43. Spherical Slider: Force vs. Displacement – After Optimization....50
Figure 44. Spherical Slider: Lateral Displacement of node #20– Before Optimization ..51
Figure 45. Spherical Slider: Lateral Displacement of node #20– After Optimization....51
Figure 46. Bilinear NSH: Hysteresis Plot – Before Optimization....54
Figure 47. Bilinear NSH: Hysteresis Plot – After Optimization....54
Figure 48. Bilinear NSH: Lateral Displacement of node #20 – Before Optimization....55
Figure 49. Bilinear NSH: Lateral Displacement of node #20 – After Optimization....55
Figure 50. Maxwell: Force vs. Displacement Plot – Before Optimization....57
Figure 51. Maxwell: Force vs. Displacement Plot – After Optimization....57
Figure 52. Maxwell: Lateral Displacement – Before Optimization....58
Figure 53. Maxwell: Lateral Displacement – After Optimization....58
Figure 54. Wen: Hysteresis Plot – Before Optimization....61
Figure 55. Wen: Hysteresis Plot – After Optimization....61
Figure 56. Wen: Lateral Displacement of node #1– Before Optimization....62
Figure 57. Wen: Lateral Displacement of node #1 – After Optimization....62
Figure 58. Wen: Hysteresis Plot – Before Optimization....65
Figure 59. Wen: Hysteresis Plot – After Optimization....65
Figure 60. Wen: Relative Lateral Displacement of node #1 – Before Optimization....66
Figure 61. Wen: Relative Lateral Displacement of node #1– After Optimization....66
Figure 62. Wen: Lateral Displacement of node #20 – Before Optimization....67
Figure 63. Wen: Lateral Displacement of node #20– After Optimization....67
Figure 64. Wen: Lateral Acceleration – Before Optimization....68
Figure 65. Wen Lateral Acceleration – After Optimization....68
Figure 66. No Isolation: Lateral Displacement of node #20....69
Figure 67. No Isolation: Lateral Acceleration of node #20....69
Figure 68. Thirty-Story Building Wire Frame (From Ref. 8)....72
Figure 69. 30-Story Building: Isolator #1 Lateral Displacement....73
Figure 70. 30-Story Building: Isolator #1 Hysteresis Plot....73
Figure 71. 30-Story Building: 15th Floor Lateral Displacement....74
Figure 72. 30-Story Building: 31st Floor Lateral Displacement....74
Figure 73. 30-Story Building: 31st Floor Acceleration....75
Figure 74. 30-Story Building: Isolator #1 Lateral Displacement....77
Figure 75. 30-Story Building: Isolator #1 Hysteresis Plot....77
Figure 76. 30-Story Building: 15th Floor Lateral Displacement....78
Figure 77. 30-Story Building: 31st Floor Lateral Displacement....78
Figure 78. 30-Story Building: 31st Floor Acceleration....79
Figure 79. No Isolation: 31st Floor Lateral Displacement....80
Figure 80. No Isolation: 31st Floor Lateral Acceleration....80

LIST OF TABLES

Table 1. Methods of Multi-Variable Unconstrained Optimization 19
Table 2. Problems Discovered with Numerical Isolator Models 22
Table 3. Optimization Results for 4-Story Building with Parallel Spring – Damper Isolators 43
Table 4. Optimization Results for 4-Story Building with Flat-Slider Restoring Spring Isolators 46
Table 5. Optimization Results for 4-Story Building with Spherical-Slider Isolators 49
Table 6. Optimization Results for 4-Story Building with Bilinear NSH Isolators 52
Table 7. Optimization Results for 4-Story Building with Maxwell Isolators 56
Table 8. Optimization Results for 4-Story Building with Wen Isolators – Sine Displacement 59
Table 9. Optimization Results for 4-Story Building with Wen Isolators – KobeJapan1995NS_US.mat 63
Table 10. Synthesis Results for30-Story Building with Wen Isolators – Sine Displacement 71
Table 11. Synthesis Results for 30-Story Building with Wen Isolators – KobeJapan1995NS_US.mat 76

THIS PAGE INTENTIONALLY LEFT BLANK

ACKNOWLEDGMENTS

In loving memory of my son.

THIS PAGE INTENTIONALLY LEFT BLANK

EXECUTIVE SUMMARY

On average, there are about 500,000 detectable earthquakes in the world per year. Only about 100,000 of these can be felt and about 100 of them have caused moderate to severe damage. Earthquakes strike without warning and can cause wide-spread damage in populated areas, particularly in third world countries where building codes are poorly enforced or non-existent.

Shear failure is the predominant failure mechanism of most structural systems experiencing a seismic event. Passive isolators have proved successful in absorbing the shear energy delivered by strong motion earthquakes. However, selection of the correct type of isolator that will respond best to the inherent dynamic characteristics of a specific structural system poses the greatest challenge. Traditional methods of transient analysis, i.e. Finite Element Analysis (FEA), for complex structural systems are computationally demanding and make it impracticable for use with existing optimization techniques.

This research focuses on the optimization of isolator parameters in order for structural systems to withstand potentially catastrophic transient vibrations. Many non-linear hysteretic, viscoelastic, and sliding friction isolators were numerically modeled using the scientific programming language, MATLAB. The existing programs used to solve the Voltera integral formulation for Transient Structural Synthesis (TSS) and the Recursive Block-by-Block (RBB) algorithm were investigated and enhanced to yield greater accuracy and increased computational speed. The final product is a user-friendly Decision Support System (DSS) for use with both civil and military applications. Based on different types of base motions and the inherent dynamics of the structure, this DSS is capable of optimizing isolator parameters to meet a user specific objective.

THIS PAGE INTENTIONALLY LEFT BLANK

I. INTRODUCTION

The U.S. Geological Survey estimates an average of 500,000 detectable earthquakes in the world per year [Ref. 1]. Only about 100,000 of these can be felt and about 100 of them have caused moderate to severe damage. Earthquakes strike without warning and can cause wide-spread damage in populated areas, particularly in third world countries where building codes are poorly enforced or non-existent.

Over the past century, scientists and engineers have investigated methods to isolate large structural systems from strong-base motion. The large lateral displacements associated with strong motion flood structural systems with high-magnitude shear forces. Shear failure is the predominant failure mechanism of most structural system undergoing an earthquake event. Passive isolators have been proven successful in absorbing the shear energy delivered by earthquakes [Ref. 2].

Even though passive structural isolators present solutions to the problem of partially decoupling structural systems from ground motion, selection of the correct type of isolators that respond best to the inherent dynamic characteristics of distinct structural systems poses the greatest challenge. This type of problem is clearly one of optimization – choose the best set of parameters to minimize or maximize an objective. Traditional methods of transient analysis, i.e. Finite Element Analysis (FEA), for complex structural systems are computationally demanding. They are impracticable for use with existing optimization techniques due to the computational demand placed by nonlinear isolators.

Transient Structural Synthesis (TSS) is a newer transient analysis method that uses normalized mode shapes, natural frequencies, and an integral equation formulation to solve the response of complex structural systems with localized nonlinearities [Ref. 3]. This time-domain synthesis method uses the Voltera Integral equation, which relies on the exact solution to the governing equations of motion. This method greatly decreases processing speed by allowing implicit model reduction and exploiting the contractive nature of the Voltera Integral equation.

Further improvements in processing speed can be achieved with the use of a Recursive Block-by-Block algorithm [Ref. 14]. This method divides the simulation time

and the impulse response function solutions into equally-sized blocks. The blocks are individually solved by convolution and retained. The solutions to the proceeding blocks are dependent on the retained solutions of previously processed blocks. This method does not degrade the solution's accuracy when compared with non-blocked solutions

These methods present excellent savings in computation speed, but they were not without fault. The existing MATLAB programs that executed the TSS and RBB algorithms had programming redundancies that decreased processing time. They also yielded less accurate results since they employed MATLAB's *conv* command, which uses a rectangular integration rule. The non-linear isolator models developed from a previous thesis research did not execute correctly with the RBB algorithm, which introduced errors into the final synthesized solutions.

Presented here is a thorough investigation of the existing MATLAB programs, which led to optimized program logic, corrected non-linear isolator models, and a method that transforms MATLAB's rectangular integration rule convolution into any integration rule with higher-order error. Also presented are numerical models for sliding-friction isolators, and a user friendly Decision Support System (DSS) tool for transient response and analysis. This program gives a user the ability to quickly change isolator parameters for TSS / RBB, change types of base motions, and optimize the isolator parameters to meet user defined objectives.

II. BACKGROUND

A. EARTHQUAKES

Earthquakes are one of the most terrifying natural phenomena known. They indiscriminately strike without warning, are felt thousands of miles away, and can cause widespread damage. The largest earthquake to strike in the twentieth century was in 1960 off the coast of Chile – 9.5 on the Richter scale. It ruptured an area 525 miles long and 80 miles wide, which devastated numerous Chilean cities, caused hundred of large landslides, and may have aggravated the Puyehue Volcano that erupted two days later [Ref. 4]. This earthquake created a deadly tsunami of more than 30 feet that completely eliminated entire villages along the Chilean coast. The tsunami continued across the Pacific Ocean where it killed 61 people in Hawaii and hundreds more in Japan, more than 8000 miles from the earthquake source.

The causes of earthquakes are explained with the theory of plate tectonics. The basic theory is that the lithosphere, the surface layer of the earth, is made up of many plates that slide over the asthenoshpere, the layer that behaves as a lubricant. Along the boundaries of the plates they will move apart, push together, or slide against each other. When two plates move apart from each other, molten lava rises from beneath the lithosphere. The lava fills the gap created from the separating plates and hardens. This divergent plate boundary is commonly seen at the bottom of an ocean.

Along convergent plate boundaries, one of the plates is usually pushed under the other. The subducted plate will sink into the lower mantel layers and melt. When neither of the plates yields to subduction, the colliding plates form mountain ranges. The peak of Mt. Everest, part of the Himalaya mountain range, increases an average of three inches per year due to the pressure created from the Asian Plate and the Indian Plate [Ref. 5]. Plates that slide against each other do so along transform boundaries and can create tension. The sudden decrease in tension or compression between moving plates releases large amounts of shear energy that propagate through the Earth's crust. Earthquakes are

more common along fault lines – areas where plates meet and move in different directions. The plate-boundary diagram presented in Figure 1 further explains these phenomena.

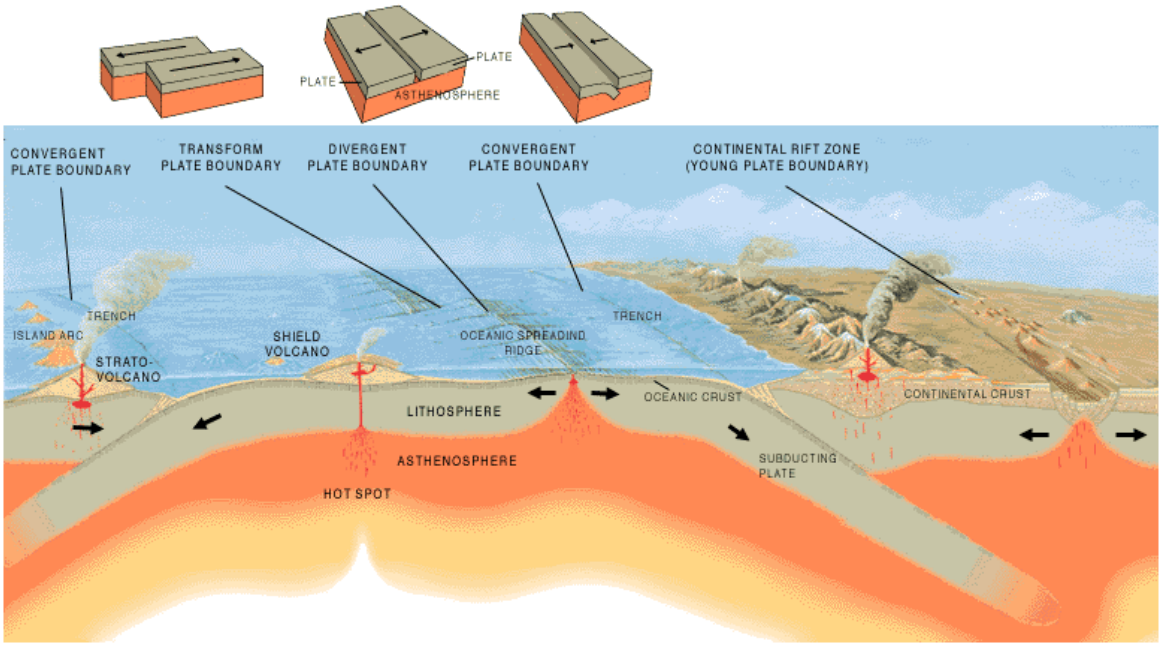

Figure 1. Plate-Boundary Diagram (From Ref. 1)

1. Fault Lines

Geologists have identified four types of fault systems, normal, reverse, thrust, and strike-slip faults. They are characterized by orientation of the fault plane, the break in the rock, and the resulting movement of the two blocks of rock. The normal fault has a nearly vertical fault plane with a hanging wall, the rock above the plane, and a foot wall, the rock below the plane. The hanging wall pushes down against the foot wall, which in turn pushes up against the hanging wall. This separation of the Earth's crust is a result of the pull from a divergent plate boundary. The reverse fault also has a nearly vertical fault plane but the compressed rock causes the hanging wall to push up and the footwall to push down. A thrust fault behaves similar to the reverse fault except that the fault plane is nearly horizontal. As a result, the hanging wall is pushed on top of the foot wall – a

common occurrence in a convergent plate boundary. The strike-slip fault commonly occurs in transform plate boundaries where the plates move in opposing horizontal directions.

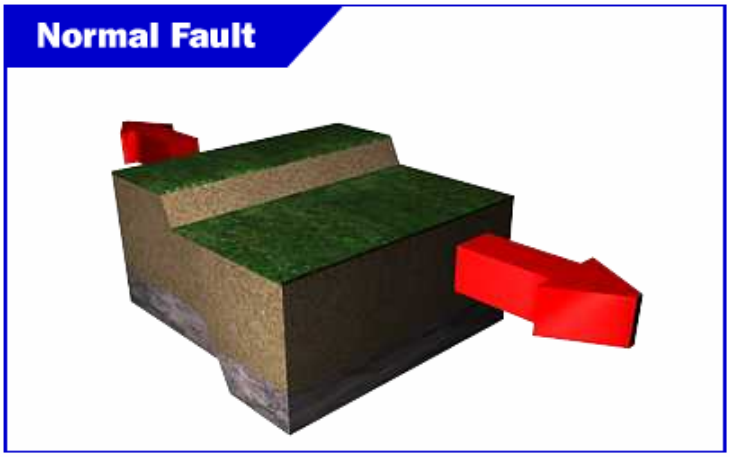

Figure 2. Normal Fault (From Ref. 6)

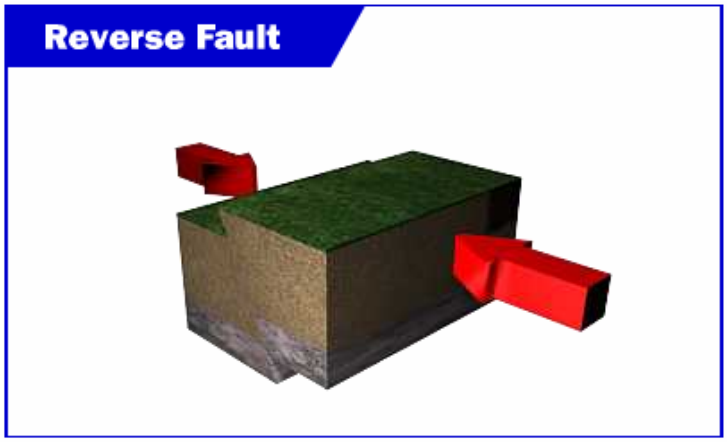

Figure 3. Reverse Fault (From Ref. 6)

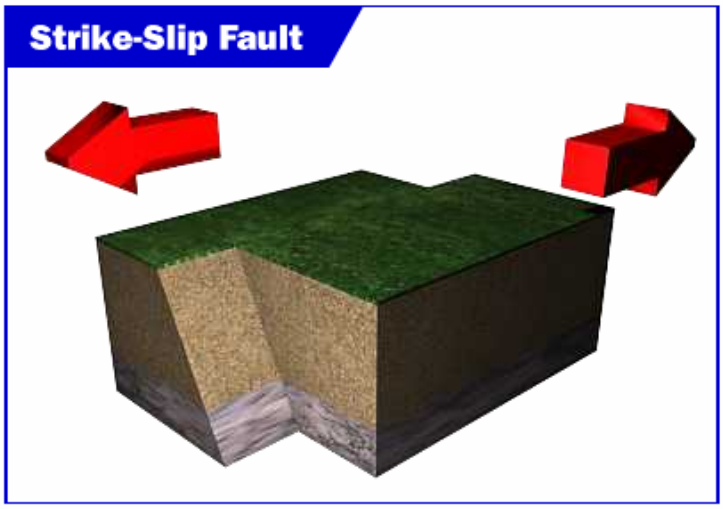

Figure 4. Strike-Slip Fault (From Ref. 6)

The movement of the plates along fault lines creates friction. When the moving rocks become locked, the restricted motion causes the build up of potential energy – the stress in the rock increases. When the rock finally yields due to the enormous stresses, the sudden release of kinetic energy propagates through the Earth's lithosphere.

2. Seismic Waves

The seismic energy wave propagates through the Earth in the same manner as disturbance in a body of water. Seismic waves are categorized into body waves and surface waves. Body waves are those that travel through the inner part of the Earth and cause primary waves (p-waves) and secondary waves (s-waves) [Ref. 6]. P-waves are compression waves that travel through to the Earth's surface the fastest and can penetrate solids, liquids, and gasses. S-waves are shear waves that travel perpendicular to the direction of the body waves. They only propagate through solid material and are thus stopped by the Earth's liquid asthenosphere.

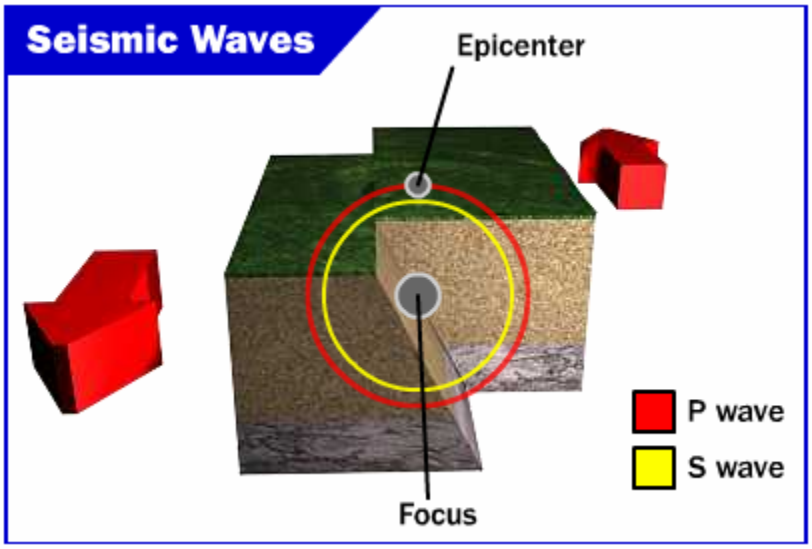

Figure 5. Body Wave Propagation (From Ref. 6)

Surface waves are caused by the body waves that reach the surface. They are also known are long waves (l-waves) due to their low frequency. L-waves produce the most intense ground displacement and are responsible for the most damage associated with earthquakes.

B. BASE MOTION ISOLATION

Base motion isolation has become an increasing requirement for structural designs in earthquake prone areas. The two types of isolation that have gained acceptance are elastomeric bearings and sliding systems. Elastomeric bearings are made of either natural rubber or neoprene and serve the purpose of decoupling a structural system from the horizontal component of strong-ground motion. The low horizontal stiffness of the elastomer gives the structural system a natural frequency that is much lower than its fixed-base frequency and lower than the larger ground motion frequencies [Ref. 2]. Since the first non-rigid body mode of a structural system relates to structural deformations, the system can be viewed as a rigid body.

Sliding systems limit the transfer of shear across the isolation interface. The sliding interface is typically made of two dissimilar metals with a low friction coefficient aided by a restoring device. The use of restoring devices with sliding systems helps reduce the diameter of the bearing plates and the support system.

Non-linear base isolation is of special interest since, unlike linear isolators that deflect earthquake energy; non-linear isolators dissipate the energy through plastic deformation of the isolator materials or with the use of viscous or coulomb damping.

1. Elastomeric and Hysteretic Isolators

Elastomeric isolators usually include high-damping rubber bearings (HDR), low-damping rubber bearings (RB) or low-damping rubber bearings with a lead core (LRB). These isolators consist of thin layers or natural rubber that are vulcanized and bonded to steel plates. Natural rubber exhibits both hysteretic and viscoelastic behavior. In particular, low-damping natural rubber exhibits an almost linear elastic and linear viscous behavior. HDR and RB isolators are practically linear since their dynamic shear modulus remains almost constant over a wide range of temperature and frequencies [Ref. 2]. Their dynamic damping coefficients remain comparatively constant at frequencies lower than 50 Hz – a desirable characteristic since strong motion frequencies are much lower.

For isolators with different types of rubber, the stiffness characteristics will change as the shear loading changes. For small displacements, the isolator stiffness is large – this is desirable to minimize the effects of wind loading. When the isolator experiences large shear strains, the stiffness is very low and effectively deflects seismic energy.

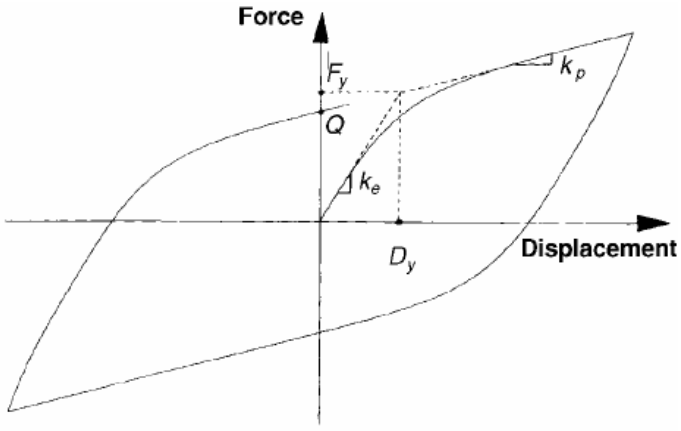

Figure 6. Idealized Hysteretic Force-Displacement Relation of a LRB (From Ref. 7)

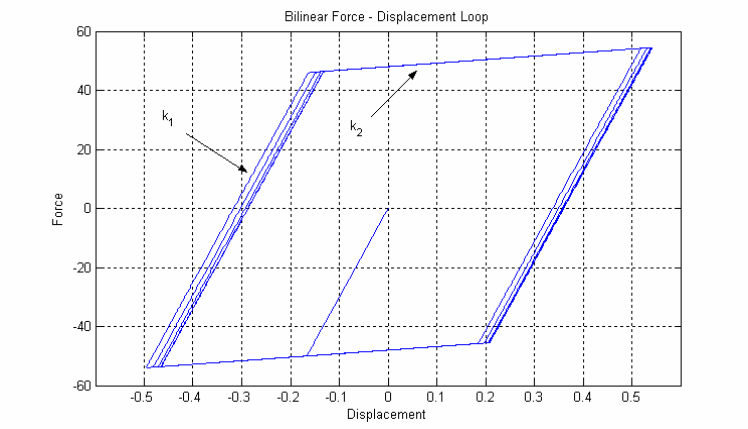

Figure 7. Bilinear Hysteretic Numerical Model of a LBR

A LRB is categorized as a hysteretic isolator because of its lead core. A hysteretic material is one that will remain permanently deformed when the disturbing force is removed. Viscoelastic and elastomeric materials do not exhibit hysteretic behavior since they return to their original position once the disturbing force is removed. LRB isolators are typically constructed of low-damping natural rubber with a press fitted lead core. During strong lateral motion, the lead core yields at low stresses, deforms in nearly pure shear, and produces stable hysteretic behavior. Repeated yielding will not cause fatigue failure since lead self-anneals at standard temperature [Ref. 7]. The behavior of LRB isolators can be represented by a bilinear hysteretic numerical model, such as the one presented in Figure 7. Equation (1) relates the characteristic strength, Q, of an LRB isolator to the lead core area, A_p, and the shear yield stress of lead, Q_{yl}.

$$Q = A_p \sigma_{yl} \tag{1}$$

Even though a bilinear numerical model will yield acceptable results for non-linear isolators, the Wen model, Figure 8, will more closely represent the hysteretic curve.

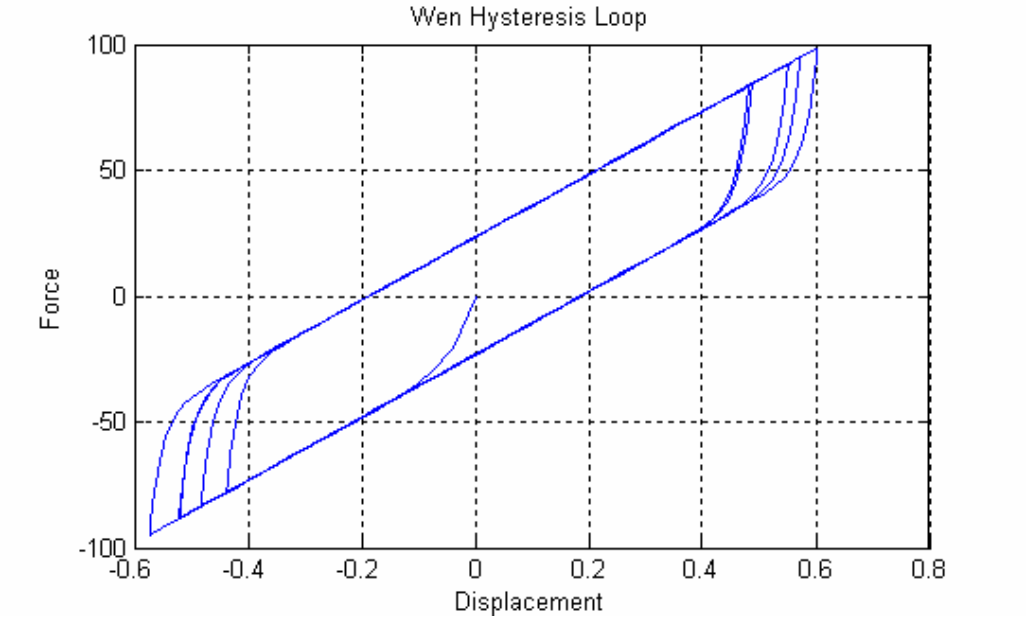

Figure 8. Wen Hysteretic Numerial Model of a LRB

2. Sliding Isolators with Restoring Force Mechanisms

Sliding bearings will limit the transmission of lateral forces to the isolated structure, but require large sliding surfaces and usually result in permanent offset displacements. To reduce the diameter of the sliding surface and prevent unwanted displacements, a restoring force mechanism is typically used. The three types of sliding isolators are shown in Figure 9.

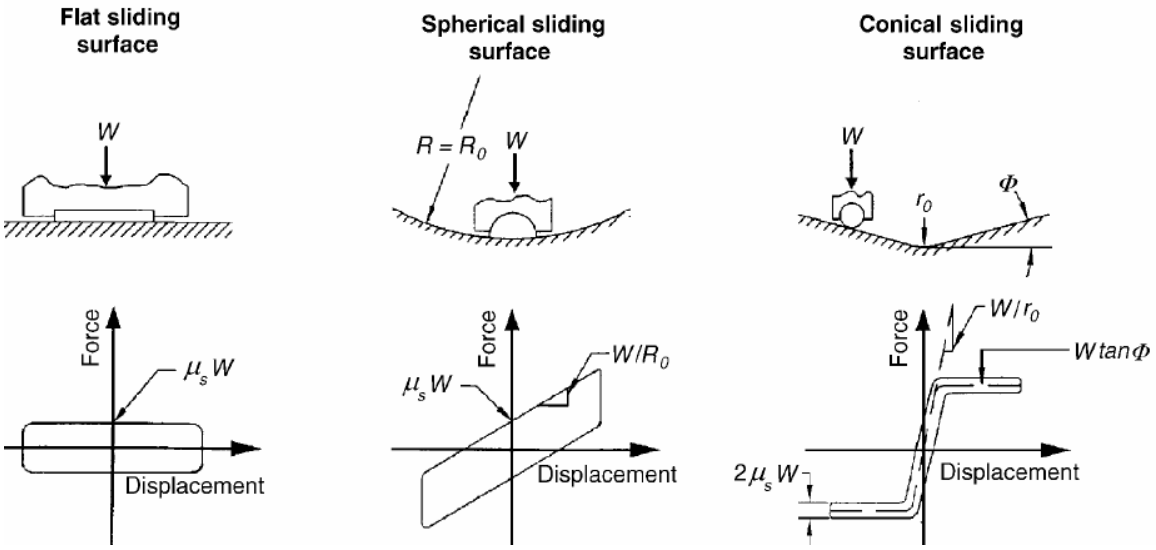

Figure 9. Idealized Force Displacement Loops of Sliding Bearings (From Ref. 7)

The lateral force developed from a sliding bearing can be calculated with Equation (2). The effects due to vertical ground acceleration and overturning moments on the normal load used to calculate the lateral force is calculated with Equation (3) [Ref. 7].

$$F = \frac{N}{R}U + \mu_s N \,\mathrm{sgn}(\dot{U}) \tag{2}$$

where

U = Displacement

U_{dot} = Sliding velocity

R = Radius of curvature of the sliding surface

μ_s = Coefficient of sliding friction

N = Normal load on the bearing

$$N = W\left(1 + \frac{\ddot{U}_v}{g} + \frac{P_s}{W}\right) \tag{3}$$

Flat sliding bearings have an infinite radius of curvature and require a restoring mechanism. This is not the case with spherical and conical sliding surfaces since self-centering is inherent to their design. Sliding bearings are commonly made from PTFE or PTFE based composites in contact with a polished stainless steel surface.

3. Viscoelastic Isolators

Viscoelastic isolators can be either frequency dependent or frequency independent. Such isolators that resemble a parallel spring-damper configuration are frequency dependent and poorly dissipate displacement energy. In turn, if the configuration resembles a spring-damper in series, such as the Maxwell model, it is considered frequency independent. Frequency independent isolators retain their characteristic force-displacement loop over a broad range of frequencies [Ref. 8].

C. RELEVANT RESEARCH

The final analysis / optimization program is a combination of the proper use of the Voltera Integral Equation, Transient Structural Synthesis (TSS), and the Recursive

Block-by-Block (RBB) algorithm. These topics are well researched and discussed in their respective references. The following sub-sections broadly discuss these topics in order for the reader to have the general knowledge need to understand the following chapters.

1. Governing Equations of Motion

Mechanical or structural systems undergo forced vibrations when external energy is applied. External energy can be applied by an external / internal force or by a change in displacement. Forces and displacements can be harmonic, non-harmonic and periodic, non-periodic, or random in nature. Harmonic excitation usually results in a harmonic system response, while suddenly applied non-periodic excitation results in a transient system response. However, suddenly applied harmonic excitation will also produce a transient response.

The basic equation of motion for a forced single degree-of-freedom (DOF) system is derived from Newton's second law of motion.

$$m\ddot{x} + c\dot{x} + kx = F(t) + F_{NL}(x, \dot{x}, t) \tag{4}$$

The solution to this 2nd order ordinary differential equation is a homogeneous and particular one. When the initial conditions are zero, such as a structural system awaiting a seismic event, the homogeneous solution will also be zero. What remains is the particular solution to the forced system. Linear systems can be solved with the correct Laplace transform, while nonlinear systems may require more advanced numerical methods.

A common method for solving linear-multi DOF systems is with eigenvector and eigenvalue solutions. For an undamped 2-DOF system, Figure 10, the equations of motion are stated here in matrix form.

$$\begin{pmatrix} m_1 & 0 \\ 0 & m_2 \end{pmatrix} \begin{Bmatrix} \ddot{x}_1 \\ \ddot{x}_2 \end{Bmatrix} + \begin{pmatrix} k_1 + k_2 & -k_2 \\ -k_2 & k_2 \end{pmatrix} \begin{Bmatrix} x_1 \\ x_2 \end{Bmatrix} = \begin{Bmatrix} F_1 \\ F_2 \end{Bmatrix} \tag{5}$$

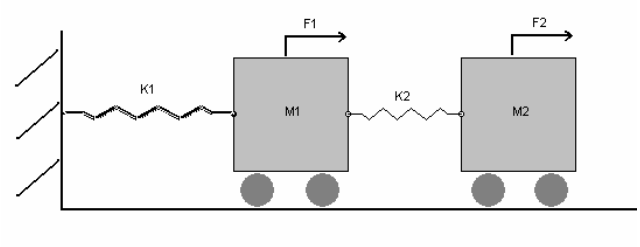

Figure 10. Forced, 2-DOF Undamped System

The mass and stiffness matrices are needed in order to solve for the eigenvalues and eigenvectors. The square root of the eigenvalues yields the natural frequencies and the eigenvectors contain the system modes. Systems with n-DOF will have n-modes and n-natural frequencies. The modes and natural frequencies are needed to later calculate the impulse response functions that will be used to solve the particular solution using the Voltera integral equation.

2. Voltera Integral Equation

This convolution integral is generally found in most college-level vibrations textbooks and is based on the idea that any force is the equivalent to a superposition of impulses of discrete duration time, τ.

$$x(t) = \int_0^t f(\tau)h(t-\tau)d\tau \tag{6}$$

Here, h are the impulse response functions (IRF) that were calculated with the modes and natural frequencies. The equation used to calculate the IRFs for a 1-DOF system is:

$$h(t) = \left(\frac{e^{-\zeta\omega_n t}}{\omega_n\sqrt{1-\zeta^2}} \sin \omega_n\sqrt{1-\zeta^2}\, t \right) \tag{7}$$

where

ω_n = Natural frequency

ζ = Damping ratio

In order to solve the convolution integral numerically, an integration rule is applied in matrix form. The following matrix equation was developed with the trapezoid

integration rule and solves for the particular solution of a system with zeros for the initial conditions.

$$\begin{Bmatrix} x_0 \\ x_1 \\ \vdots \\ \vdots \\ x_m \end{Bmatrix} = \Delta t \begin{bmatrix} \frac{1}{2}h\,(0\Delta t) & 0 & \cdots & 0 \\ \frac{1}{2}h\,(1\Delta t) & \frac{1}{2}h\,0\Delta t & \cdots & 0 \\ \vdots & \vdots & \cdots & \vdots \\ \vdots & \vdots & \cdots & \vdots \\ \frac{1}{2}h\,(m\Delta t) & h((m-1)\Delta t) & \cdots & \frac{1}{2}h\,(0\Delta t) \end{bmatrix} \begin{Bmatrix} F_0^{iso} \\ F_1^{iso} \\ \vdots \\ \vdots \\ F_m^{iso} \end{Bmatrix} \tag{8}$$

The forcing vector F^{iso} represents the isolator force due to the base motion excitation. Reference [8] presents a detailed discussion of the Voltera Integral Equation in modal space.

3. Transient Structural Synthesis

Transient Structural Synthesis (TSS) is a topic that is thoroughly discussed in [Ref. 3] and broadly presented here since it is the core of the program developed for this thesis. In a time domain, TSS is used to calculate the dynamic response of coupled substructures and allows for model reduction to only the coordinates of interest. System modifications can quickly be calculated with pre-modification transient response data. The object is to solve for the nonlinear isolator forces, which are retained to later solve for the response of other coordinates of interest. This is an iterative process that requires an initial guess for $\mathbf{f}^{iso}$, the vector of isolator forces – usually a vector of ones. Chapter III, Section C presents a method of improving the initial guess for accuracy by modifying $\mathbf{f}^{iso}$ with a vector of integration rule weightings. The following flowchart explains this iterative method.

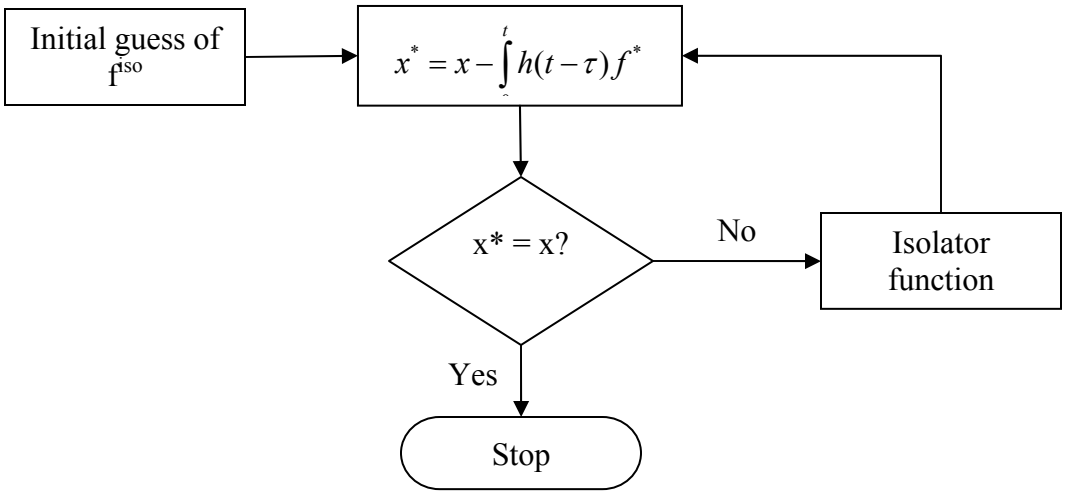

Figure 11. Iterative method used to solve for the isolator forces

The converged solution for the vector of isolator forces is used to calculate the dynamic response of other coordinates of interest. The response of such a point is the linear combination of its IRF convolved with each isolator force that couples the system.

4. Recursive Block-by-Block Algorithm

The recursive block-by-block (RBB) algorithm [Ref. 14] further reduces processing time by dividing the total simulation time into several blocks of equal lengths. This method divides the simulation time and the impulse response function solutions into equally sized blocks. The blocks are individually solved by convolution and retained. The solutions to the proceeding blocks are dependent on the retained solutions of previously processed blocks. This method does not degrade the solution's accuracy when compared with non-blocked solutions.

D. OPTIMIZATION – NONLINEAR PROGRAMMING

Optimization problems can be divided into either linear programming (LP) or nonlinear programming (NLP) – most engineering problems are nonlinear in nature. NLP algorithms start at any point within the feasible solution region of the NLP problem. It then attempts to move from the starting point in a direction through the feasible region that results in an improved objective function. If the algorithm determines there is a better direction, it will adjust its step size and move in that direction to a better feasible solution. The process continues until the algorithm determines that movement in any direction will degrade the solution. The algorithm terminates when it has found a local

optimal solution. – a solution that is better than any other feasible solution in its immediate area within the feasible region. However, a given local optimal solution might not be the best possible solution. It is common practice with NLP problems to use different starting points in search of the best feasible solution [Ref. 10].

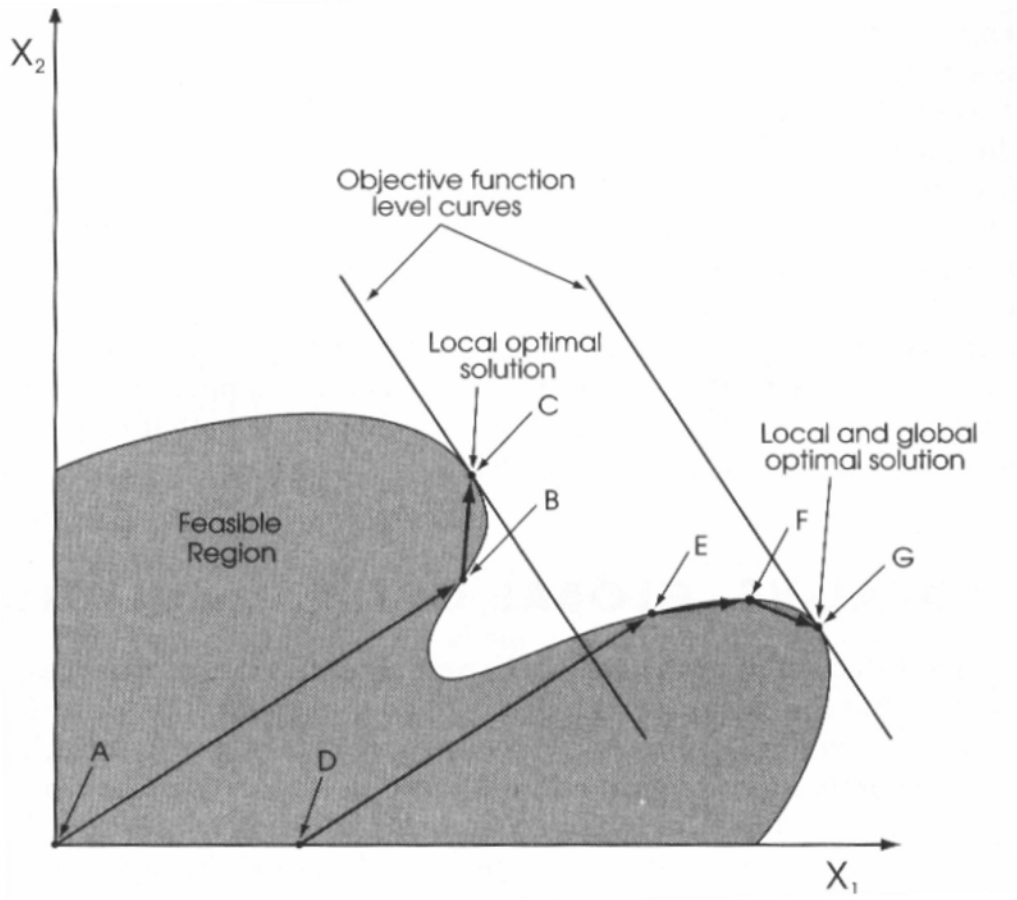

Figure 12. Multiple Solutions to a NLP Problem (From Ref. 10)

NLP problems have three combinations of objectives with constraints: linear objective with nonlinear constraints, nonlinear objective with linear constraints and nonlinear objective with nonlinear constraints. The Decision Support System (DSS) tool written for this thesis uses a linear objective function of either displacements, accelerations, or both, with nonlinear constraints. These combinations are graphically described in Figure 13.

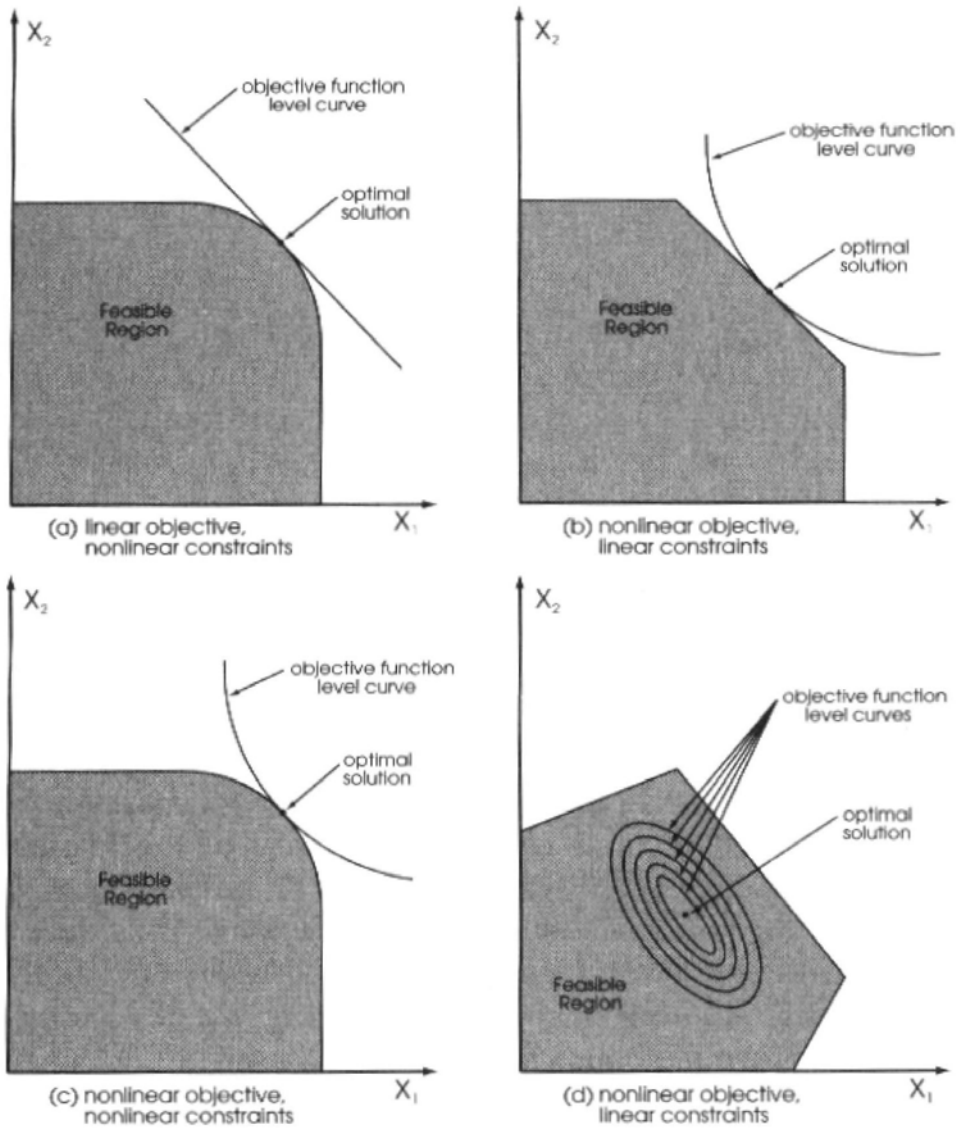

Figure 13. Different Combinations of Objectives with Constraints (From Ref. 10)

1. One-Variable Optimization Problems

For multivariable functions, a one-dimensional minimization routine may be called numerous times to find a local minimum. Interval bounding and Golden Section interval refinement algorithms are useful in searching for the minimum of one-variable functions.

The interval bounding function starts at a point on a curve and "marches" at a fixed space step in a descending direction. When the function encounters an ascending

direction, it stops and saves the current and last two points for the interval refinement function. This function should be run several times at different starting points to find the interval that may yield an optimal solution.

The interval refinement function uses the Golden Section algorithm to isolate the contained minimum point to a predetermined tolerance. This algorithm uses the Golden Ratio (0.618034) to refine an interval. It first determines the interval length and then adds a fraction of the interval length (the length multiplied by the Golden Ratio) to the lower bound of the interval. It subtracts the same length fraction from the upper bound. Depending on the magnitude of the two new points within the interval, the algorithm eliminates the portion of the interval that is no longer needed – Figure 14 clarifies this methodology [Ref. 11].

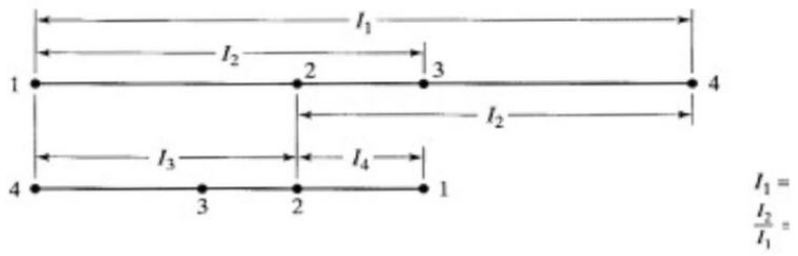

Figure 14. Golden Section Interval Refinement (From Ref. 11)

2. Multi-Variable Optimization Problems

Common methods for multi-variable unconstrained optimization include Steepest Descent, Newton's Method, Marquardt's Compromise, and Modified Newton's Methods. The Steepest Descent and Modified Newton methods incorporate the bounding phase and Golden Section algorithms. The MATLAB Optimization Toolbox used for this thesis automatically chooses a method; however, a user can easily change the method and optimization parameters by changing the *optimset* values within MATLAB. The advantages and disadvantages of each method are summarized in Table 1.

Method	Advantages	Disadvantages
Steepest Descent	-Maintains a descent property -Only uses the gradient information -Converges from any starting point -Reliable and stable	-Requires a line search -Slows down near a minimum -Very slow convergence
Newton	-Can exhibit quadratic convergence -No line search -Very fast convergence	-Requires the Hessian and its inverse (will fail if singular) -Needs to solve a linear system of equations -Only converges near optimal function values -May diverge for non-quadratic functions or with poor starting points
Marquardt	-Maintains a descent property -No line search -Excellent convergence rate -Uses Newton when it gives good descent results and Steepest Descent where it doesn't	-Requires the Hessian -Needs to solve a linear system of equations
Modified Newton	-Maintains a descent property -Avoids divergence	-Requires a line search

Table 1. Methods of Multi-Variable Unconstrained Optimization

3. Constrained Optimization

Constrained optimization is the minimization of an objective function subject to the constraints of the possible values of the independent variables. Constraints can be linear or nonlinear with either equality or inequality constraints.

The typical equality constrained optimization problem has the form:

$$\text{minimize} \quad f(x)$$

$$\text{subject to} \quad h(x) = 0$$

where $f(x)$ is the scalar valued function and $h(x)$ is the vector valued constraint function. Because of the constraint, stationary points (minimum, maximum, or saddle points) of $f(x)$ may not be valid solutions since they may not satisfy the constraints. The common approach to solving constrained optimization problems is with the method of

Lagrange multipliers. This method converts the constrained optimization problem into an unconstrained one, which is then solved with one of the methods listed on Table 1. The stationary points of the Lagrangian are potential solutions of the constrained optimization problem [Ref. 12].

$$L = f + \sum_{j=1}^{l} \lambda_j h_j \tag{9}$$

The typical inequality constrained optimization problem has the form:

$$\text{minimize} \quad f(x)$$

$$\text{subject to} \quad g(x) \leq 0$$

where $f(x)$ is the scalar valued function and $g(x)$ is the vector valued constraint function. The discussion of inequality constraints is lengthy and thoroughly discussed in [Ref. 11] and [Ref. 12].

E. DECISION SUPPORT SYSTEMS

Decision Support Systems (DSS) are a specific class of computerized information systems that support the decision makers. DSS are typically interactive computer-based systems intended to aide decision makers by using communications technologies, data, documents, knowledge and/or models to identify, solve problems, and make decisions. The type of DSS developed for this thesis is a model-driven DSS. The model-driven DSS emphasizes access and manipulation of optimization and simulation models. It uses data and parameters provided by the designer, are not usually data intensive, and do not use large databases.

III. INVESTIGATION AND ENHANCEMENTS

A. CORRECTIONS TO EXISTING NUMERICAL ISOLATOR MODELS

The Bilinear, Maxwell, and Wen models were adopted from [Ref. 8]. In this reference, the author presents their use with TSS and RBB to solve the base isolation and structural response for three structural models. The MATLAB programs inherited from this research failed to duplicate the results presented in [Ref. 8]. The isolator model programs were thoroughly investigated for model theory, accuracy, program flow, and compatibility with RBB. The results of this investigation are presented in Table 2. Other errors of minor importance include:

- The El Centro time history plot on [Ref. 8, Page 53] is incorrectly presented in inches. The maximum and minimum displacement points are consistent with the measurements in centimeters. The data presented in this reference contains unit dimension errors.
- The starting vector of isolator forces used for TSS was a vector of zeros. A better vector of starting values is a vector of ones, as recommended in [Ref.14].

If a simulation is performed with only one block, RBB is not used. Any isolator model not written to "remember" forces and displacements from previous blocks will function correctly. Once the number of blocks exceeded one, RBB is employed and isolator models that don't "remember" will report a zero force value at the beginning of each block. Examples of these force discontinuities are show in Figures 15 – 17. The program-logic flowchart for processing RBB blocks is presented in Figure 18. It is imperative that MATLAB's persistent variables, those that retain the final force and displacement values for the previously processed block, be clear from memory. Otherwise the persistent variables will remain in memory until the user terminates the MATLAB session. Any further processing without first clearing these variables will result in incorrect results.

Isolator Model	Problems	Corrections
Bilinear	• No functionality with RBB. • Force discontinuities for more than one block. • Poor program flow. • Poorly documented.	• Model re-written to function properly with RBB. • Logic and program flow improved – properly documented • Wrote a separate model that does not account for strain hardening since LRB are self annealing at standard temperature.
Maxwell	• No functionality with RBB. • Force discontinuities for more than one block. • Runge-Kutta 4th order method solved incorrectly for range of time steps. • Poor program flow. • Poorly documented.	• Model re-written to function properly with RBB. • Logic and program flow improved • Runge-Kutta 4th order method solves correctly for any user-defined time step. • Logic and program flow improved – properly documented
Wen	• Incorrect Wen equation • No functionality with RBB. • Force discontinuities for more than one block. • Runge-Kutta 4th order method solved incorrectly for range of time steps. • Poor program flow. • Poorly documented.	• Model re-written with correct equations [Ref. 13] and to function properly with RBB. • Logic and program flow improved • Runge-Kutta 4th order method solves correctly for any user-defined time step. • Logic and program flow improved – properly documented

Table 2. Problems Discovered with Numerical Isolator Models

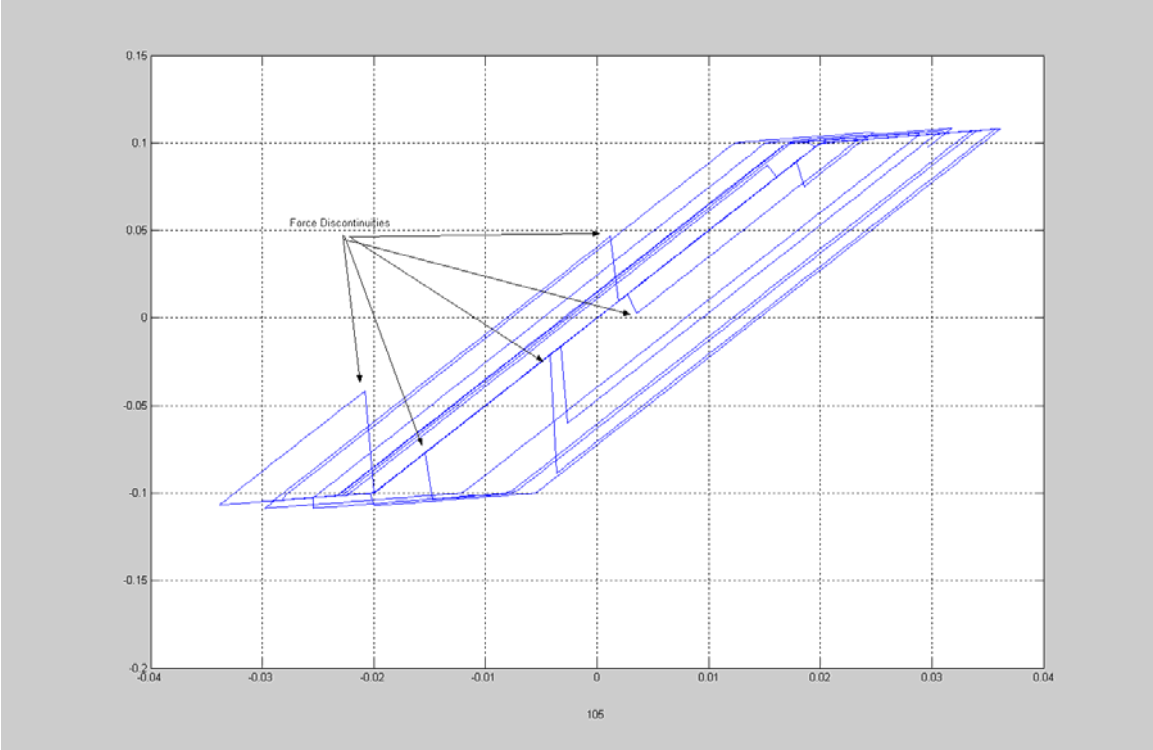

Figure 15. Force Discontinuities in with the Bilinear Model (Force vs. Disp)

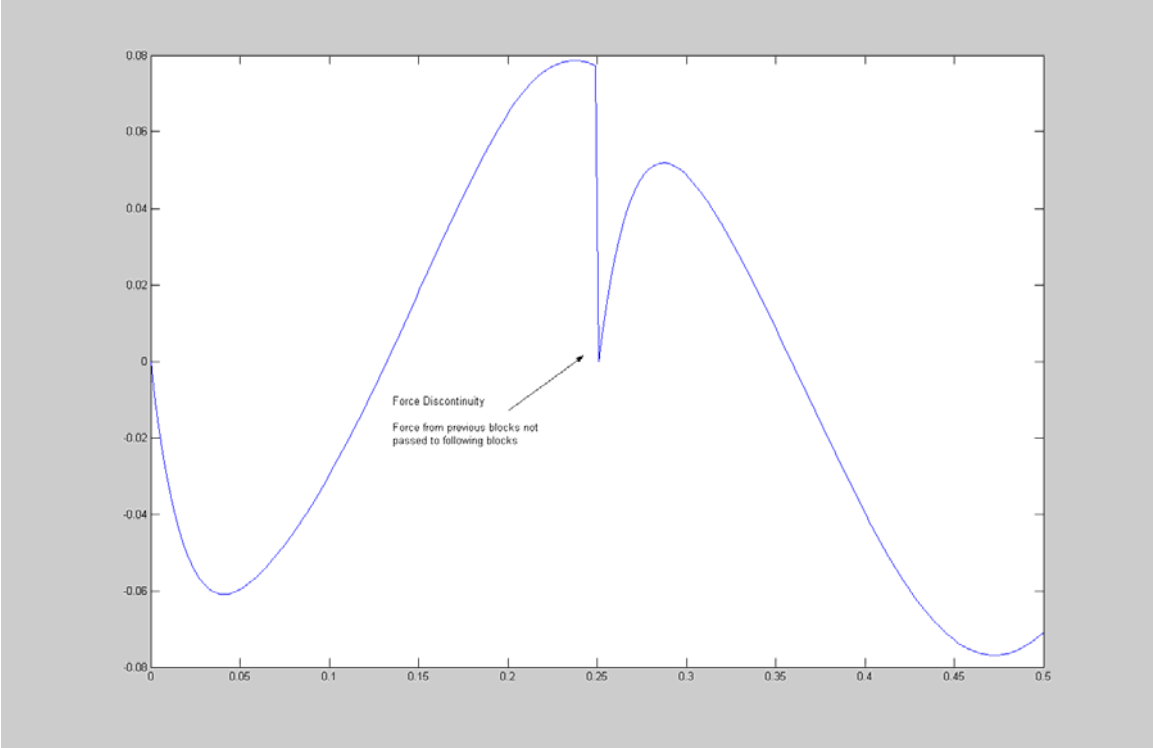

Figure 16. Force Discontinuities with the Maxwell Model (Force vs. Time)

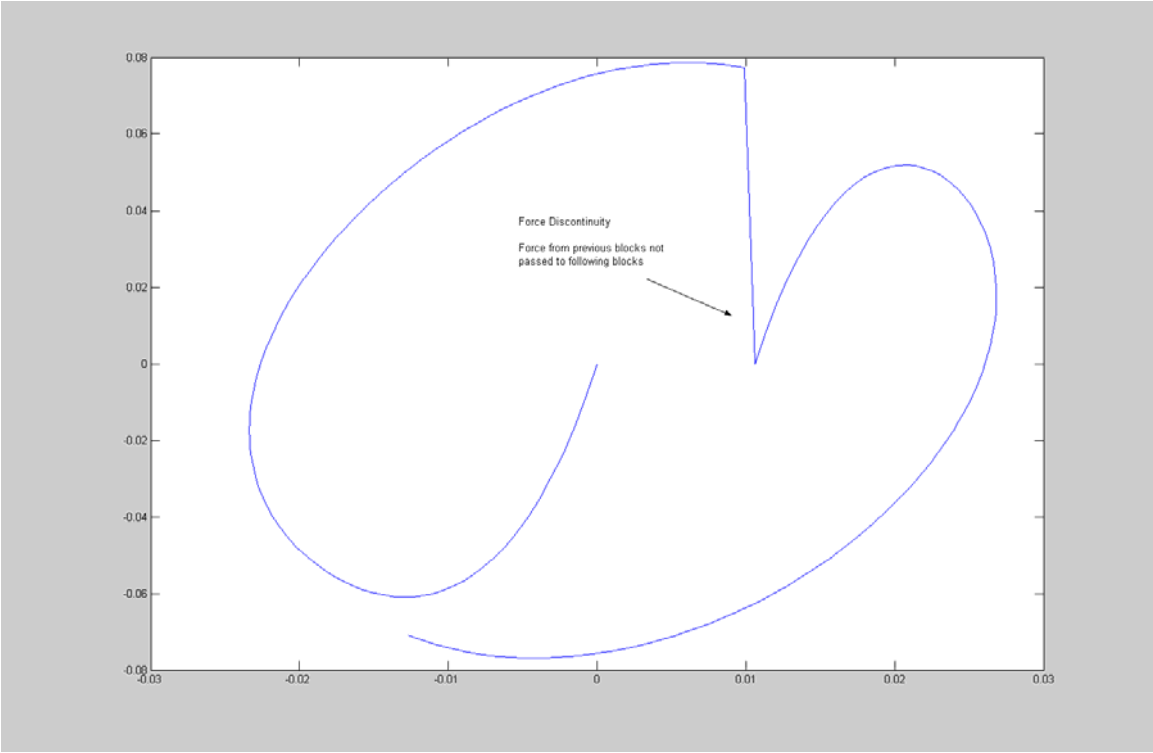

Figure 17. Force Discontinuities with the Maxwell Model (Force vs. Disp)

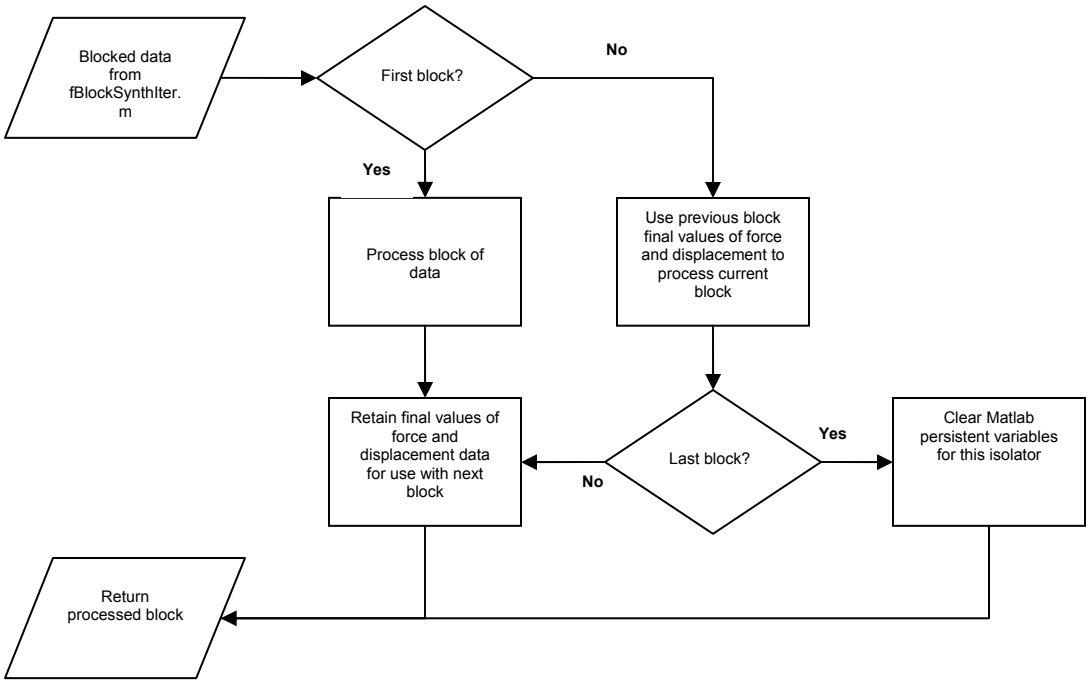

Figure 18. Blocked Data Flow for an Isolator Model that Requires Retained Values

1. Wen Model Validation

The Wen isolator model is of particular interest due to its ability to represent all varieties of hysteretic behavior by the proper selection of parameters for its governing equation. [Ref. 13] The restoring force for this hysteretic damper is:

$$Q(x,\dot{x}) = \alpha \frac{F_y}{\Upsilon} x + (1-\alpha) F_y Z \tag{10}$$

Here, Z is the dimensionless hysteretic component, which satisfies the following nonlinear first order differential equation:

$$\Upsilon \dot{Z} = -\gamma |\dot{x}| Z |Z|^{\eta-1} - \beta \dot{x} |Z|^{\eta} + A\dot{x} \tag{11}$$

The Wen numerical model program developed for this thesis accurately reproduced the results presented by Constantinou and Tadjbakhsh [Ref. 13]. The following figure shows the duplicated results for the base displacement of 5.5 inches with a frequency of 0.9 Hz used for their study.

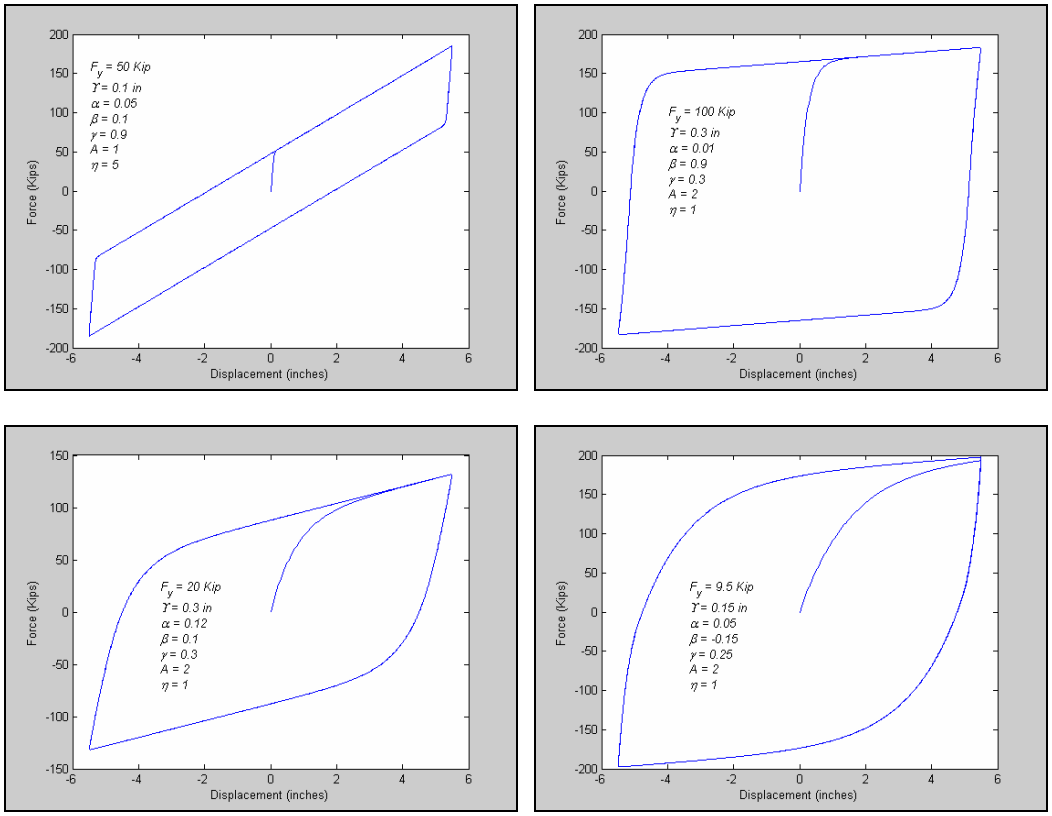

Figure 19. Hysteresis Loops for Different Wen Parameters

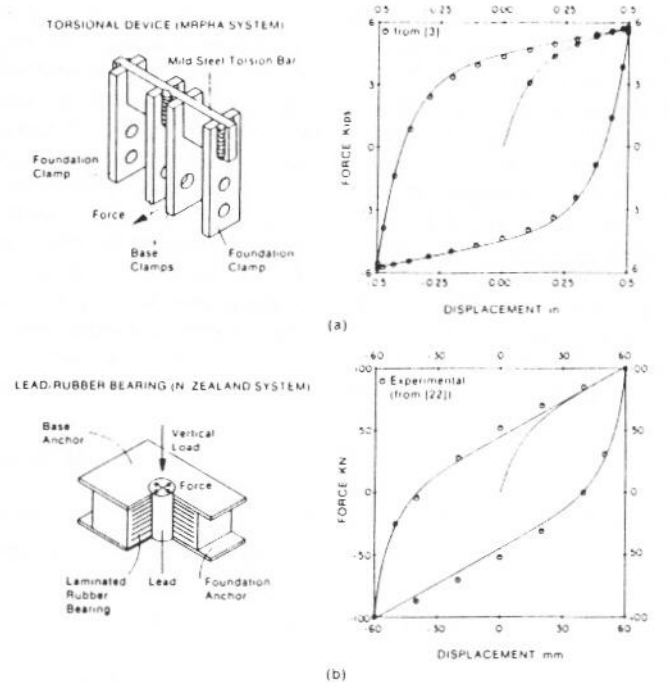

Figure 20. Hysteresis of: (a) Torsional Device; (b) LRB from Ref [13]

For a detailed review of the dimensionless parameters α, β, γ, A, and η, please refer to [Ref. 13].

B. SLIDING NUMERICAL ISOLATOR MODELS

Sliding bearings will limit the transmission of lateral forces to the isolated structure. The three sliding models presented here were adopted from [Ref. 7]. This reference is maintained by the Federal Emergency Management Agency (FEMA) and sets guidelines the analysis and design of passive seismic isolation and energy dissipation systems. These models do not take into account the effects of slipping and sticking, which can transform low-frequency base vibrations into high-frequency structural vibrations [Ref. 2].

1. Flat Sliding Surface with Restoring Device

This friction model resembles a linear spring in parallel with a linear damper. The governing equation for this model is stated in Equation (10) and does not require retained values from previous blocks to function correctly with RBB.

$$F = kx + \mu_s N \operatorname{sgn}(\dot{x}) \tag{12}$$

This equation uses the coefficient of static friction, μ_s, since the isolator is at rest before a disturbance. Also, the dynamic friction coefficients for materials commonly used with sliding bearings differs very little from the static friction coefficient [Ref. 2]. This model accepts the base displacement, base velocity, normal force (the distributed force of the structure on each isolator), and a friction coefficient in order to process and return the isolator restoring force. Flat sliding bearings with restoring capabilities are usually the combination of a sliding and elastomeric bearing.

2. Spherical Sliding Surface

In this model the spherical sliding surface acts as the restoring device. Notice that as the sphere's radius of curvature, *R*, increases, the restoring force part of Equation (11) becomes irrelevant and degrades to a flat sliding bearing with out a restoring force. This model does not require retained values from previous blocks to function correctly with RBB.

$$F = \frac{N}{R}x + \mu_s N \operatorname{sgn}(\dot{x}) \tag{13}$$

3. Conical Sliding Surface

The conical sliding surface model does require the last force value from the previous block in order to function correctly with RBB. This is due to the transition between the cone's spherical surface and the inclined surface. Note that the force vs. displacement plot from Figure 9 shows two possible force values for the same displacement. Retention of the previous force is needed to determine if the displacement is causing an increase in force (top line) or a decrease (bottom line). The program uses Equation (14), which was derived from plane geometry, to determine the transition between the spherical surface and the inclined surface.

$$s_{transition} = \sqrt{\frac{r_o}{\frac{1}{\tan(\phi)^2}+1}} \tag{14}$$

If the criteria of $-s_{transition} \le x \le s_{transition}$ is met, then the program uses Equation (14) calculate the resulting force. Outside of the transition boundaries, the program uses

Equation (15) to calculate the restoring force. Note that the value of $s_{transition}$ decreases as the incline angle decreases, which makes Equation (13) the dominating one.

$$F = F_{previous} \pm 2\mu_s N \tan(\phi) \tag{15}$$

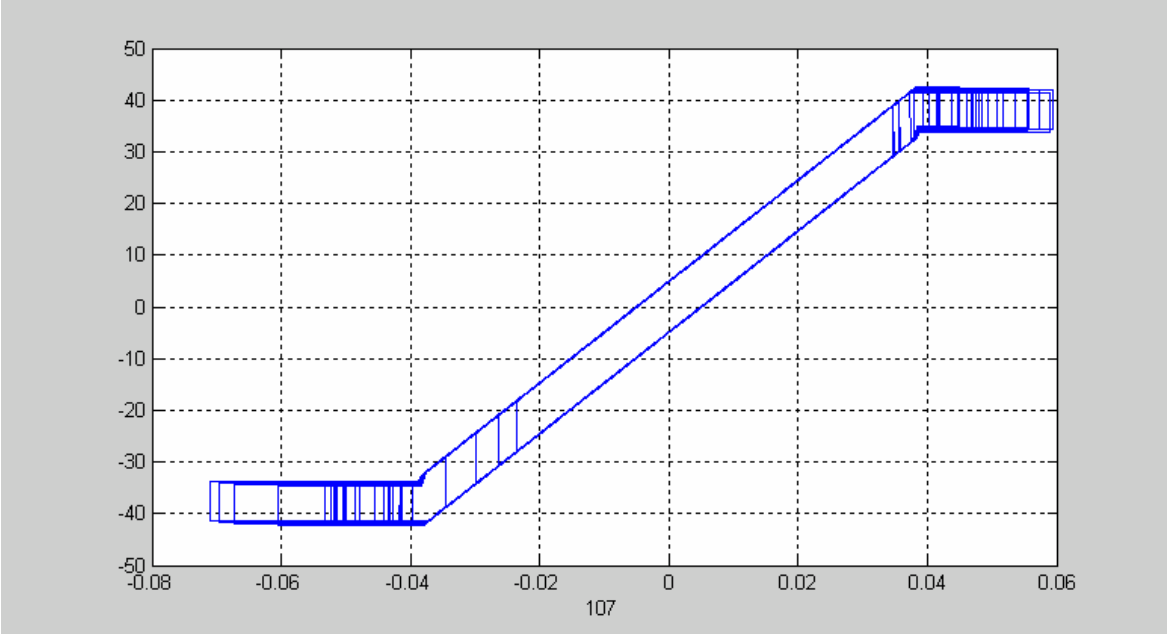

Figure 21. Conical Sliding Surface Numerical Model (Force vs. Disp)

C. CONVOLUTION-DRIVEN NUMERICAL INTEGRATION

The programs that run TSS and RBB exploit MATLAB's *conv* command for numerical integration. The convolution theorem states that the convolution of two vectors is the same as multiplying their Fourier transforms. MATLAB's Signal Processing Toolbox is optimized for speed and can perform convolutions very efficiently. The following convolution example should help the reader understand and appreciate convolution-driven numerical integration.

To integrate the line $y = x$, let $\boldsymbol{x}$= [0 1 2 3 4 5] and $\boldsymbol{v}$ = [1 1 1 1 1 1]^T. Before convolving these two vectors, we apply a filter matrix to x and discard the last four columns.

$$x_{convmtx} = \begin{pmatrix} 0 & 1 & 2 & 3 & 4 & 5 & 0 & 0 & 0 & 0 & 0 \\ 0 & 0 & 1 & 2 & 3 & 4 & 5 & 0 & 0 & 0 & 0 \\ 0 & 0 & 0 & 1 & 2 & 3 & 4 & 5 & 0 & 0 & 0 \\ 0 & 0 & 0 & 0 & 1 & 2 & 3 & 4 & 5 & 0 & 0 \\ 0 & 0 & 0 & 0 & 0 & 1 & 2 & 3 & 4 & 5 & 0 \\ 0 & 0 & 0 & 0 & 0 & 0 & 1 & 2 & 3 & 4 & 5 \end{pmatrix} \tag{16}$$

The transpose of $x_{\underline{convmtx}}$ is now multiplied by v,

$$x^{T}_{convmtx} = \begin{pmatrix} 0 & 0 & 0 & 0 & 0 & 0 \\ 1 & 0 & 0 & 0 & 0 & 0 \\ 2 & 1 & 0 & 0 & 0 & 0 \\ 3 & 2 & 1 & 0 & 0 & 0 \\ 4 & 3 & 2 & 1 & 0 & 0 \\ 5 & 4 & 3 & 2 & 1 & 0 \end{pmatrix} \times \begin{pmatrix} 1 \\ 1 \\ 1 \\ 1 \\ 1 \\ 1 \end{pmatrix} \tag{17}$$

The answer is $y_r = [0\ 1\ 3\ 6\ 10\ 15]^T$, which is the rectangular rule integration of $y=x$. The analytical answer is $\boldsymbol{y_a} = [0\ 1\ 4\ 9\ 16\ 25]^T$. In order to improve the convolution accuracy, we weight $\boldsymbol{v}$ with the Composite Trapezoid Rule, therefore $\boldsymbol{v} = [1\ 2\ 2\ 2\ 2\ 1]^T$. After a matrix multiplication as in Equation (15), the new solution is $\boldsymbol{y_t} = [0\ 1\ 4\ 9\ 16\ 25]^T$, which for this case happens to be the exact answer. This method allows the easy application of any integration rule by using a vector of weightings characteristic to the integration rule desired. The only requirement for this method to work correctly is that the square matrix must be lower triangular and the diagonal must be zero. This is not a problem with TSS since the diagonal of the Impulse Response Function (IRF) matrix is always zero at $t = 0$. The following is a list of integration rules with their respective characteristic weighting vector.

1. Trapezoid Rule – Error $\boldsymbol{Oh^3}$

$$\int_a^b f(x)dx = \frac{h}{2}[f(x_0) + 2f(x_1) + f(x_3)] \tag{18}$$

$$v = \frac{1}{2}\begin{pmatrix} 1 & 2 & 2 & \dots & 2 & 2 & 1 \end{pmatrix}^T \tag{19}$$

2. Simpson's Rule – Error Oh^5

$$\int_a^b f(x)dx = \frac{h}{3}[f(x_0) + 4f(x_1) + 2f(x_2) + 4f(x_3) + f(x_4)] \tag{20}$$

$$v = \frac{1}{3}\begin{pmatrix}1 & 4 & 2 & 4 & 2 & \dots & 2 & 4 & 2 & 4 & 1\end{pmatrix}^T \tag{21}$$

3. Weddle's Rule – Error Oh^9

$$\int_a^b f(x)dx = \frac{h}{140}[41f(x_0) + 216f(x_1) + 27f(x_2) + 272f(x_3) + 27f(x_4) + 216f(x_5) + 41f(x_6)] \tag{22}$$

$$v = \frac{1}{140}\begin{pmatrix}41 & 216 & 27 & 272 & 27 & 216 & \dots & 216 & 27 & 272 & 27 & 216 & 41\end{pmatrix}^T \tag{23}$$

When using these integration weightings with TSS, the length of $\boldsymbol{v}$ must be the same length as the vector of isolator synthesized forces. The following example will demonstrate how RBB works and how to incorporate the vector of integration weightings. Figure 22 presents a process in its fourth iteration with the following conditions:

- This data was divided into four equally-sized blocks and manipulated as in Equation (17).
- The initial guess was $\boldsymbol{f} = [1\ 1\ 1\ 1\ 1\ 1\ 1\ 1\ 1\ 1]^T$.
- First three blocks have converged and $\boldsymbol{f}$ was updated.

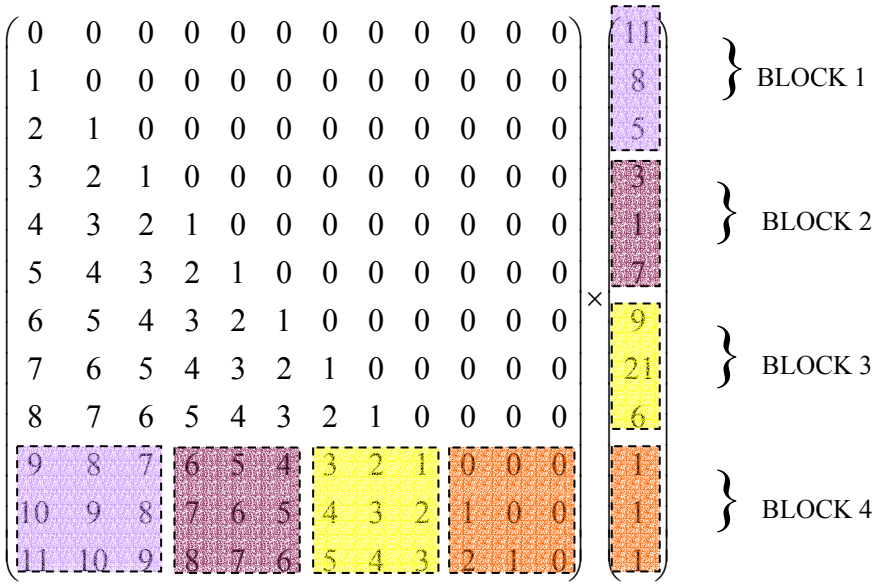

Figure 22. Example of a Recursive Block-by-Block Process

Each successive block will solve faster since it relies on the synthesized answers from prior blocks. Before the fourth block can be synthesized, the following pre-process must take place.

$$\begin{pmatrix} 9 & 8 & 7 \\ 10 & 9 & 8 \\ 11 & 10 & 9 \end{pmatrix} \times \begin{pmatrix} 11 \\ 8 \\ 5 \end{pmatrix} \rightarrow update\ x(10:12)$$

$$\begin{pmatrix} 6 & 5 & 4 \\ 7 & 6 & 5 \\ 8 & 7 & 6 \end{pmatrix} \times \begin{pmatrix} 3 \\ 1 \\ 7 \end{pmatrix} \rightarrow update\ x(10:12) \qquad (24)$$

$$\begin{pmatrix} 3 & 2 & 1 \\ 4 & 3 & 2 \\ 5 & 4 & 3 \end{pmatrix} \times \begin{pmatrix} 9 \\ 21 \\ 6 \end{pmatrix} \rightarrow update\ x(10:12)$$

The fourth ***f*** block and the updated fourth ***x*** block are then processed by the TSS algorithm. To improve the accuracy of RBB, apply the blocked vector of integration weightings, ***IW***, as shown in Figure 23 – pad with zeros to match the length of ***f***.

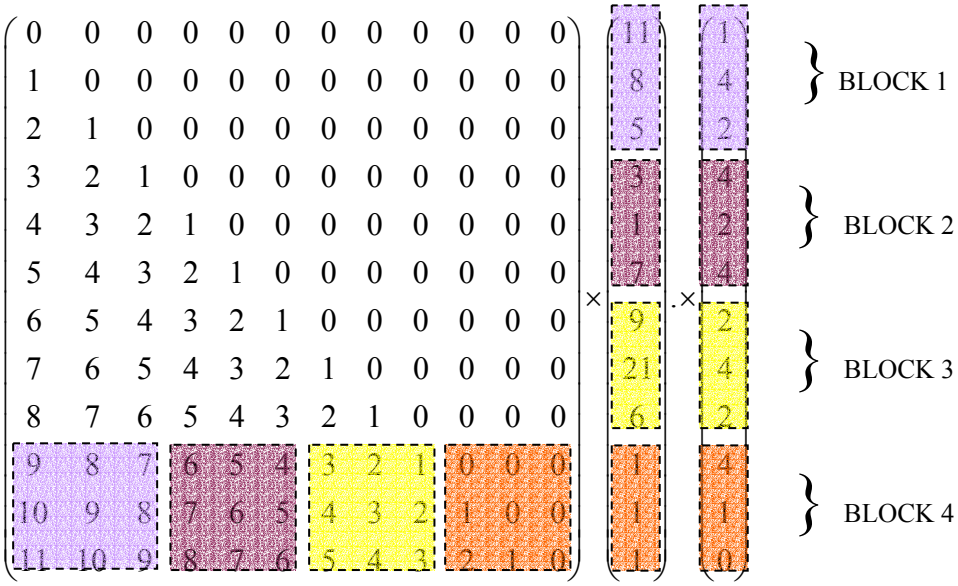

Figure 23. Example of a Recursive Block-by-Block Process with Simpson's Rule

The vector of integration weightings is element-wise multiplied with the vector of forces. Note that the padded zero has no effect on the answer since the matrix diagonal is already zero. Figure 24 shows the accuracy improvements for a 2-DOF spring-mass-damper system solved with TSS / RBB (8 blocks) and Simpson's Rule integration. The results were compared to a Working Model 2-D simulation with the same parameters.

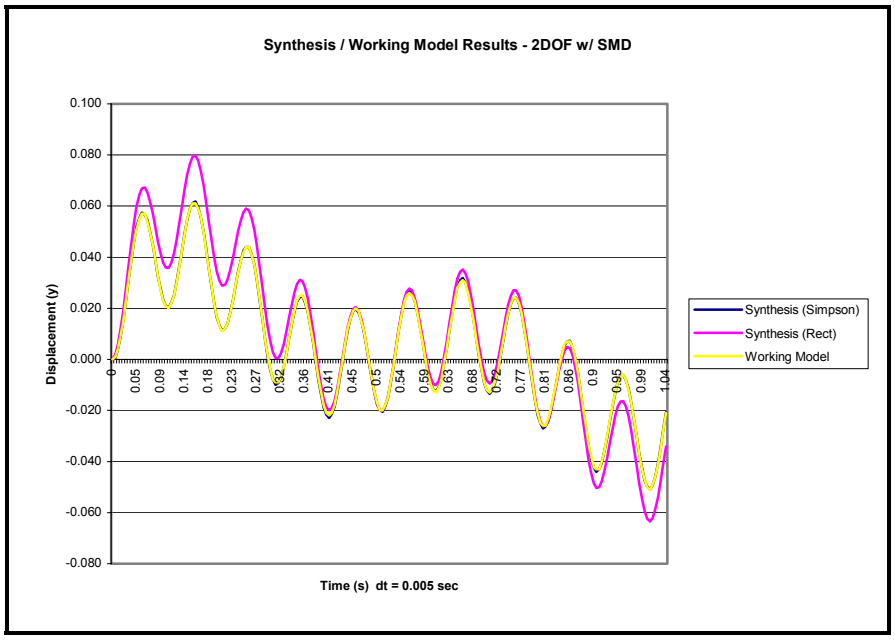

Figure 24. Accuracy Improvement for a 2-DOF SMD System

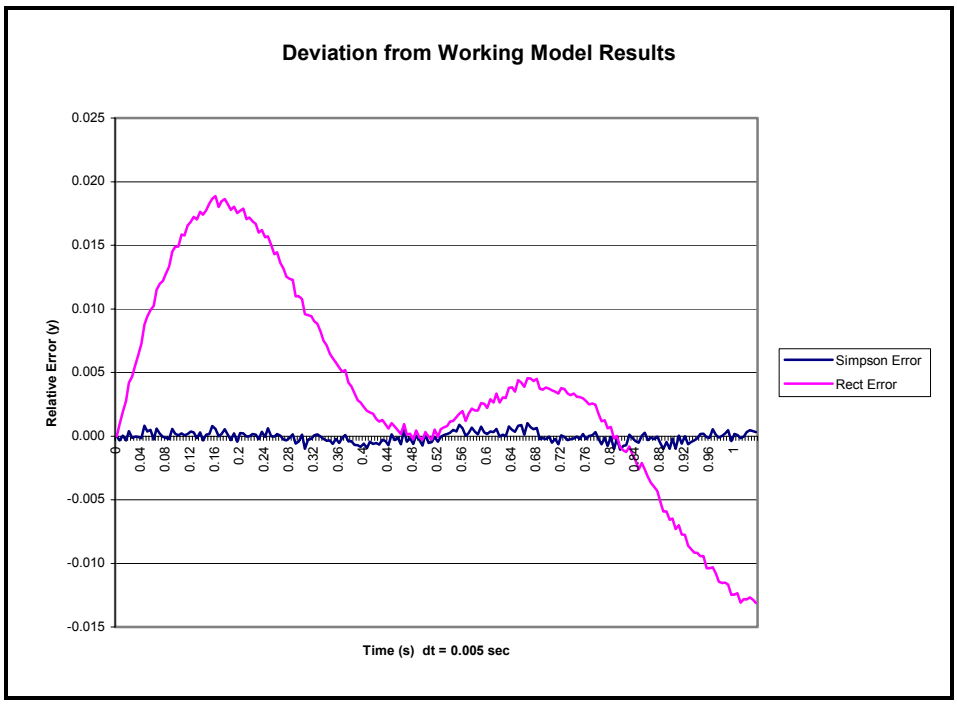

Figure 25. Differential Integration Error for 2-DOF SMD System

D. PROGRAM OPTIMIZATION FOR SPEED

The MATLAB programs presented here were thoroughly investigated, modified, and/or re-written to remove process redundancies and improve program flow and inter-compatibility. Heavy use was made of MATLAB's vectorization and convolution capabilities, which are optimized for speed and commonly used for signal processing. The Wen and Maxwell isolator models employ a Runge-Kutta 4th order method to solve the governing differential equations (GDE). The GDEs could have been solved faster with MATLAB's ODE 45 solver, but it was decided that the present method, which uses FOR: NEXT loops, would suffice. The compiled version of this program, like other programs, will execute faster than in its native programming environment.

THIS PAGE INTENTIONALLY LEFT BLANK

E. OASIS (GUI)

Optimization and Analysis of Structural Isolation Systems (OASIS) is the DSS tool developed to bring together and automate the optimization and analysis process. The following figures show screen shots of the GUI modules.

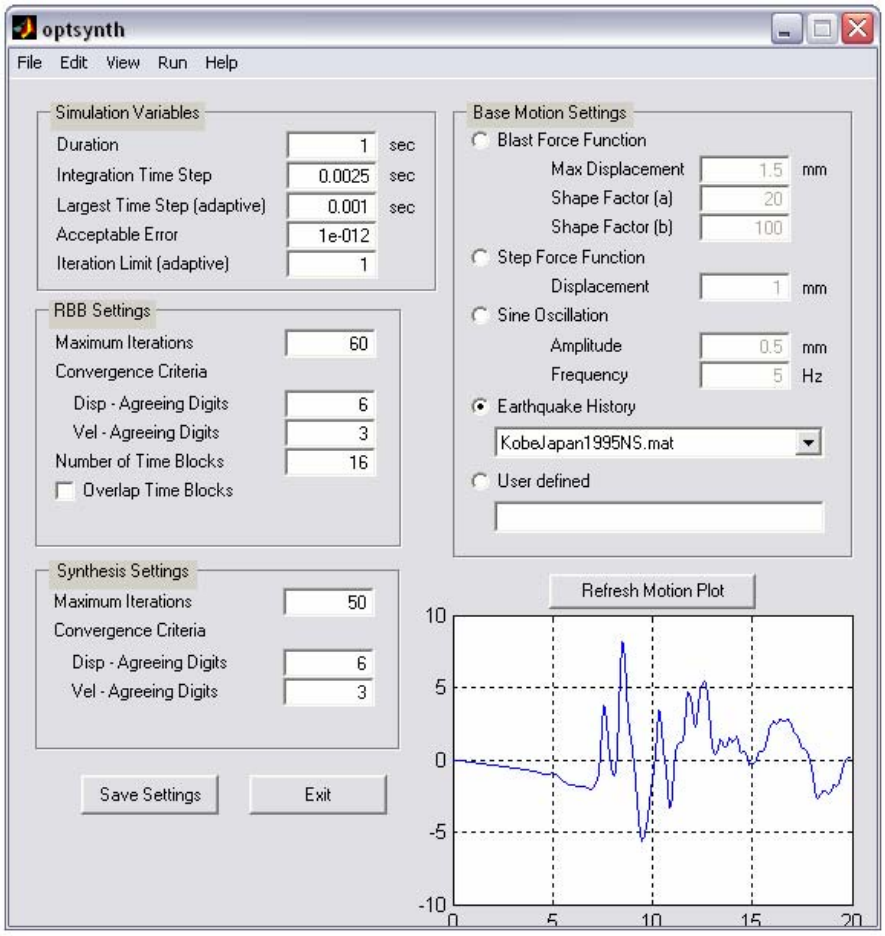

Figure 26. Main GUI Module

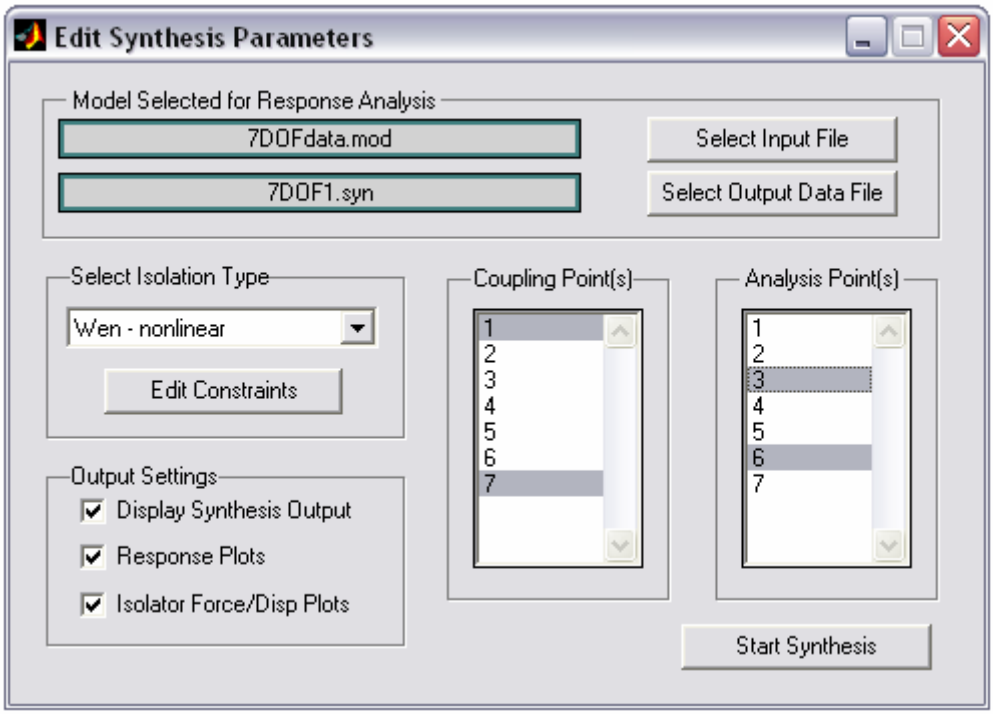

Figure 27. Transient Structural Synthesis Module

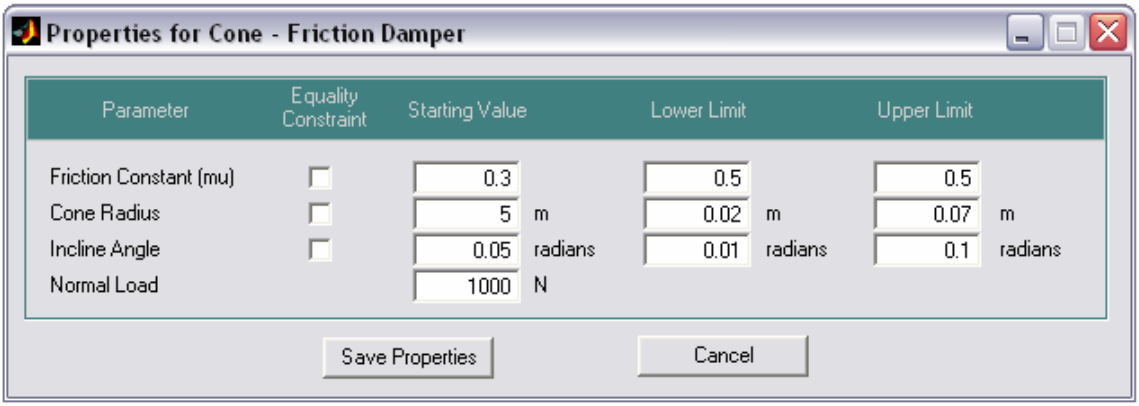

Figure 28. Isolator Options and Constraints

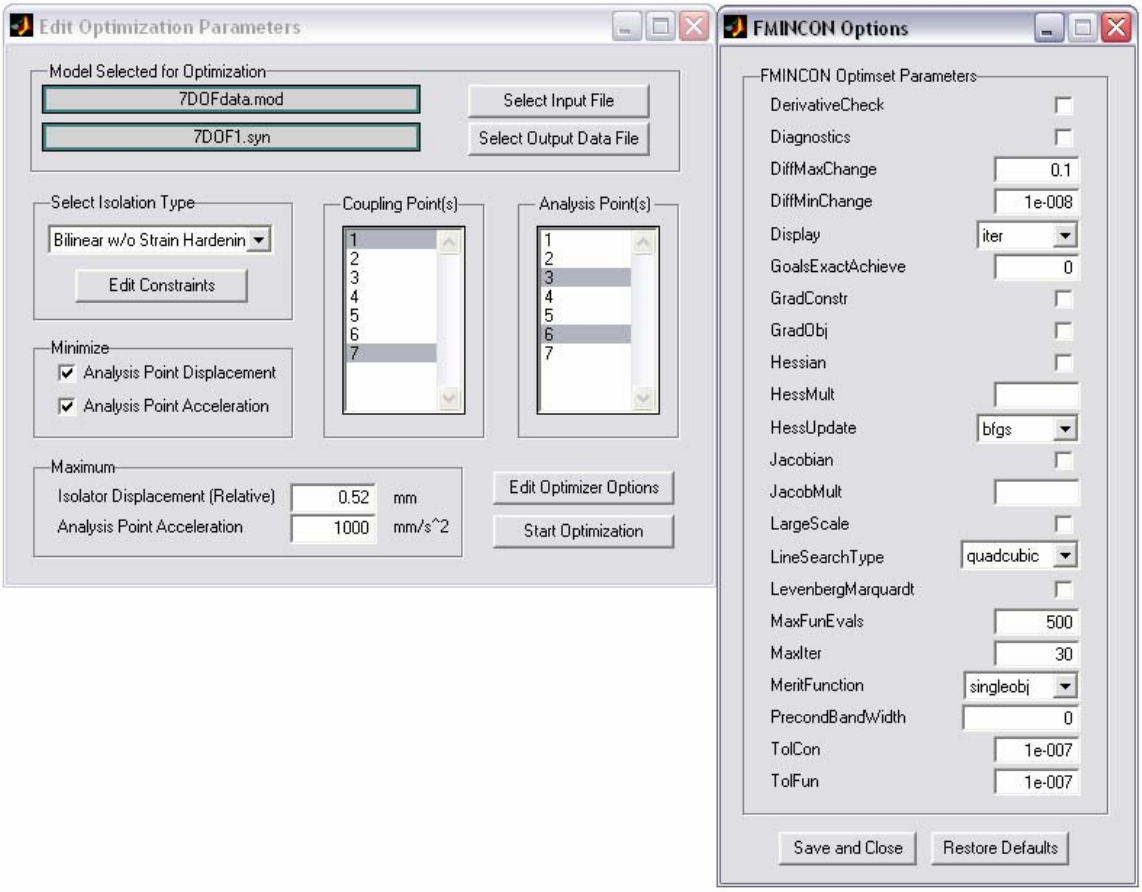

Figure 29. Optimization Module with Advanced FMINCON Options

THIS PAGE INTENTIONALLY LEFT BLANK

IV. PROGRAM VERIFICATION

A. WORKING MODEL 2-D

Working Model 2-D is a conceptual design tool that allows users to create and analyze real-life mechanical systems. It was extensively used to verify the accuracy of the results generated with OASIS. Presented in the following tables and figures are the validation results for 2-DOF and 7-DOF models with parallel spring-dampers respectively. Cset is a vector with the index value of the coupling node(s). For example, the following 2DOF system is coupled at m_1 (node #1), therefore Cset = [1].

1. 2DOF System

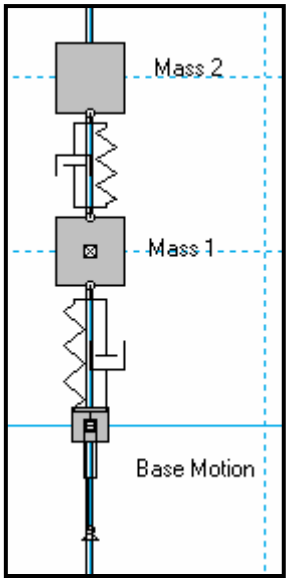

Problem: Determine the response of m_2.
Model: m_1 = 1 slug
m_2 = .5 slug
k = 50 lbf / ft
c =0 lbf-s / ft
Isolator: Spring – Damper in parallel
k = 10 lbf / ft
c = 0.5 lbf-s / ft
Cset: [1]
Base Motion: Sinusoidal
A = 0.0833 in
f = 10 Hz
Duration: 2 sec.

Results: Baseline results from WM2D.
Max Disp: 0.0037 ft

Statistics: Synthesis deviation from WM2D.
Average: 9.6100×10^{-6}
Standard Deviation: 2.7574×10^{-5}
Maximum Error: 6.3873×10^{-5}

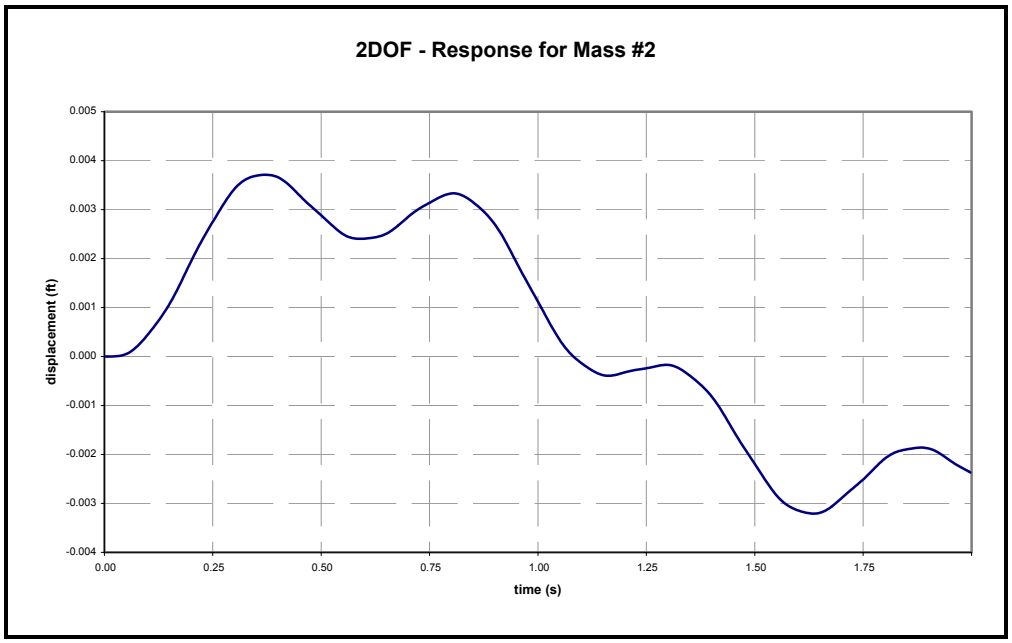

Figure 30. 2DOF Validation Model – Response for Mass #2

2. 7DOF System

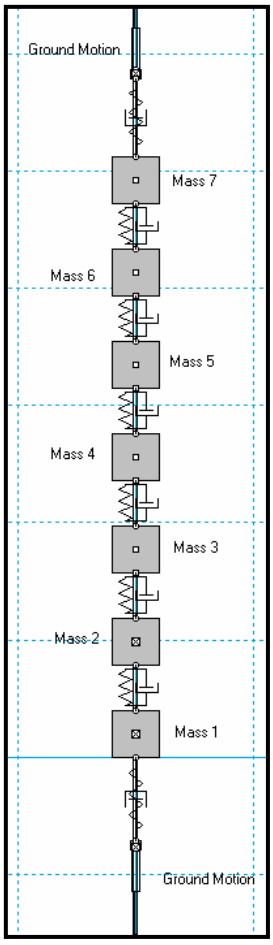

Problem: Determine the response of m_2.
Model: $m_1 = 3.5$ slug
$m_2 = 3$ slug
$m_3 = 2.5$ slug
$m_4 = 2$ slug
$m_5 = 1.5$ slug
$m_6 = 1$ slug
$m_7 = 0.5$ slug
$k_1 = k_2 = k_3 = k_4 = k_5 = k_6 = 50$ lbf / ft
$c_1 = c_2 = c_3 = c_4 = c_5 = c_6 = 0$ lbf-s / ft

Isolator: Spring – Damper in parallel:
k = 200 lbf / ft
c = 2.5 lbf-s / ft

Cset: [1 7]

Base Motion: Sinusoidal
A = 0.08333 ft
f = 10 Hz
Duration: 2 sec

Results: Baseline results from WM2D.
Max Disp: 0.0054 ft

Statistics: Synthesis deviation from WM2D.
Average: 8.9500×10^{-5}
Standard Deviation: 3.6670×10^{-4}
Maximum Error: 9.6700×10^{-4}

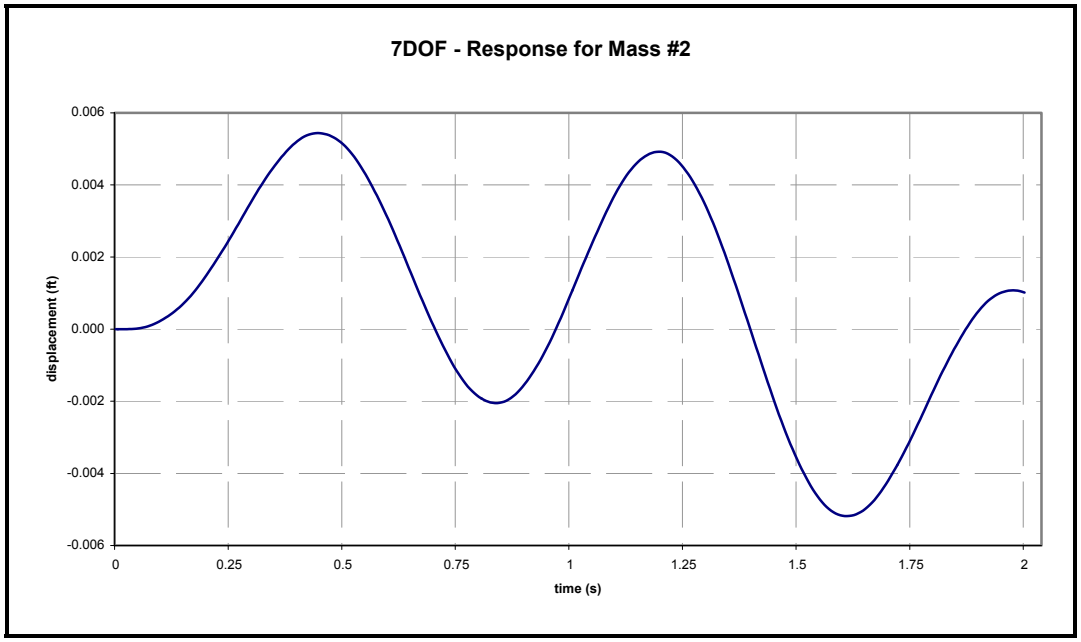

Figure 31. 7DOF Validation Model – Response for Mass #2

B. SINGLE BAY – FOUR STORY BUILDING FRAME

Presented here is a validation of a four story building isolated with Maxwell elements. The force vs. displacement plot of the Maxwell isolator, [Ref. 8, Page 59], is presented correctly, but was most likely processed in one block since no force discontinuities are present. The following validation was preformed to reproduce the results from [Ref. 8] with the RBB algorithm.

1. Four Story Building Frame

Problem: Determine a corner lateral displacement
Model: bldg4storyfree_hor.mat
Isolator: Maxwell Isolator
k = 300 lbf / in
c = 51 lbf-s / in
Cset: [1 2 3 4]
Base Motion: ElCentro1940NS.mat
Duration: 50 sec.

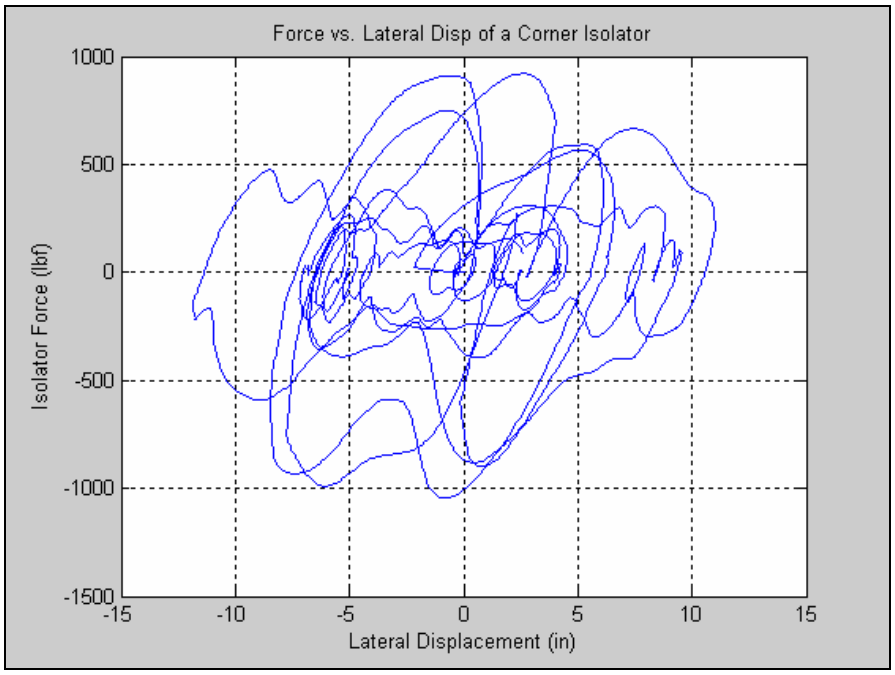

Figure 32. Lateral Hysteresis of Corner Node , 16 blocks

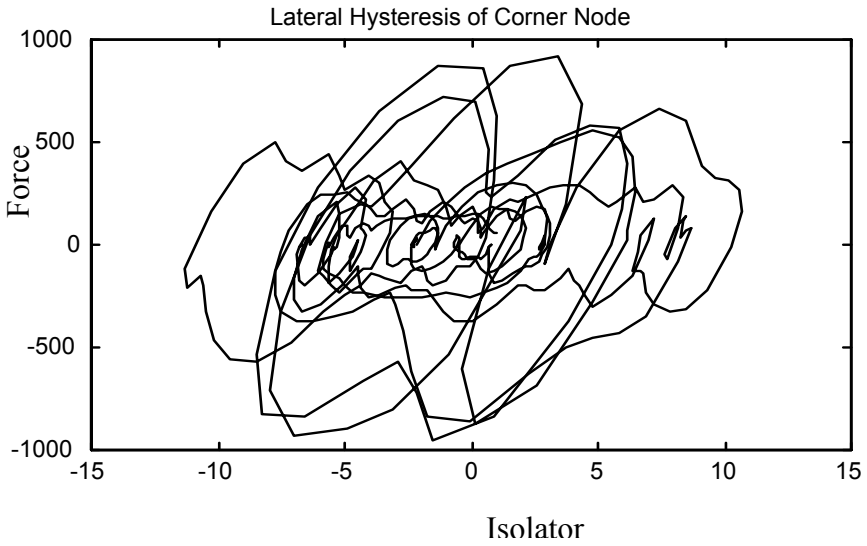

Figure 33. Hysteresis of Corner Node (From Ref. 8)

V. SAMPLE OPTIMIZATION PROBLEMS

A. SINGLE BAY FOUR-STORY BULDING

The four-story building used for [Ref. 8] is revisited here with a variety of isolators. This structure is assembled with 50 ksi steel structural members with the following specifications:

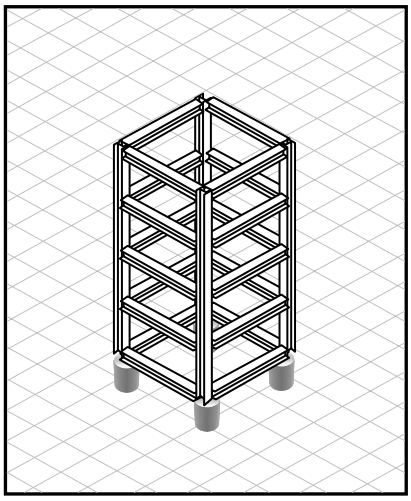

- Columns: W36x486
- First floor beams: W36x170
- Second floor beams: W36x170
- Third floor beams: W36x160
- Fourth floor beams: W36x150
- Roof beams: W36x135

The following objective functions use the absolute values of the design variables to ensure the minimum values are not interpreted as large negative values.

1. Parallel Spring and Damper

Base Motion	Sine, 1in, 10 Hz, 7 sec
Coupling Nodes (cset)	[1 2 3 4]
Analysis Node (rset)	[20] – 5th floor node
Starting Isolator Values	k = 15 lb/in ; c = 0.5 lb-s/in
Objective	Minimize 5th floor lateral displacement (node 15)
Optimal Isolator Values	k = 15 lb/in ; c = 0.05 lb-s/in
Max Displacement	Max 5th floor lateral disp = 0.0032 in
Process Time	00:09:42

Table 3. Optimization Results for 4-Story Building with Parallel Spring – Damper Isolators

Objective Function:

MIN:	x_{20}		(5^{th} floor lateral displacement)
Subject to:	k - 30	≤ 0	(Isolator constraints)
	-k + 10	≤ 0	
	c – 0.7	≤ 0	
	-c + 0.01	≤ 0	
	$-x_{20}$	≤ 0	(Nonnegativity)

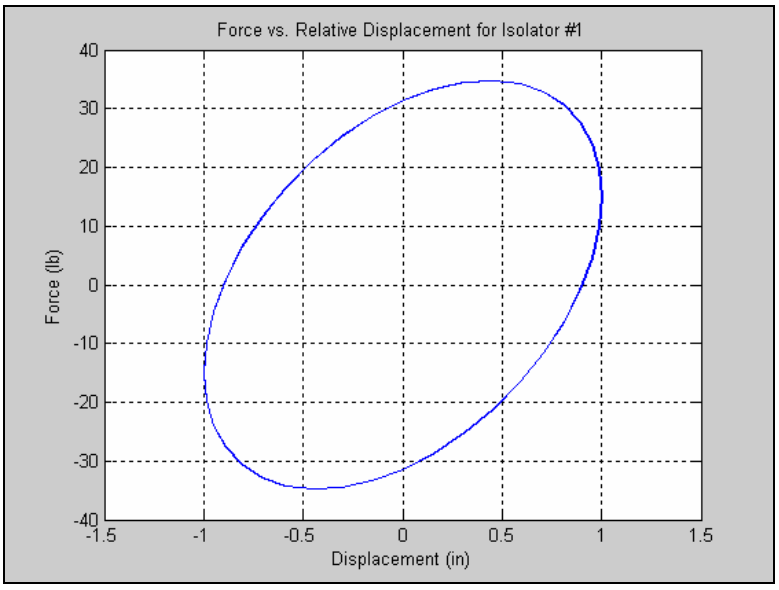

Figure 34. Parallel Spring – Damper: Force vs. Displacement – Starting Values

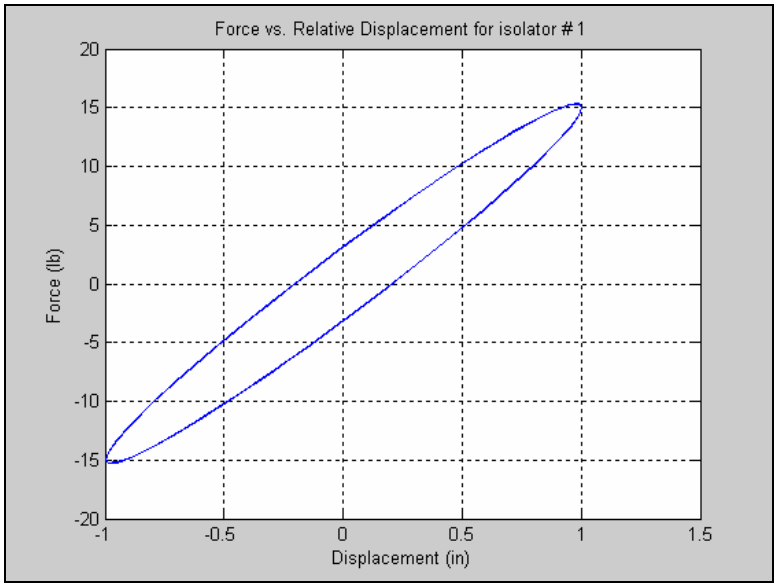

Figure 35. Parallel Spring – Damper: Force vs. Displacement – Optimal Values

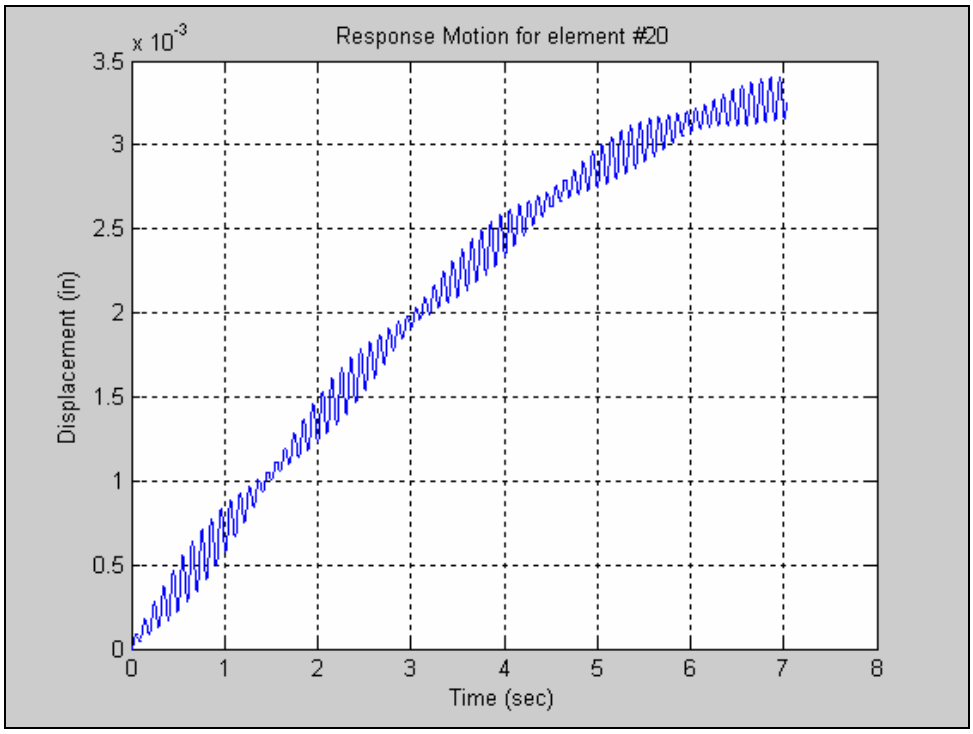

Figure 36. Parallel Spring – Damper: Displacement of node #20– Before Optimization

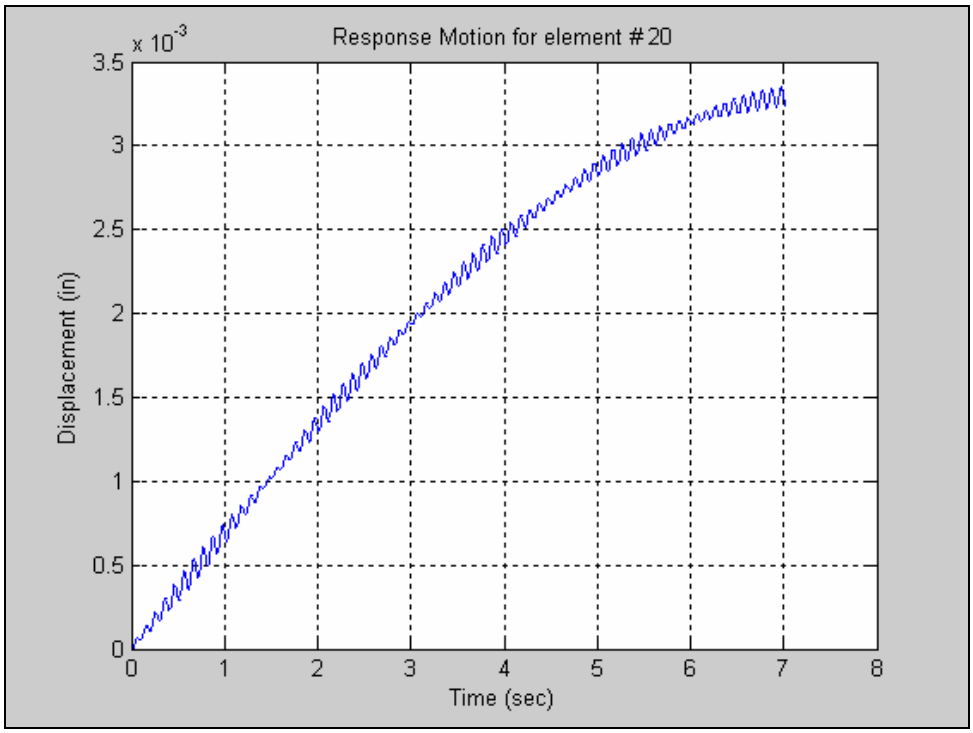

Figure 37. Parallel Spring – Damper: Displacement of node #20– After Optimization

2. Flat Slider with Restoring Spring

Base Motion	Sine, 1in, 10 Hz, 7 sec
Coupling Nodes (cset)	[1 2 3 4]
Analysis Node (rset)	[20] – 5th floor node
Starting Isolator Values	k = 10 lb/in ; μ = 0.5 ; N = 2183 lb
Objective	Minimize 5th floor lateral acceleration
Optimal Isolator Values	k = 23.3 lb/in ; μ = 0.1
Max Displacement	Max 5th floor lateral accel = 13.0446 in/sec^2
Process Time	00:03:50

Table 4. Optimization Results for 4-Story Building with Flat-Slider Restoring Spring Isolators

Objective Function:

MIN:	$\ddot{x}_{20}$		(5th floor lateral acceleration)
Subject to:	k - 30	≤ 0	(Isolator constraints)
	-k + 5	≤ 0	
	μ – 0.7	≤ 0	
	-μ + 0.1	≤ 0	
	- $\ddot{x}_{20}$	≤ 0	(Nonnegativity)

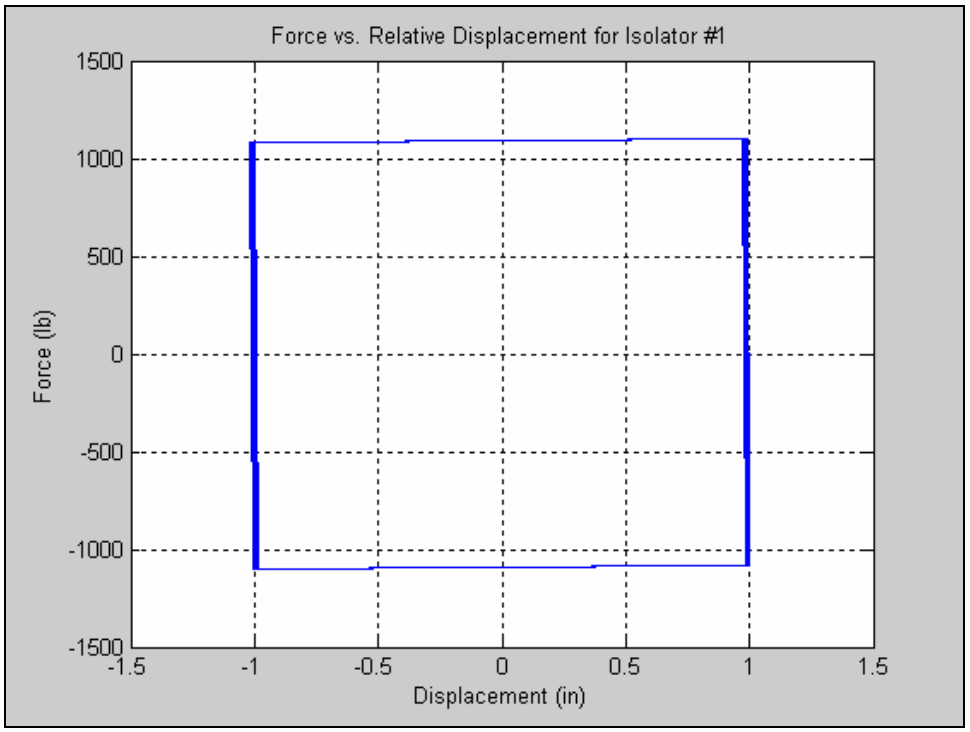

Figure 38. Flat Slider with Restoring Spring: – Before Optimization

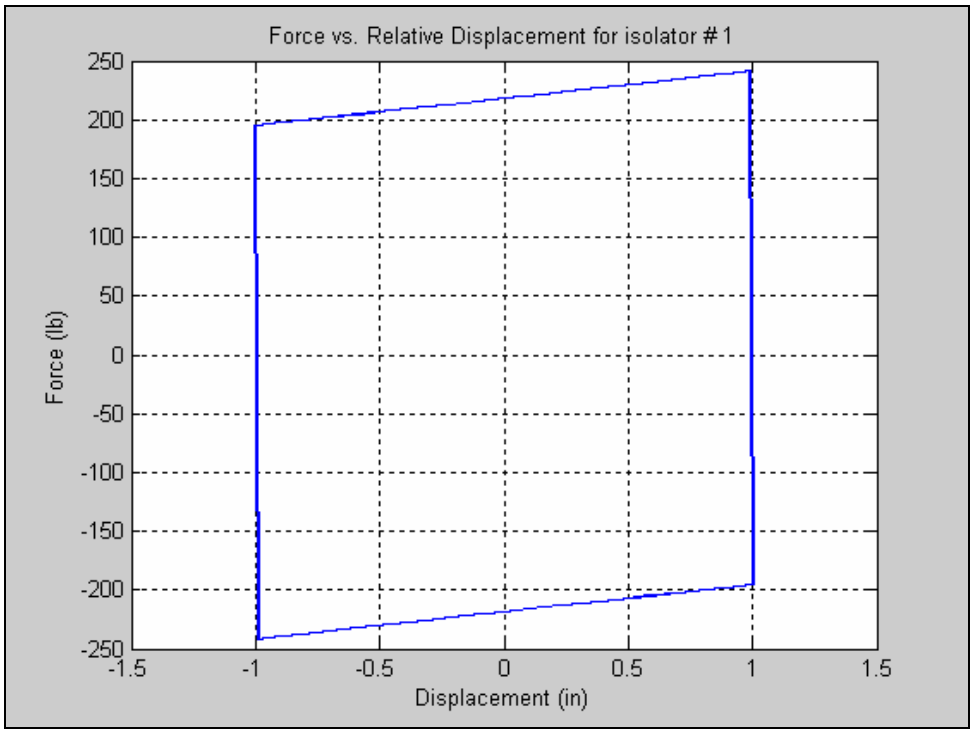

Figure 39. Flat Slider with Restoring Spring: – After Optimization

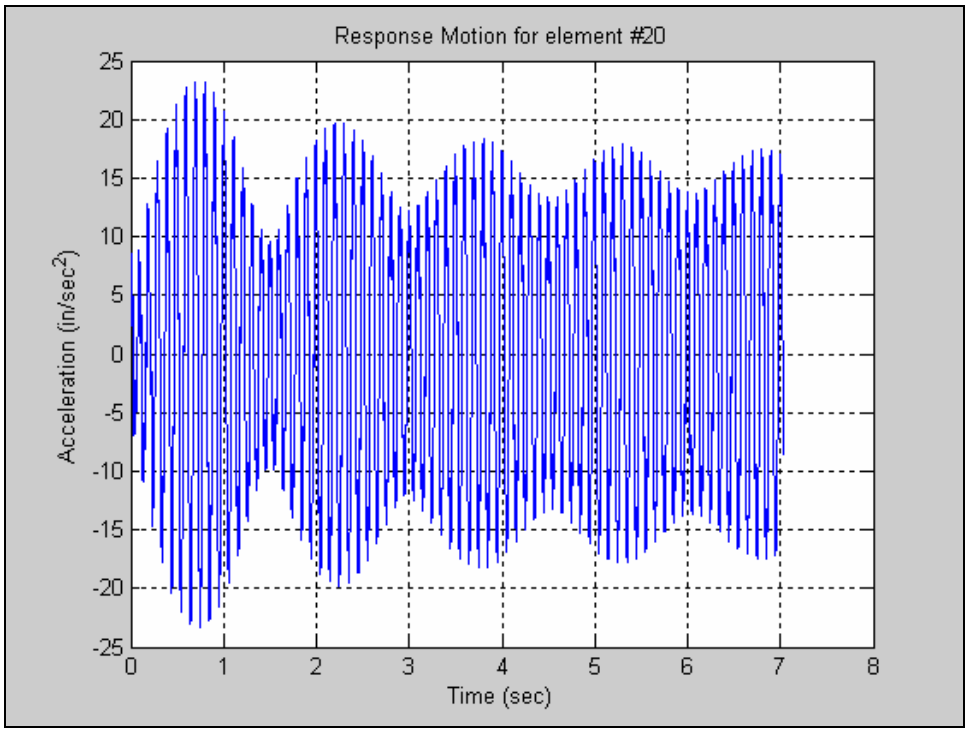

Figure 40. Flat Slider with Restoring Spring: Lateral Acceleration of node #20 – Before Optimization

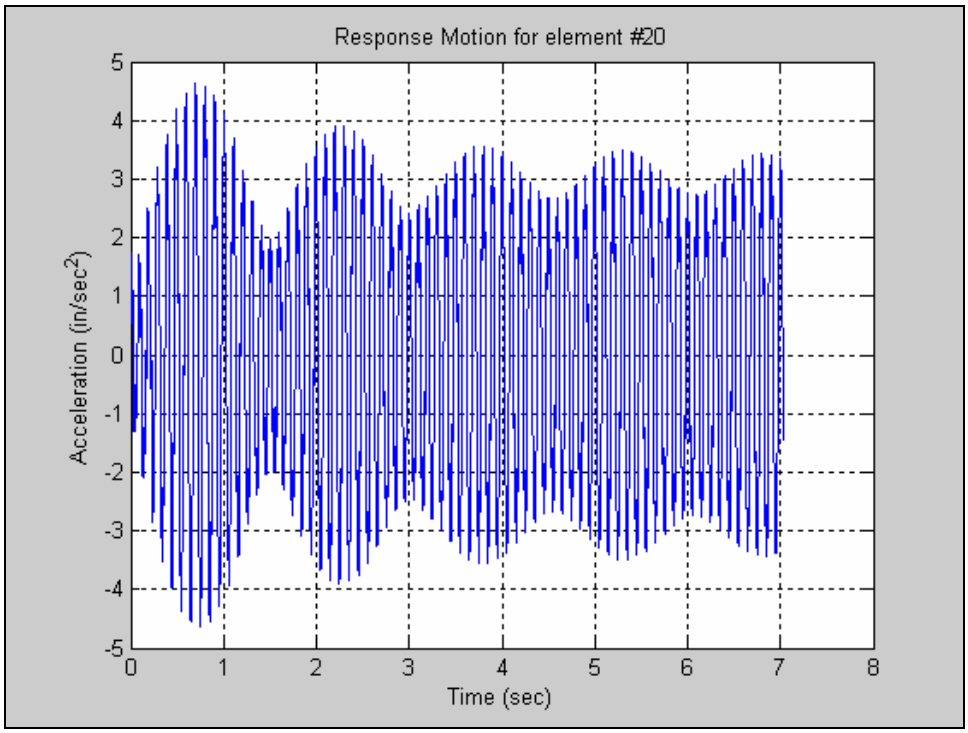

Figure 41. Flat Slider with Restoring Spring: Lateral Displacement of node #20 – After Optimization

3. Spherical Slider

Base Motion	Sine, 1in, 10 Hz, 7 sec
Coupling Nodes (cset)	[1 2 3 4]
Analysis Node (rset)	[20] – 5th floor node
Starting Isolator Values	$\mu = 0.5$; r = 60 in; N = 2183 lb
Objective	Minimize 5th floor lateral displacement
Optimal Isolator Values	$\mu = 0.1$; r = 120 in
Max Displacement	Max 5th floor lateral disp = 0.0021 in
Process Time	00:04:06

Table 5. Optimization Results for 4-Story Building with Spherical-Slider Isolators

Objective Function:

MIN:	x_{20}		(5th floor lateral displacement)
Subject to:	$\mu - 30$	≤ 0	(Isolator constraints)
	$-\mu + 5$	≤ 0	
	$r - 0.7$	≤ 0	
	$-r + 0.1$	≤ 0	
	$-x_{20}$	≤ 0	(Nonnegativity)

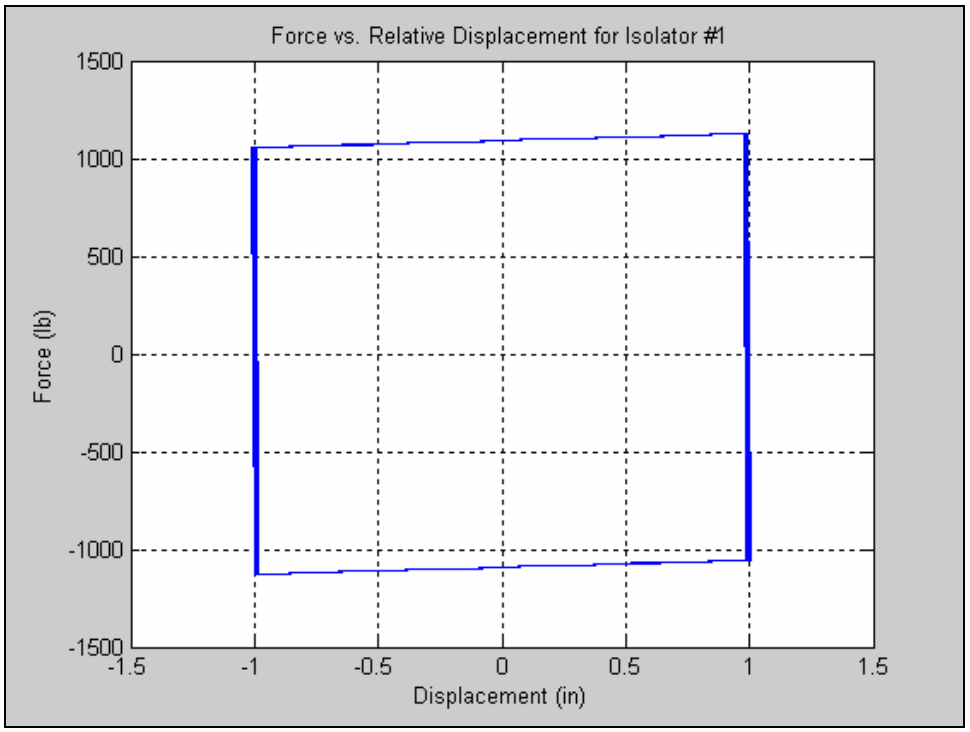

Figure 42. Spherical Slider: Force vs. Displacement – Before Optimization

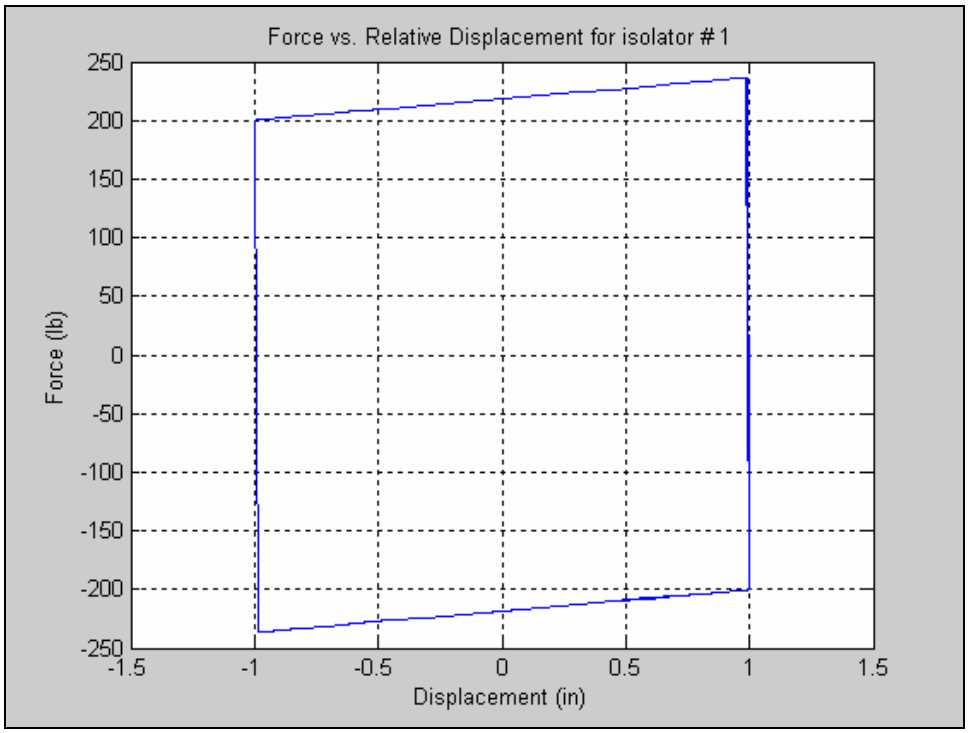

Figure 43. Spherical Slider: Force vs. Displacement – After Optimization

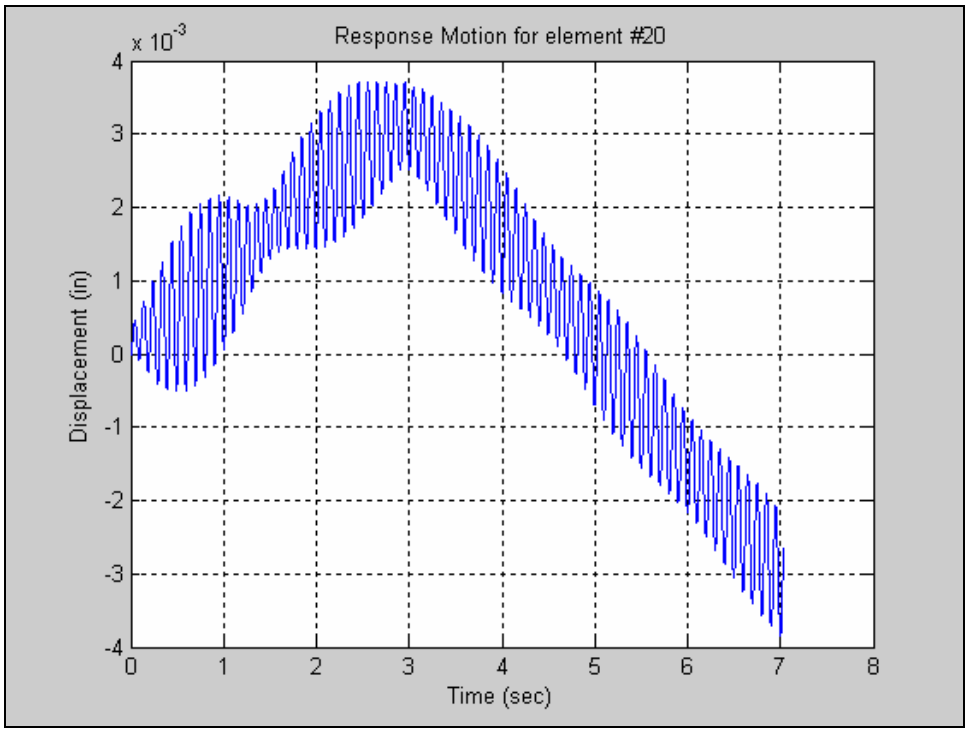

Figure 44. Spherical Slider: Lateral Displacement of node #20– Before Optimization

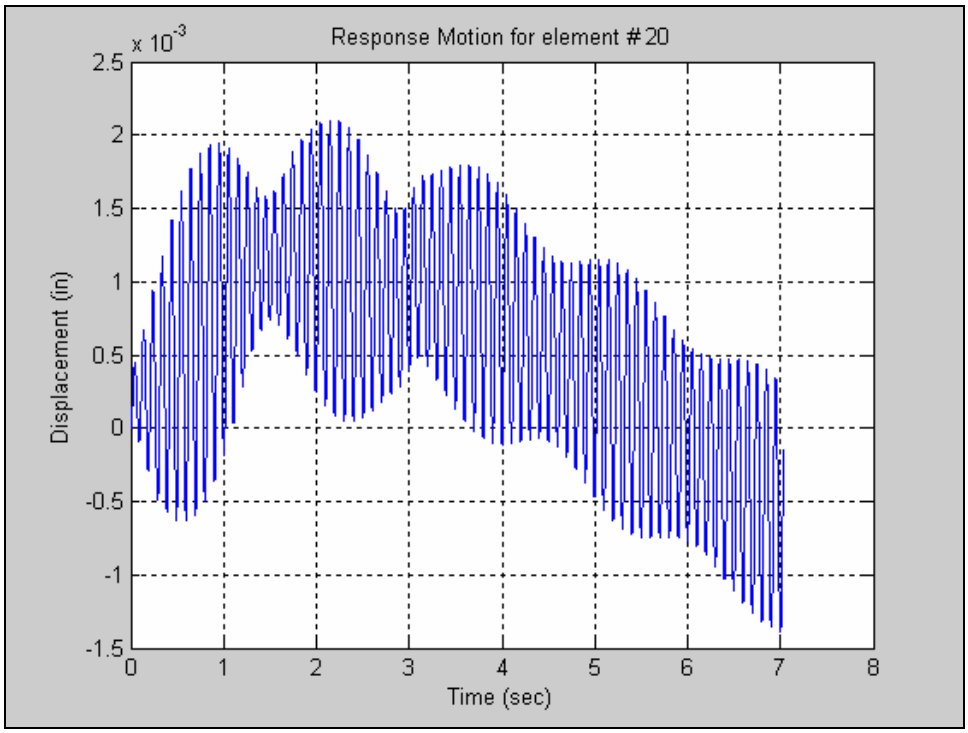

Figure 45. Spherical Slider: Lateral Displacement of node #20– After Optimization

4. Bilinear – No Strain Hardening

Base Motion	Sine, 1in, 10 Hz, 10 sec
Coupling Nodes (cset)	[1 2 3 4]
Analysis Node (rset)	[20]– 5^h floor node
Starting Isolator Values	k_1= 4937 lb/in; yp = 0.4; F_{yt} = 1997 lb F_{yc} = -1993 lb
Objective	Minimize 5^h floor lateral displacement Maximum relative isolator displacement = 2 in
Optimal Isolator Values	k_1= 4933 lb/in; yp = 0.25; F_{yt} = 2100 lb F_{yc} = -1900 lb
Max Displacement	Max 5^h floor lateral disp = 0.041 in
Process Time	00:07:12
Bearing Data	High-Damping Natural Rubber Dia: 19.68 in Length: 19.68 in Shear Mod: 79.77 Psi Stiffness: 4933.21 lb / in

Table 6. Optimization Results for 4-Story Building with Bilinear NSH Isolators

Objective Function:

MIN:	x_{20}		(5^{th} floor lateral displacement)
Subject to:	k_1 -5200	≤ 0	(Isolator constraints)
	$-k_1 + 4800$	≤ 0	
	yp – 0.5	≤ 0	
	-yp + 0.1	≤ 0	
	$F_{yt} – 2200$	≤ 0	
	$-F_{yt} + 1800$	≤ 0	
	$F_{yc} – 2200$	≤ 0	
	$-F_{yc} + 1800$	≤ 0	
	$-x_{20}$	≤ 0	(Nonnegativity)

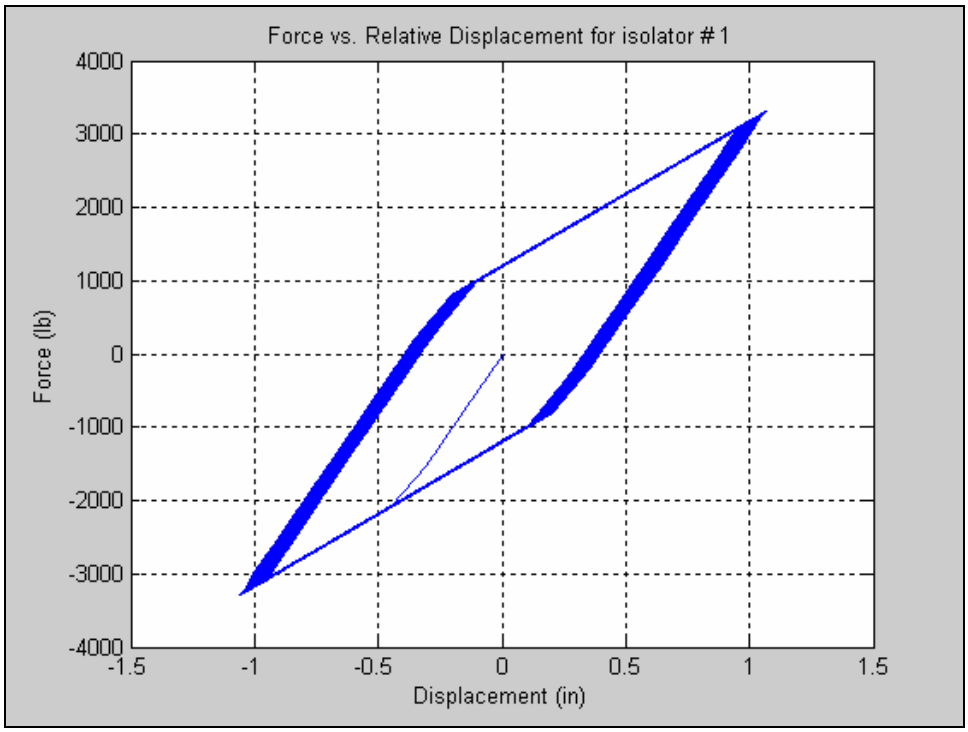

Figure 46. Bilinear NSH: Hysteresis Plot – Before Optimization

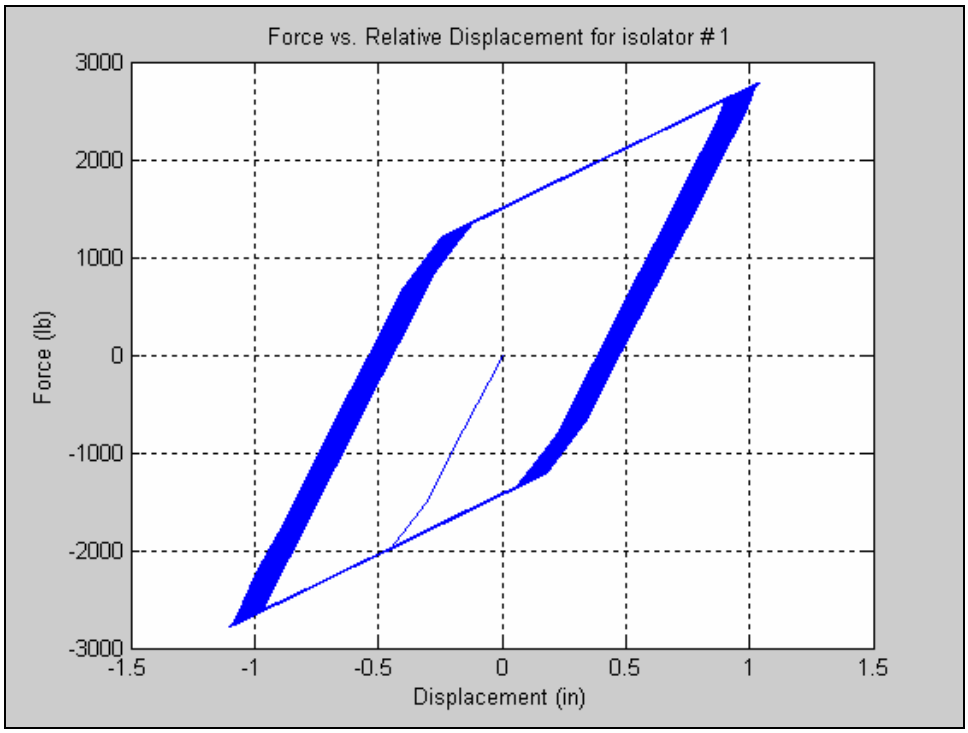

Figure 47. Bilinear NSH: Hysteresis Plot – After Optimization

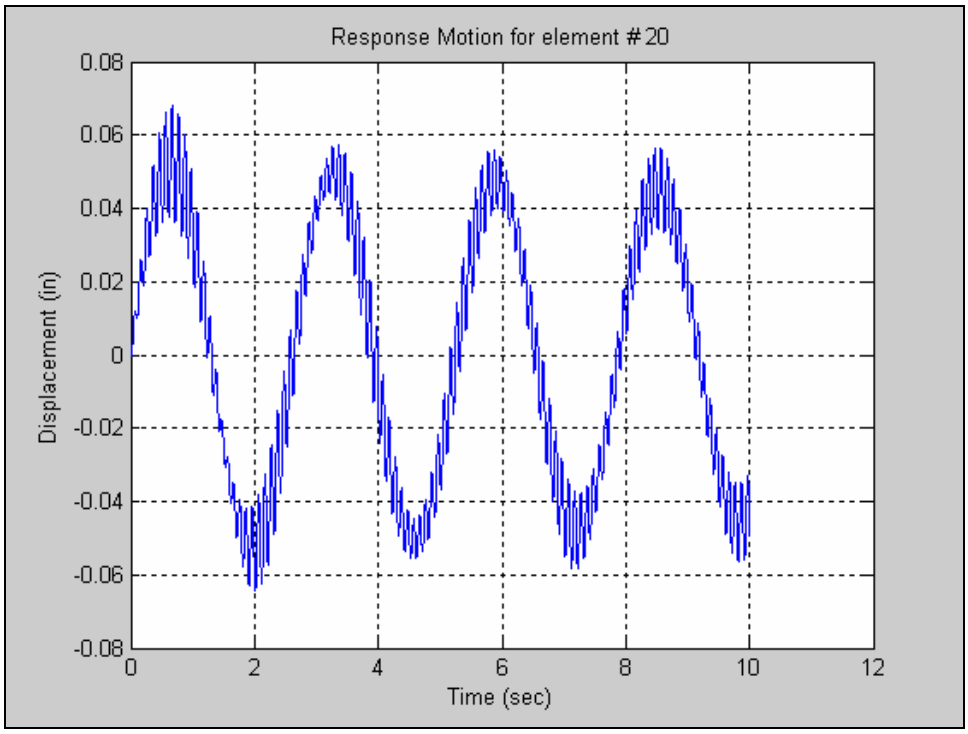

Figure 48. Bilinear NSH: Lateral Displacement of node #20 – Before Optimization

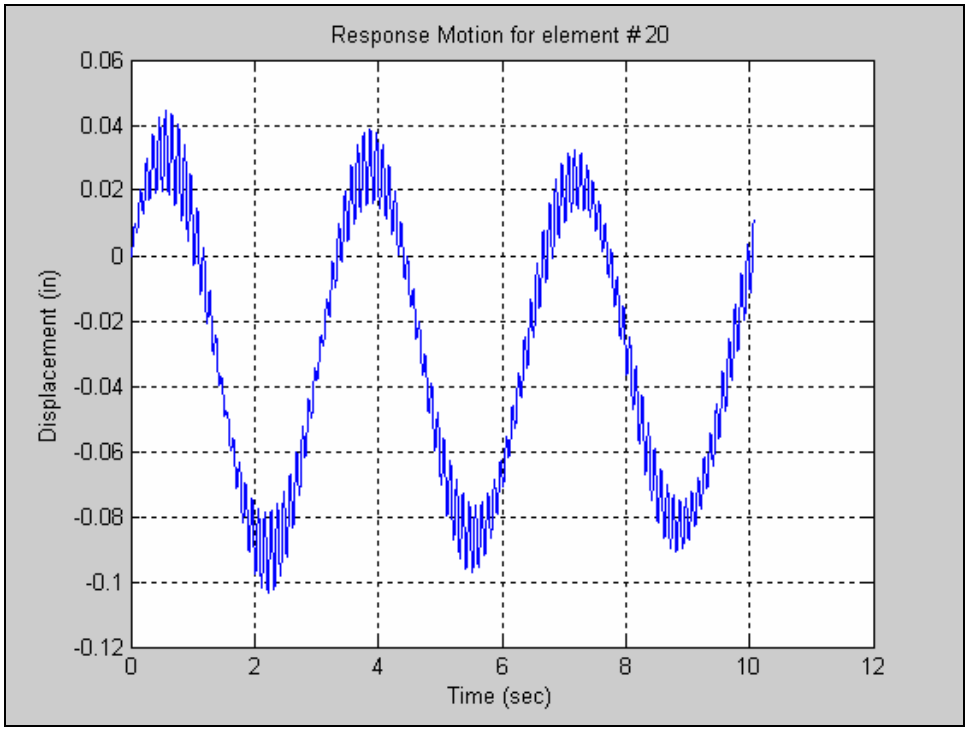

Figure 49. Bilinear NSH: Lateral Displacement of node #20 – After Optimization

5. Maxwell

Base Motion	Sine, 12in, 5 Hz, 10 sec
Coupling Nodes (cset)	[1 2 3 4]
Analysis Node (rset)	[1 2 3 4] – Isolator Node
Starting Isolator Values	k = 3000 lb/in; c = 50 lb-s/in
Objective	Minimize isolator node absolute displacement
Optimal Isolator Values	k = 3000 lb/in; c = 40 lb-s/in
Max Displacement	Max isolator ode absolute disp = 0.08 in
Process Time	00:01:55

Table 7. Optimization Results for 4-Story Building with Maxwell Isolators

Objective Function:

MIN: $x_1 + x_2 + x_3 + x_4$ (Isolator lateral displacements)

Subject to: $k - 3000 = 0$ (Isolator constraints)
$c - 60 \leq 0$
$-c + 40 \leq 0$

$x_1, x_2, x_3, x_4 \geq 0$ (Nonnegativity)

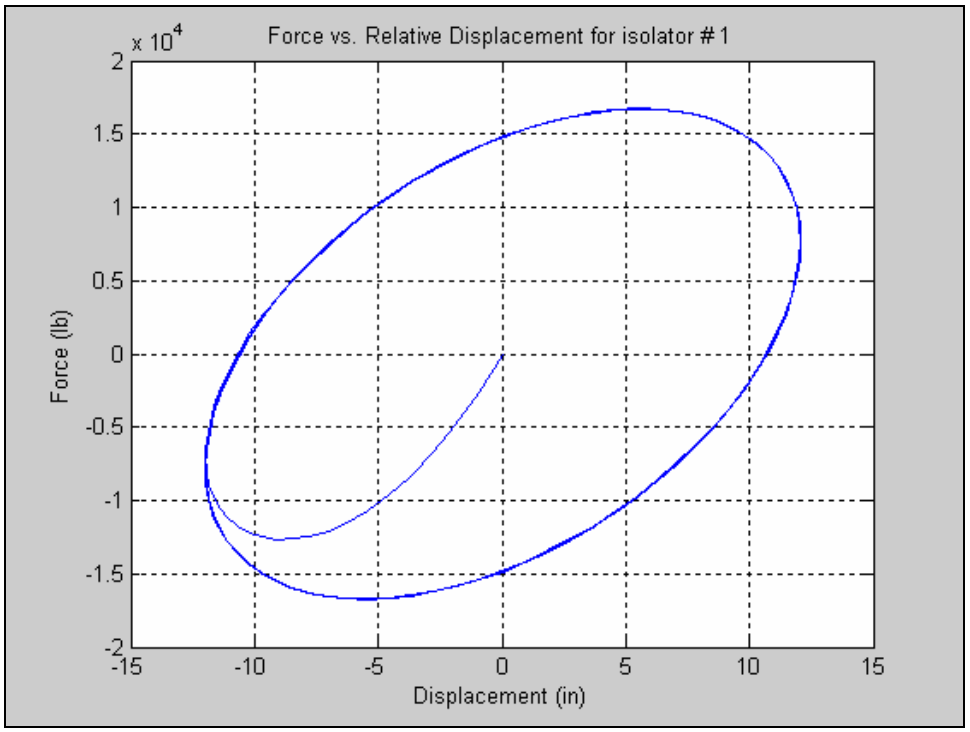

Figure 50. Maxwell: Force vs. Displacement Plot – Before Optimization

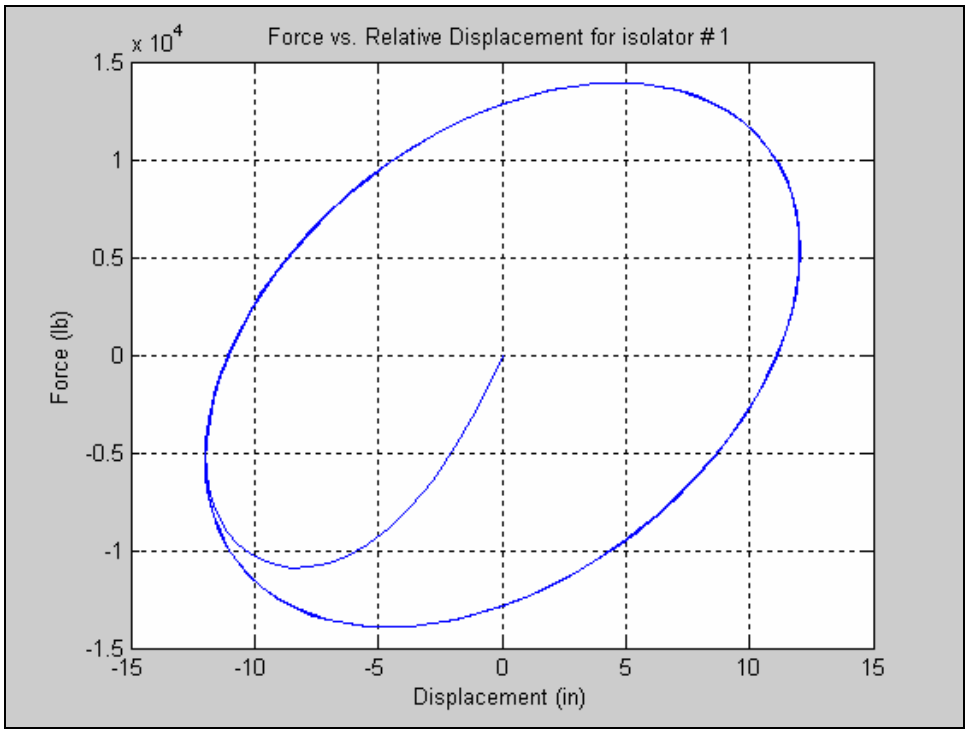

Figure 51. Maxwell: Force vs. Displacement Plot – After Optimization

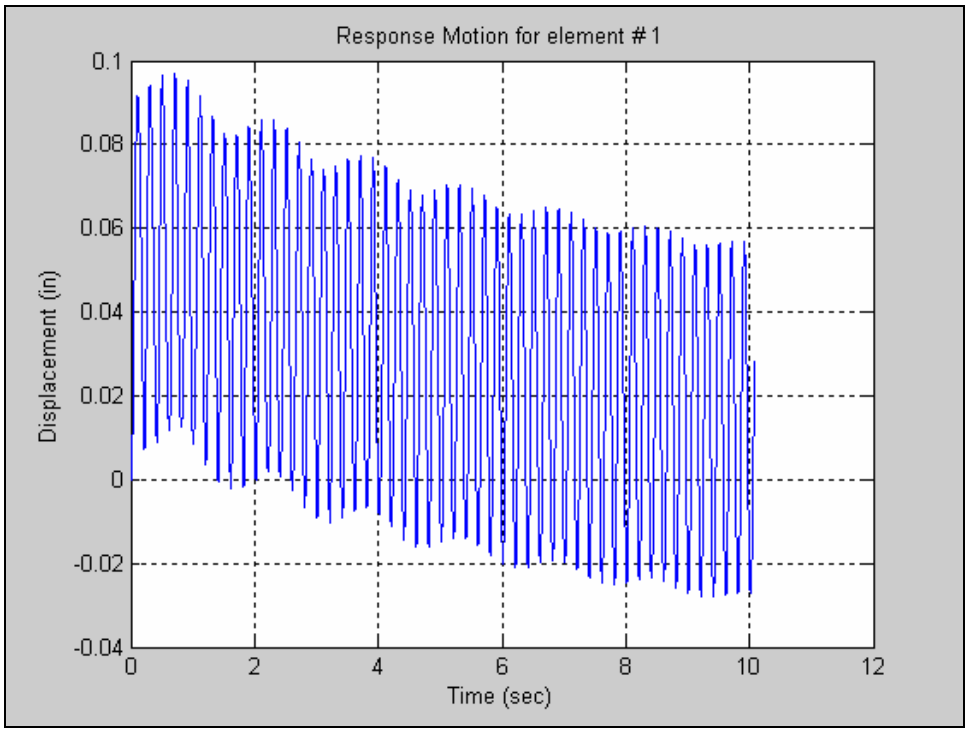

Figure 52. Maxwell: Lateral Displacement – Before Optimization

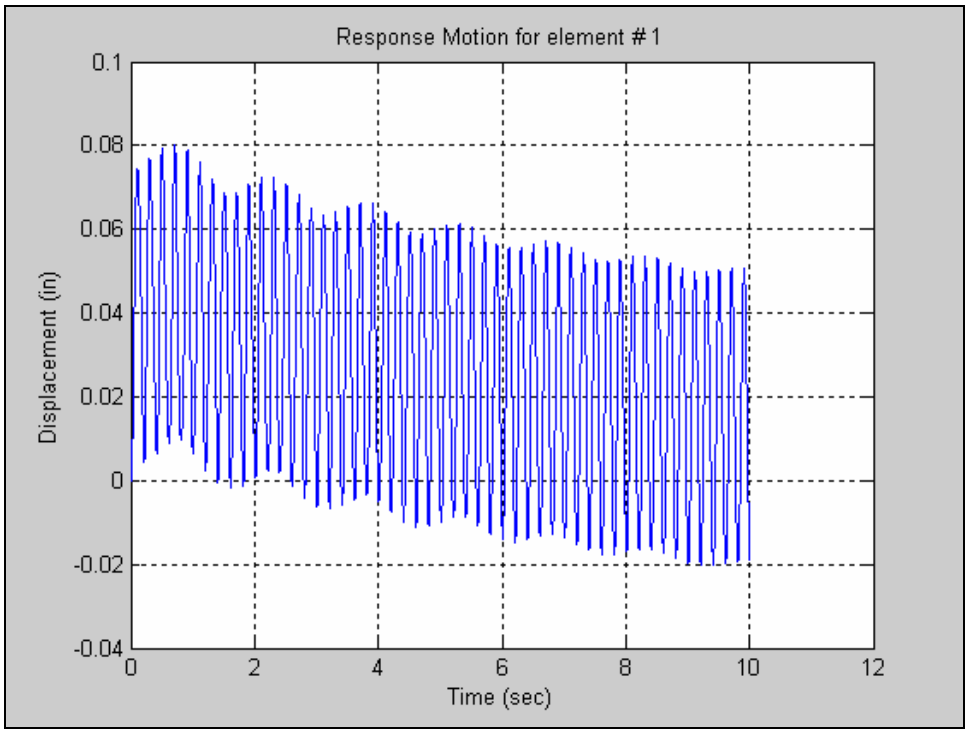

Figure 53. Maxwell: Lateral Displacement – After Optimization

6. Wen – Sine Base Motion

Base Motion	Sine, 12in, 5 Hz, 10 sec
Coupling Nodes (cset)	[1 2 3 4]
Analysis Node (rset)	[1 2 3 4] – Isolator Nodes
Starting Isolator Values	Yield Force = 3000 lb Yield Displacement(Y) = 3 in Yield to Post (α) = 0.1 β = 5 Γ = 5 A = 3 η = 3
Objective	Minimize isolator node absolute displacement
Optimal Isolator Values	Yield Force = 2970 lb Yield Displacement(Y) = 10.8 in Yield to Post (α) = 0.1 β = 100 Γ = 313.4 A = 2 η = 3
Max Displacement	Max isolator node absolute disp = 0.1350 in
Process Time	02:01:53

Table 8. Optimization Results for 4-Story Building with Wen Isolators – Sine Displacement

Objective Function:

MIN: $x_1 + x_2 + x_3 + x_4$ (Isolator lateral displacements)

Subject to:

$Fy - 3500$	≤ 0	(Isolator constraints)
$-Fy + 2500$	≤ 0	
$Y - 100$	≤ 0	
$-Y + 2.7$	≤ 0	
$\alpha - 0.5$	≤ 0	
$-\alpha + 0.05$	≤ 0	
$\beta - 1000$	≤ 0	
$-\beta + 3$	≤ 0	
$\Gamma - 1000$	≤ 0	
$-\Gamma + 3.5$	≤ 0	
$A - 5$	≤ 0	
$-A + 1$	≤ 0	
$\eta - 5$	≤ 0	
$-\eta + 1$	≤ 0	
x_1, x_2, x_3, x_4	≥ 0	(Nonnegativity)
η, A	= Integer	

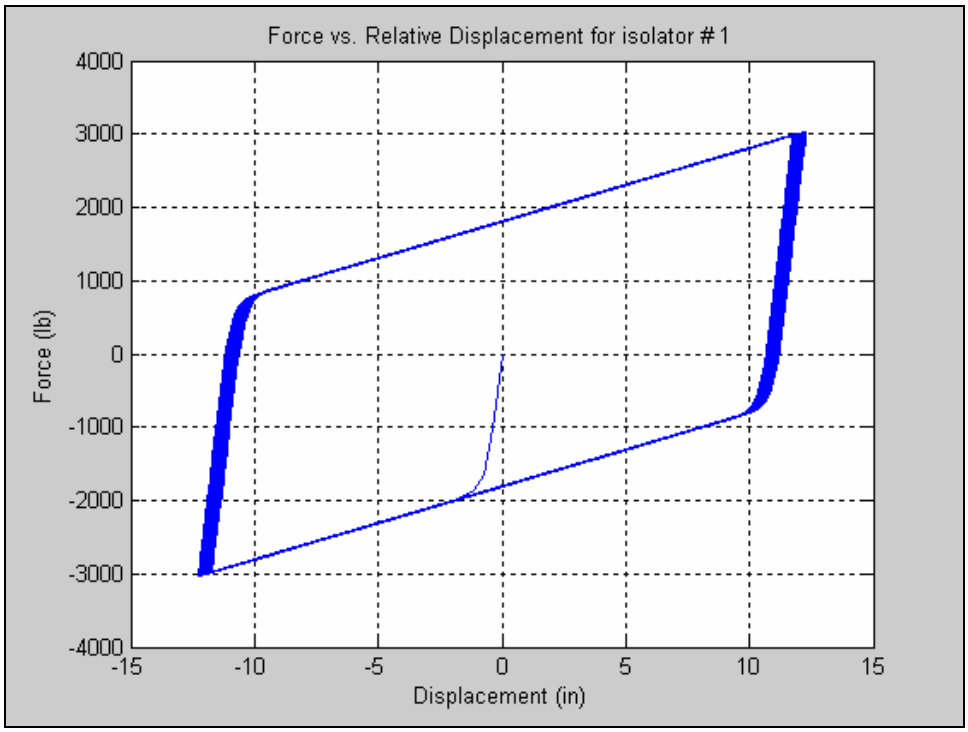

Figure 54. Wen: Hysteresis Plot – Before Optimization

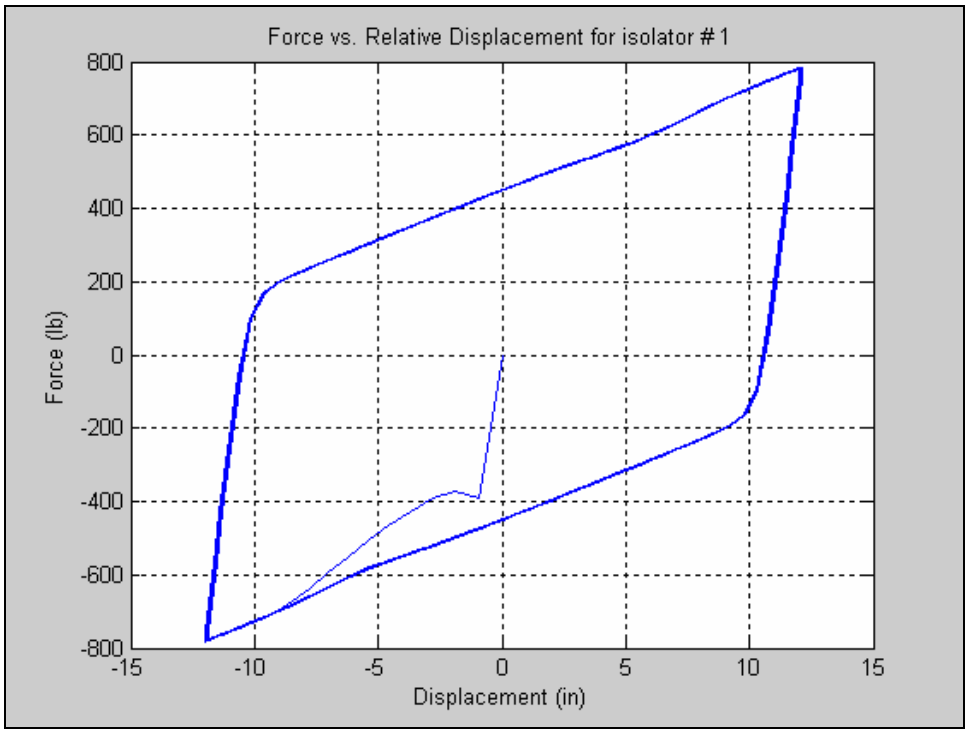

Figure 55. Wen: Hysteresis Plot – After Optimization

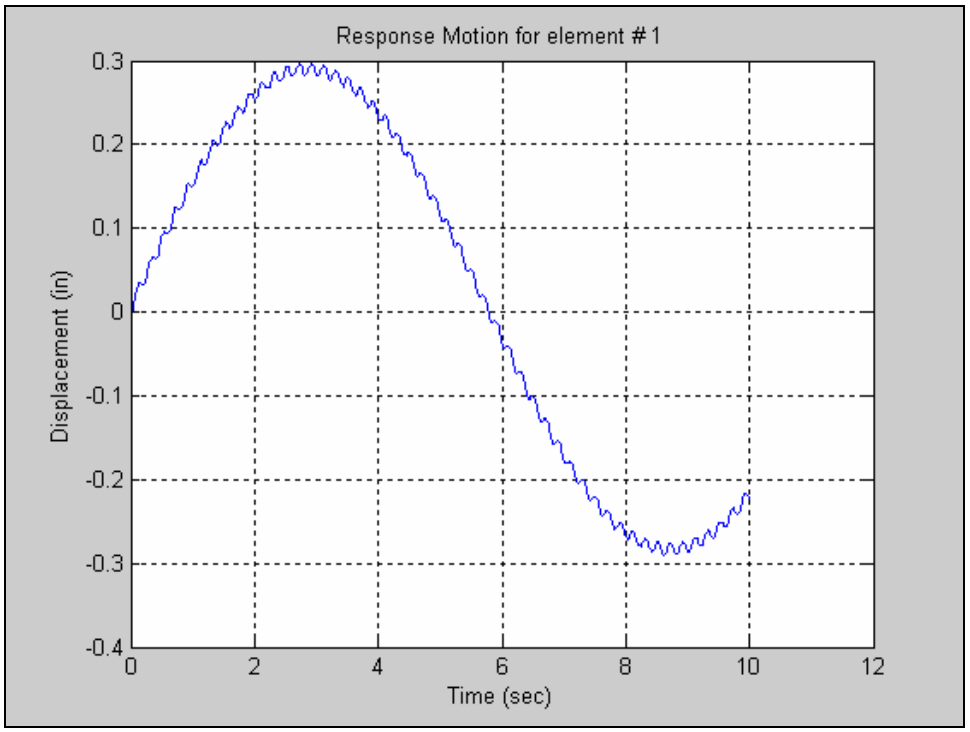

Figure 56. Wen: Lateral Displacement of node #1– Before Optimization

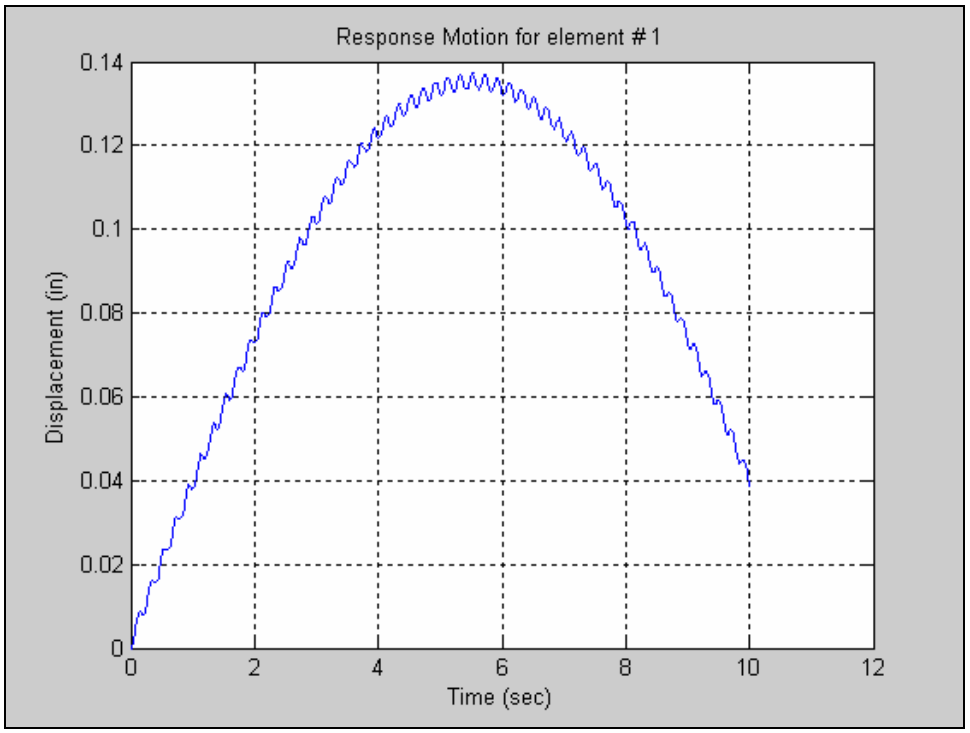

Figure 57. Wen: Lateral Displacement of node #1 – After Optimization

7. Wen – Kobe Japan 1995 NS

Base Motion	KobeJapan1995NS_US.mat 20 sec
Coupling Nodes (cset)	[1 2 3 4]
Analysis Node (rset)	[20] – 5th floor node
Starting Isolator Values	Yield Force = 3000 lb Yield Displacement(Y) = 3 in Yield to Post (α) = 0.1 β = 5 Γ = 5 A = 3 η = 3
Objective	Minimize 5th floor lateral displacement. Isolator displacement relative to ground motion cannot exceed 10 in.
Optimal Isolator Values	Yield Force = 2968 lb Yield Displacement(Y) = 5.9 in Yield to Post (α) = 0.5 β = 98.1 Γ = 313.4 A = 2 η = 3
Max Displacement	Max 5th floor node lateral disp. = 3.193 in Max isolator node relative disp = 9.1371 in
Process Time	02:05:44

Table 9. Optimization Results for 4-Story Building with Wen Isolators – KobeJapan1995NS_US.mat

Objective Function:

MIN:	x_{20}		(5^{th} floor lateral displacements)
Subject to:	Fy -3500	≤ 0	(Isolator constraints)
	- Fy + 2500	≤ 0	
	Y – 100	≤ 0	
	- Y + 2.7	≤ 0	
	α – 0.5	≤ 0	
	- α + 0.05	≤ 0	
	β – 1000	≤ 0	
	-β + 3	≤ 0	
	Γ – 1000	≤ 0	
	- Γ + 3.5	≤ 0	
	A – 5	≤ 0	
	-A + 1	≤ 0	
	η – 5	≤ 0	
	-η + 1	≤ 0	
	z_1, z_2, z_3, z_4	≤ 10 in	(Isolator relative displacements)
	x_{20}	≥ 0	(Nonnegativity)
	η, A	=	Integer

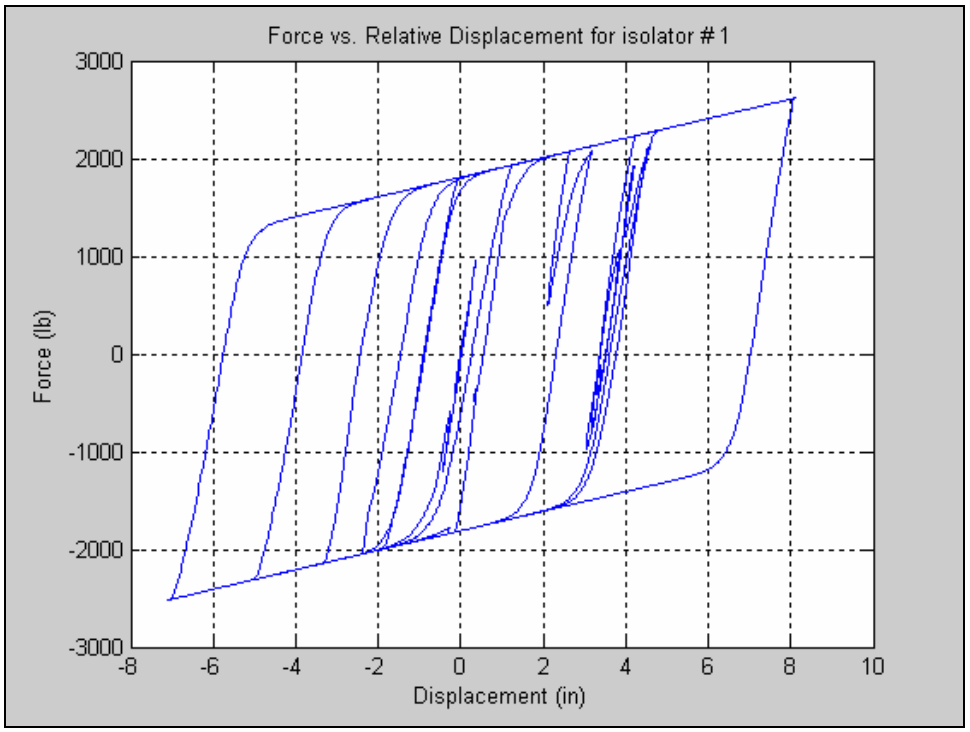

Figure 58. Wen: Hysteresis Plot – Before Optimization

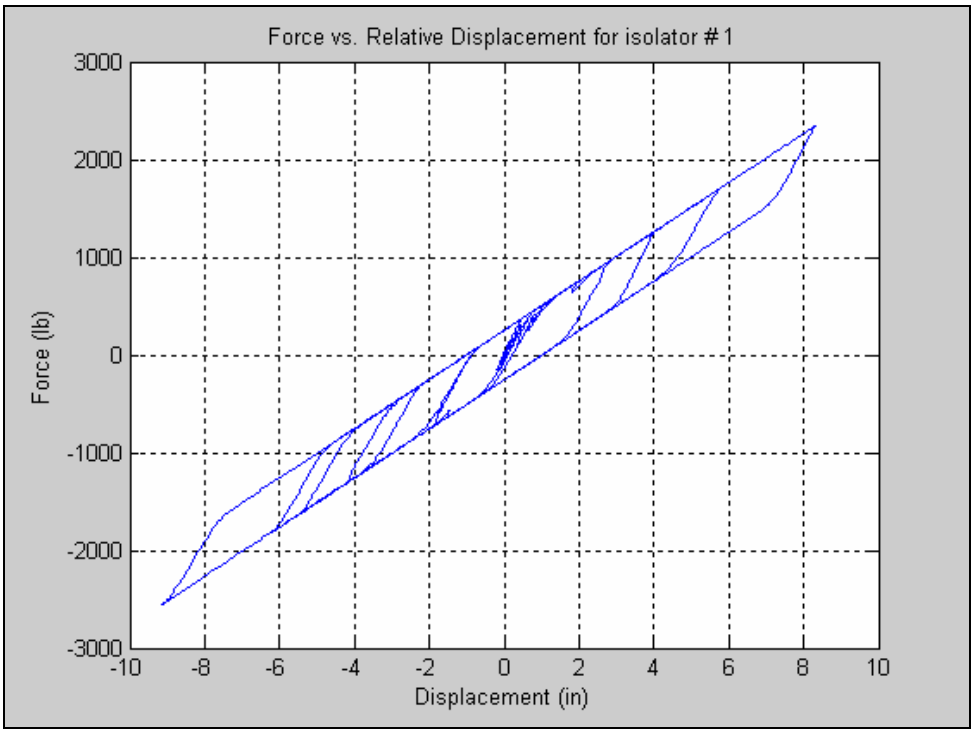

Figure 59. Wen: Hysteresis Plot – After Optimization

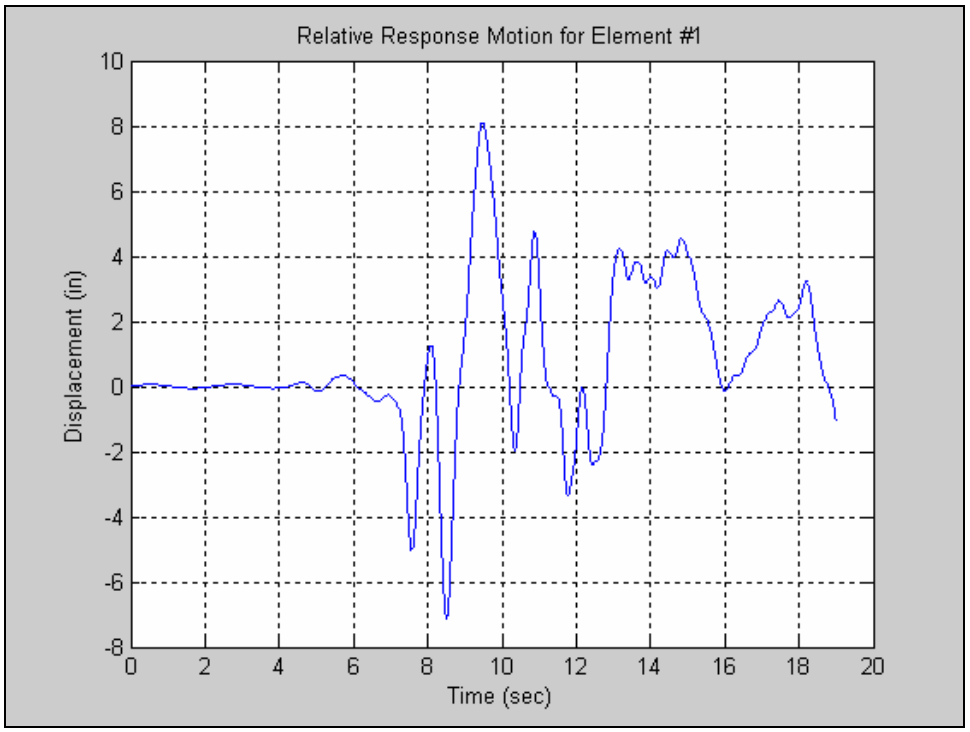

Figure 60. Wen: Relative Lateral Displacement of node #1 – Before Optimization

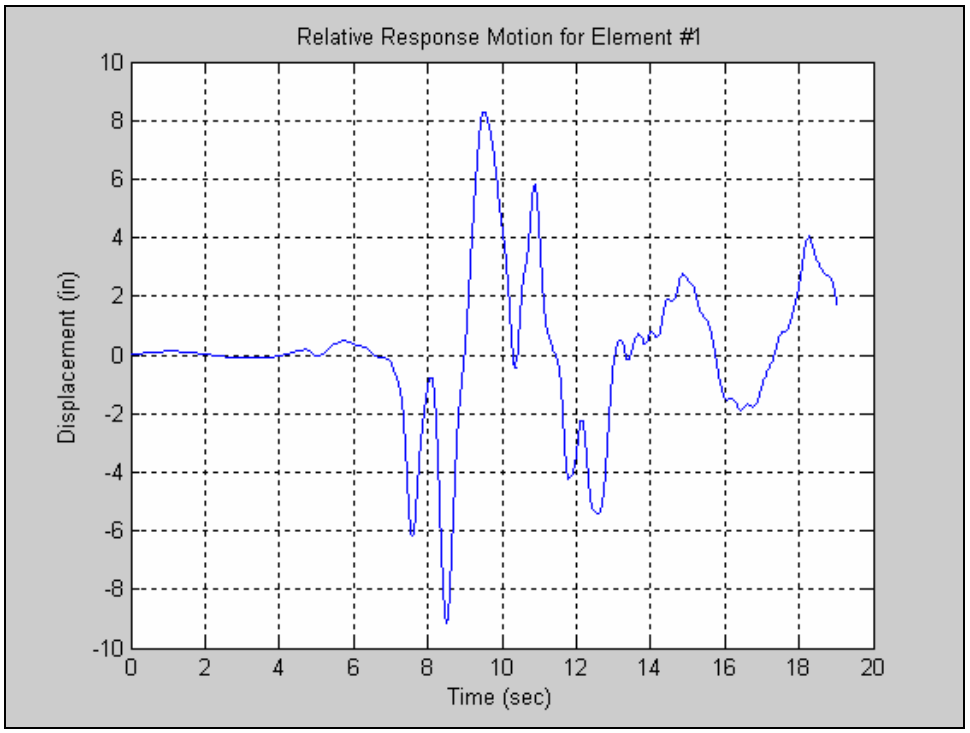

Figure 61. Wen: Relative Lateral Displacement of node #1– After Optimization

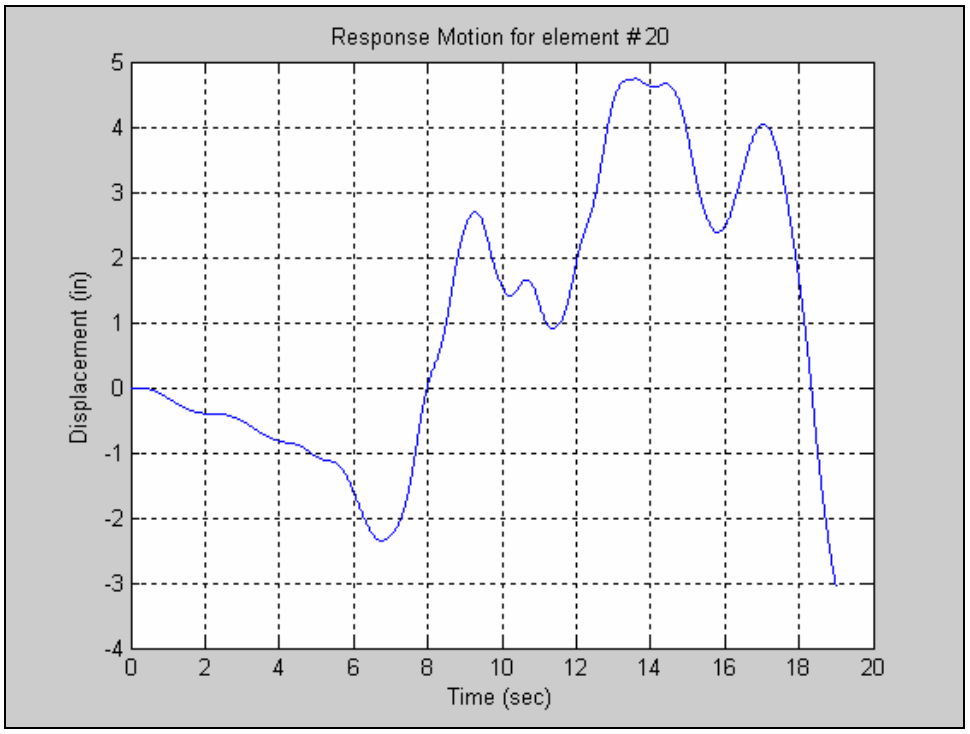

Figure 62. Wen: Lateral Displacement of node #20 – Before Optimization

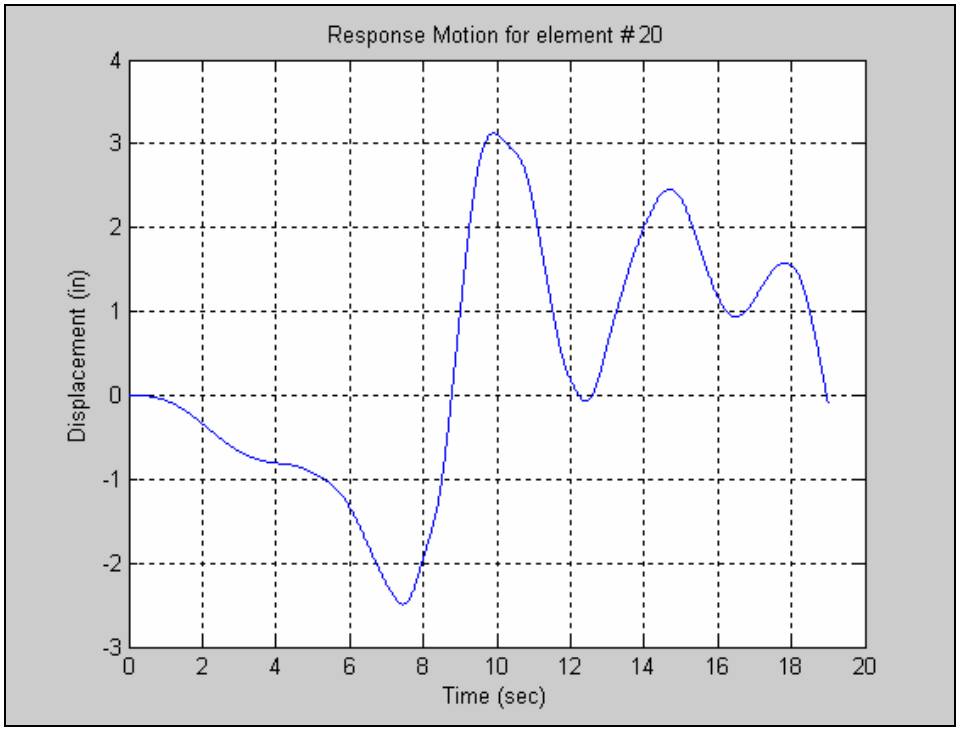

Figure 63. Wen: Lateral Displacement of node #20– After Optimization

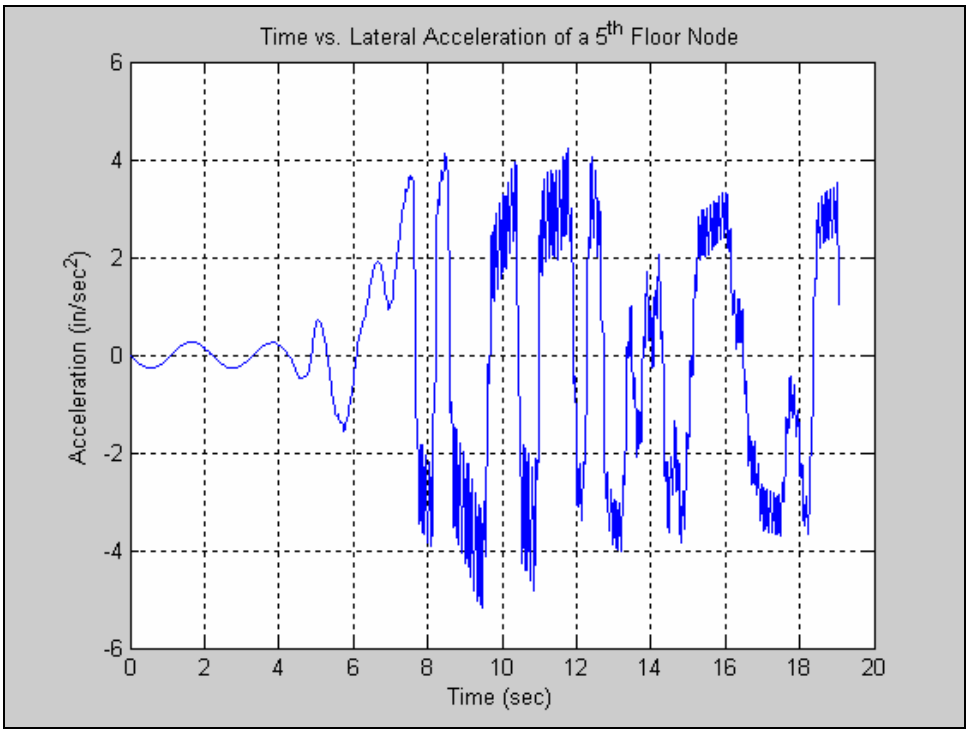

Figure 64. Wen: Lateral Acceleration – Before Optimization

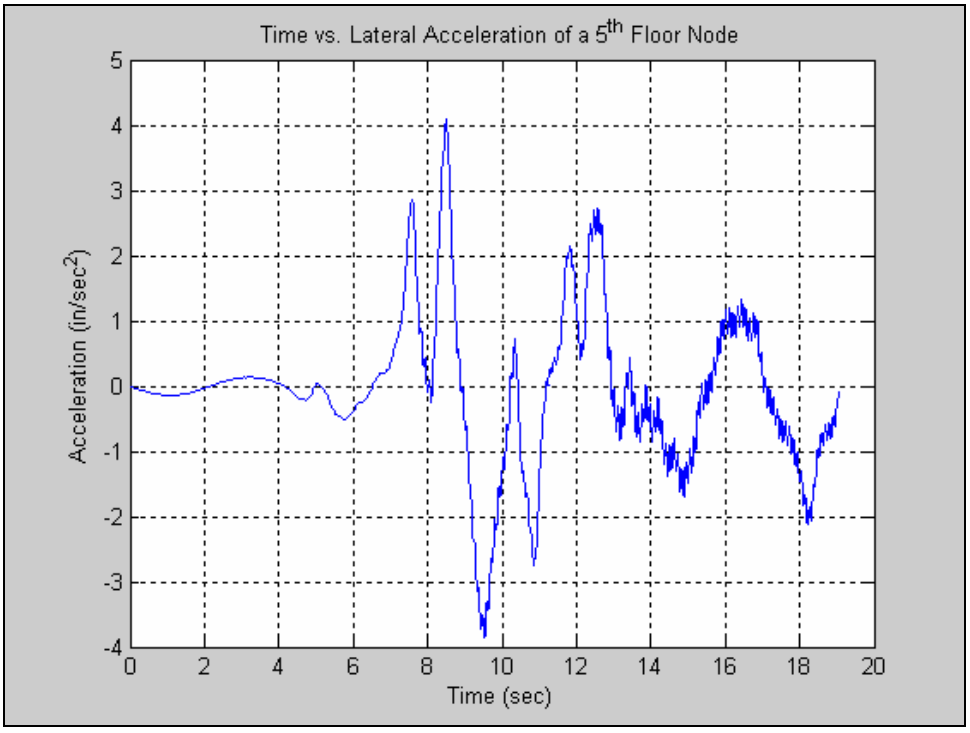

Figure 65. Wen Lateral Acceleration – After Optimization

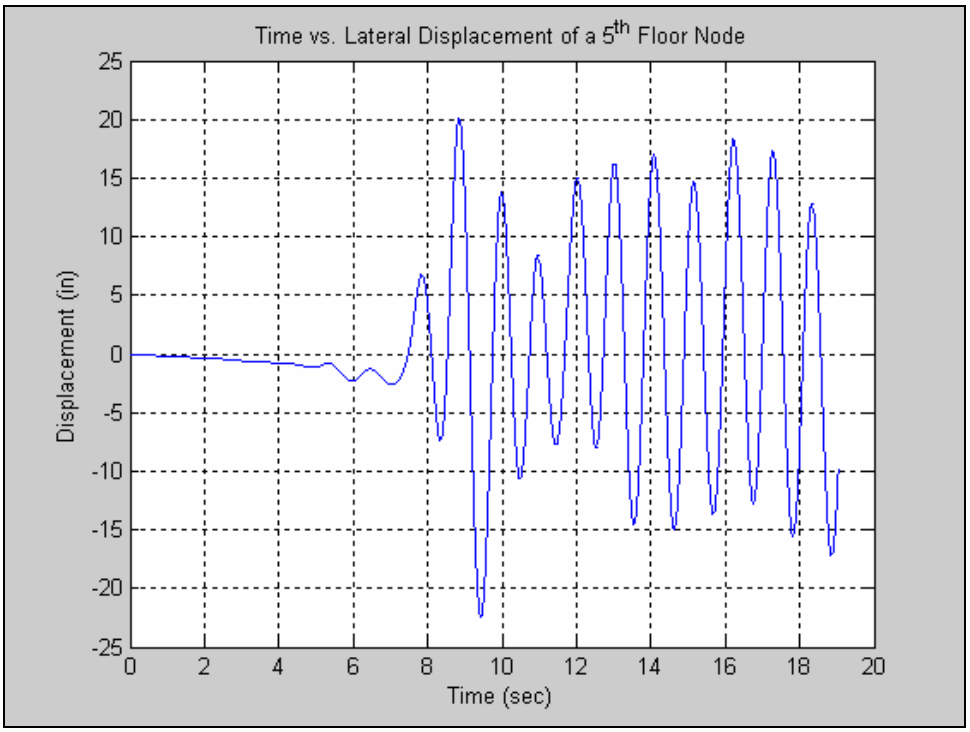

Figure 66. No Isolation: Lateral Displacement of node #20

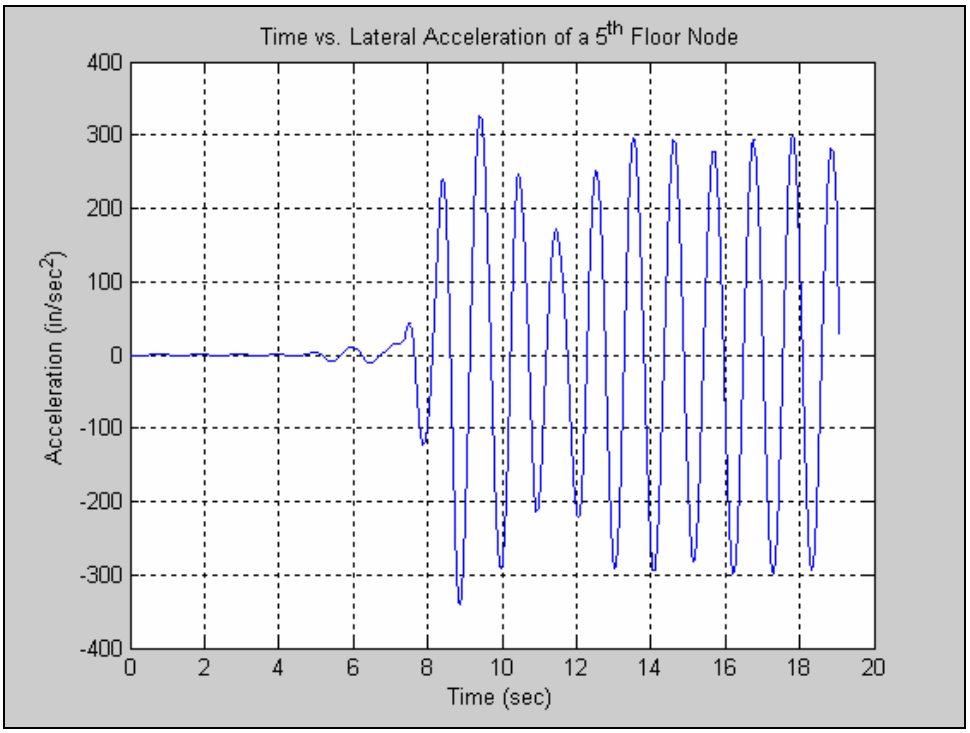

Figure 67. No Isolation: Lateral Acceleration of node #20

THIS PAGE INTENTIONALLY LEFT BLANK

B. FIFTEEN BAY THIRTY-STORY BULDING

The thirty-story building used for [Ref. 8] is revisited here with Wen isolation. This structure is coupled with 81 isolators and exposed to both sinusoidal and Kobe earthquake base motions. This model was processed to demonstrate OASIS's ability to quickly process large-complex structural systems.

1. Wen – Sine Base Motion

Base Motion	Sine, 12in, 5 Hz, 10 sec
Coupling Nodes (cset)	[1 2 3 4 … 77 78 79 80 81] (81 nodes)
Analysis Node (rset)	[1215 2511] – 15th and 31st floors
Isolator Values	Yield Force = 2970 lb Yield Displacement(Y) = 10.8 in Yield to Post (α) = 0.1 β = 100 Γ = 313.4 A = 2 η = 3
Objective	Determine the response of the 15th and 31st floor nodes.
Max Displacement	Max Lateral Disp 15th Floor: 0.0246 in Max Lateral Disp: 31st Floor: 0.0251 in
Process Time	03:37:43

Table 10. Synthesis Results for30-Story Building with Wen Isolators – Sine Displacement

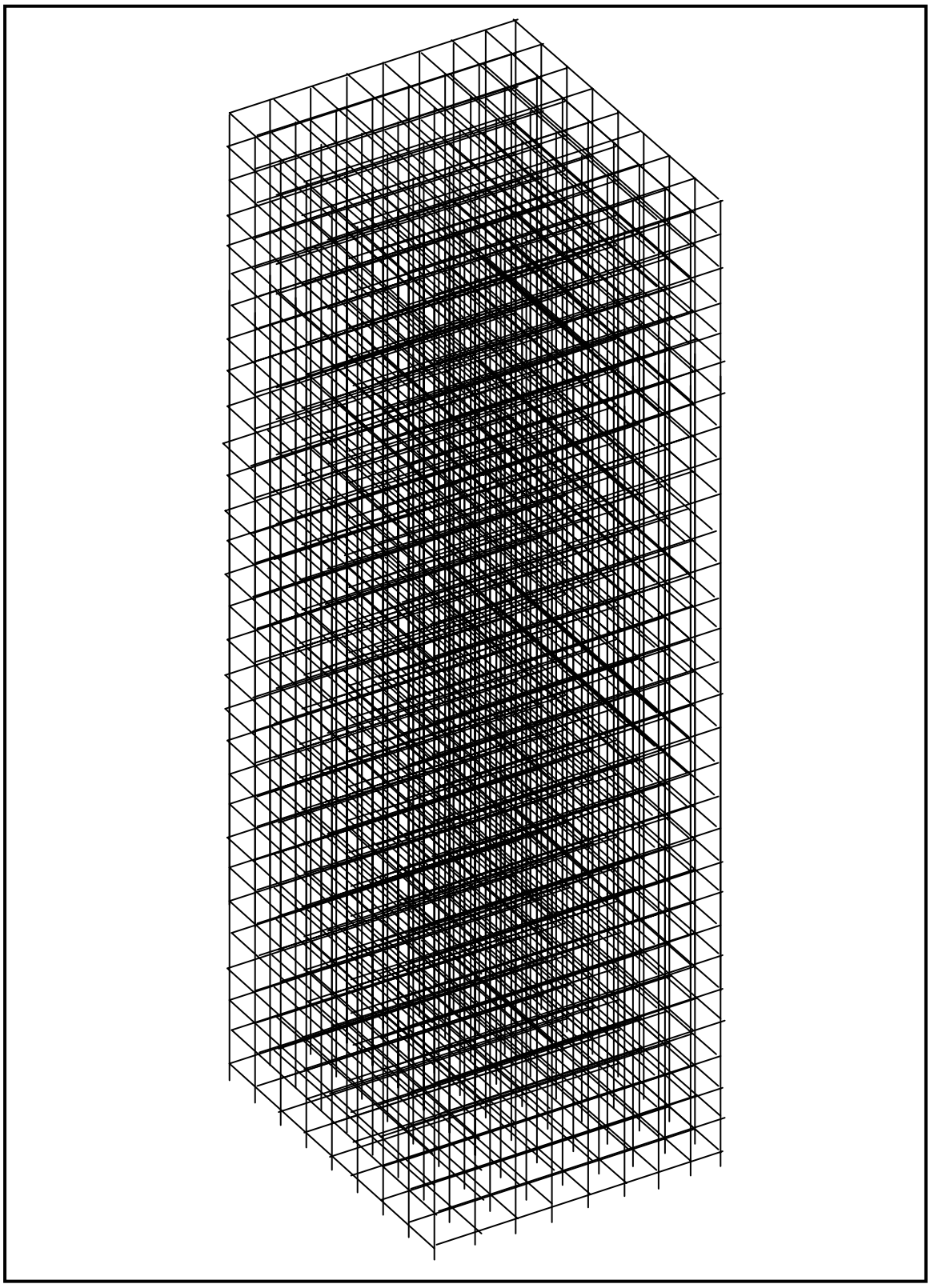

Figure 68. Thirty-Story Building Wire Frame (From Ref. 8)

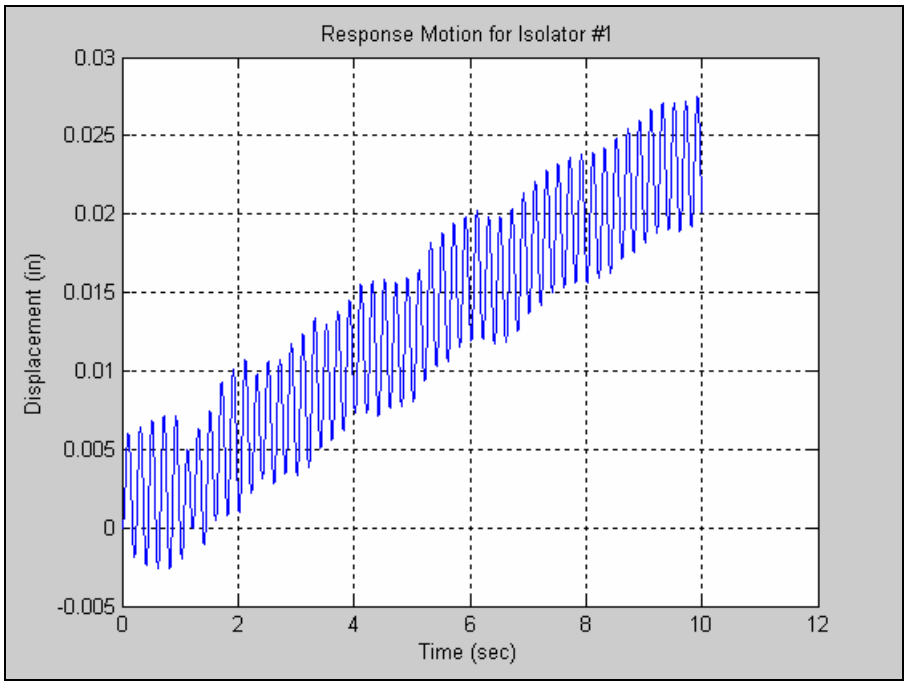

Figure 69. 30-Story Building: Isolator #1 Lateral Displacement

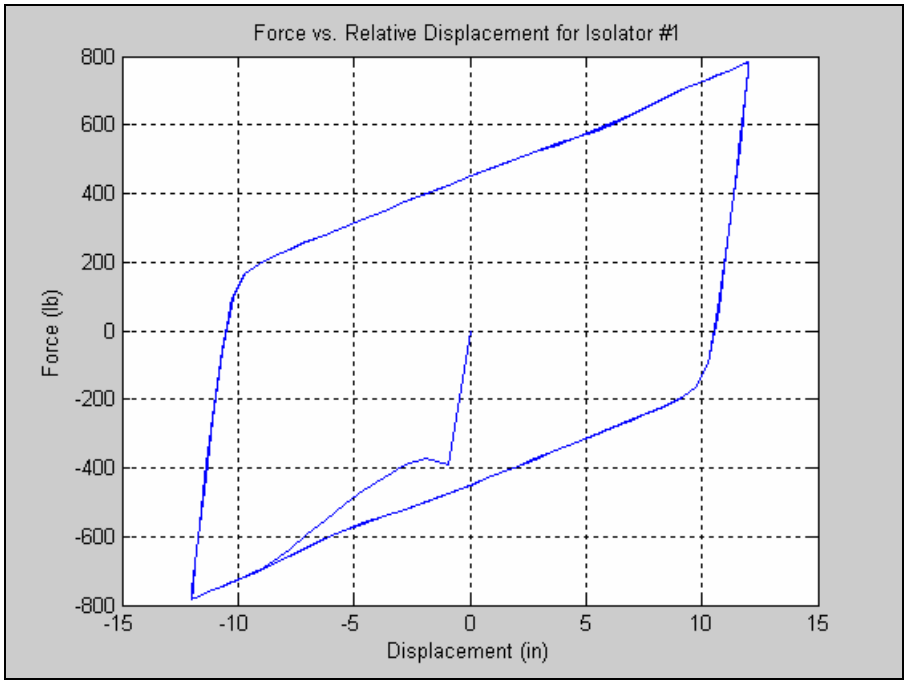

Figure 70. 30-Story Building: Isolator #1 Hysteresis Plot

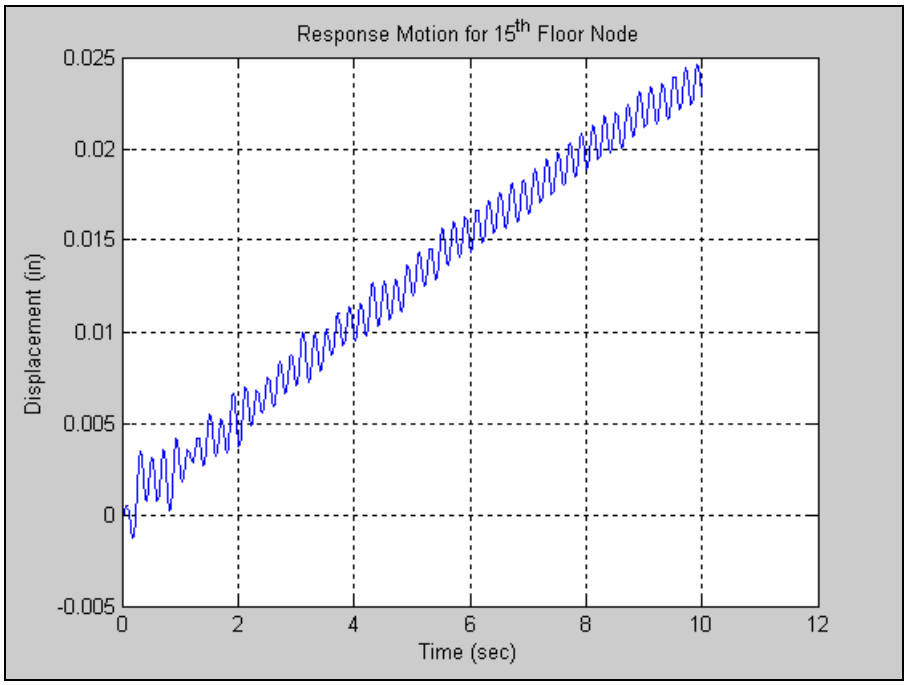

Figure 71. 30-Story Building: 15th Floor Lateral Displacement

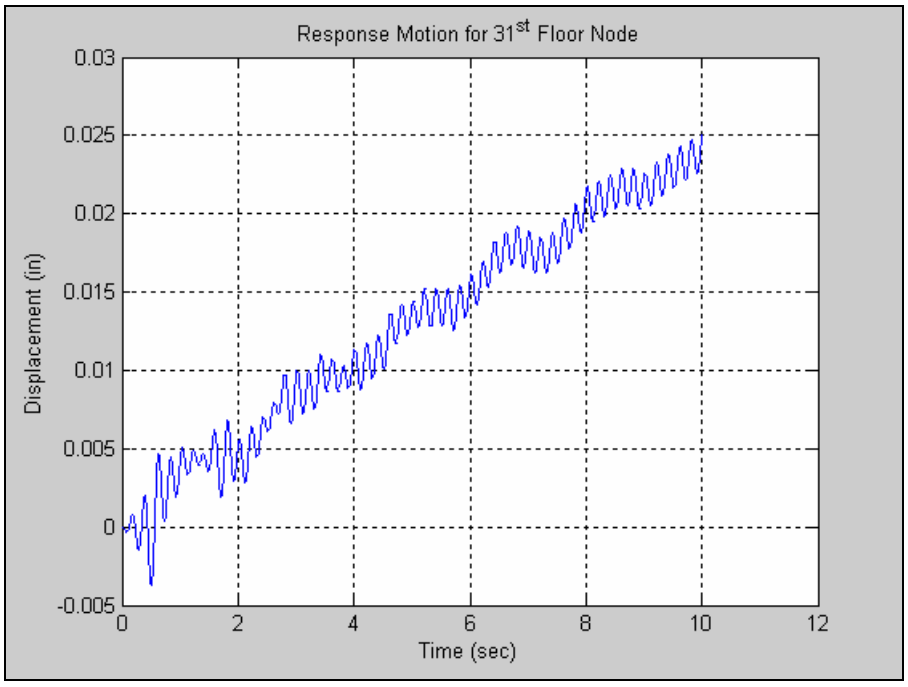

Figure 72. 30-Story Building: 31st Floor Lateral Displacement

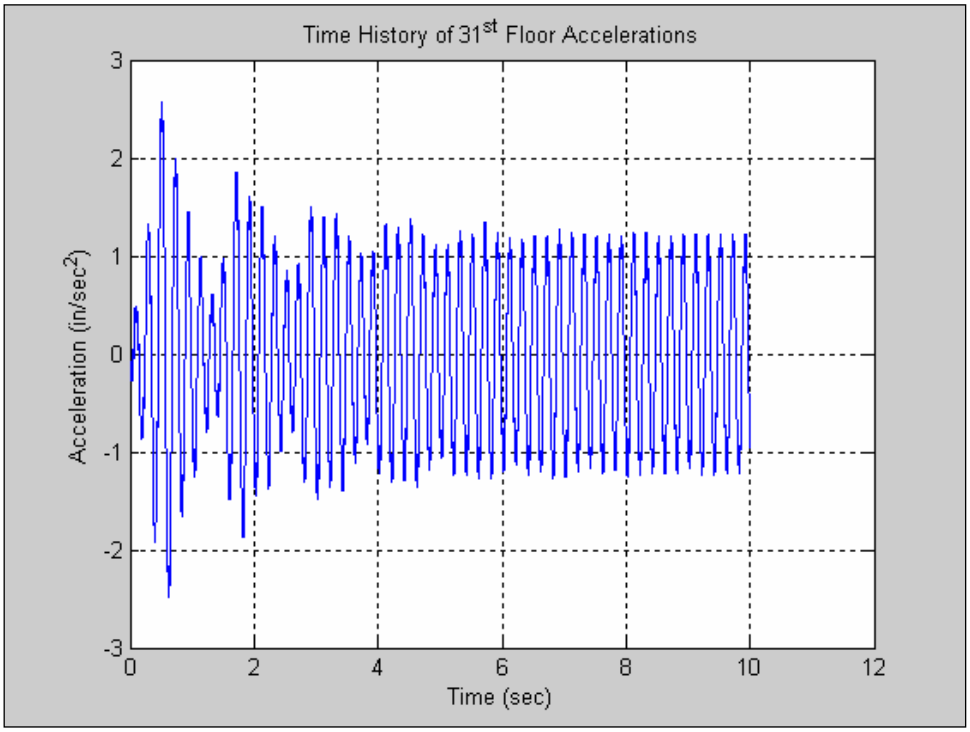

Figure 73. 30-Story Building: 31st Floor Acceleration

2. Wen – Kobe Japan 1995 US Base Motion

Base Motion	KobeJapan1995NS_US.mat 20 sec
Coupling Nodes (cset)	[1 2 3 4 … 77 78 79 80 81] (81 nodes)
Analysis Node (rset)	[1215 2511] – 15th and 31st floors
Isolator Values	Yield Force = 2970 lb Yield Displacement(Y) = 10.8 in Yield to Post (α) = 0.1 β = 100 Γ = 313.4 A = 2 η = 3
Objective	Determine the response of the 15th and 31st floor nodes.
Max Displacement	Max Lateral Disp 15th Floor: 3.6817 in Max Lateral Disp: 31st Floor: 3.6841 in
Process Time	06:27:36

Table 11. Synthesis Results for 30-Story Building with Wen Isolators – KobeJapan1995NS_US.mat

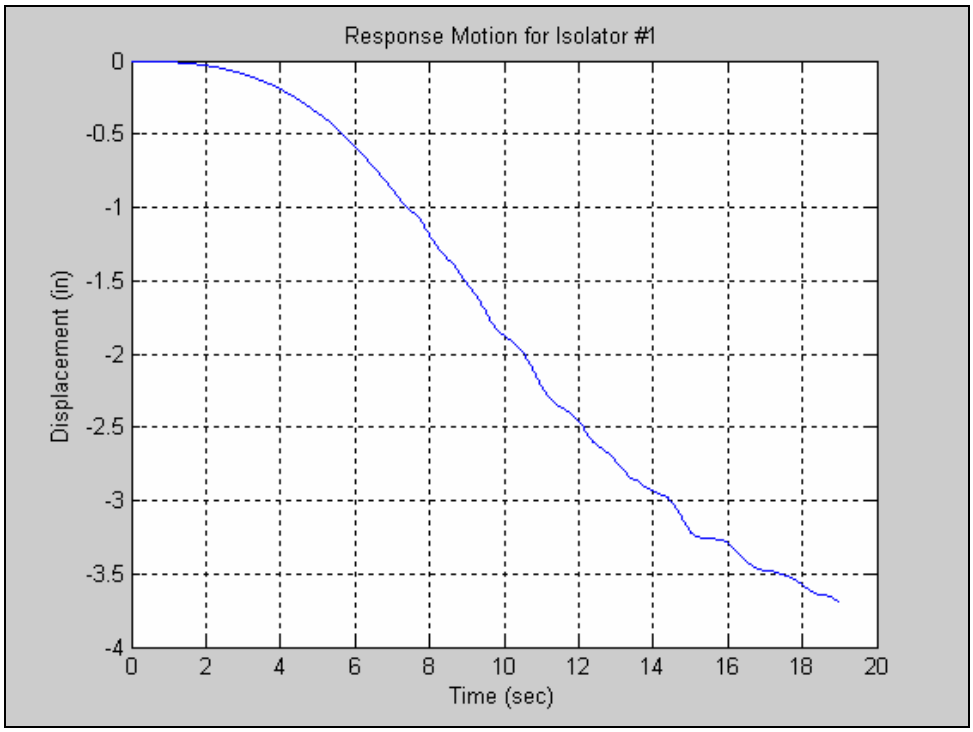

Figure 74. 30-Story Building: Isolator #1 Lateral Displacement

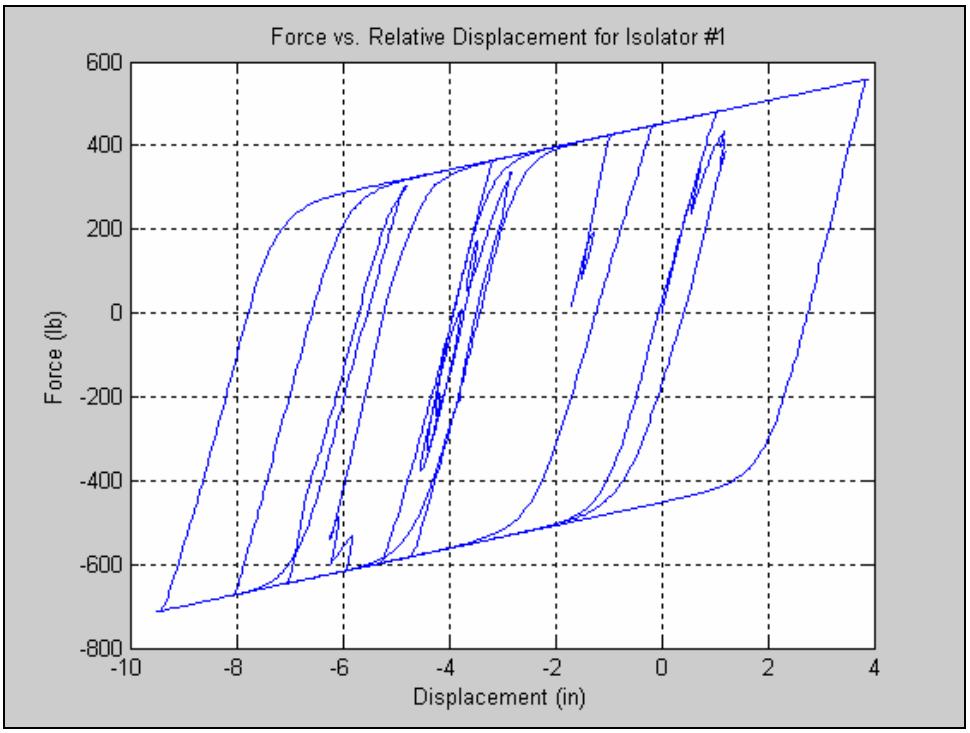

Figure 75. 30-Story Building: Isolator #1 Hysteresis Plot

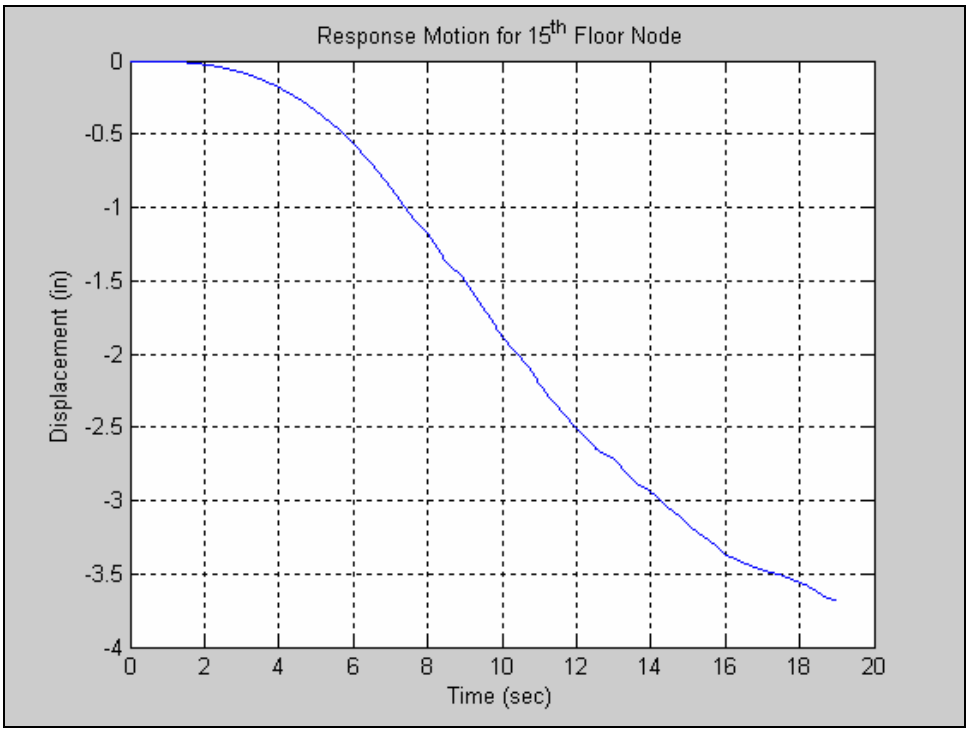

Figure 76. 30-Story Building: 15th Floor Lateral Displacement

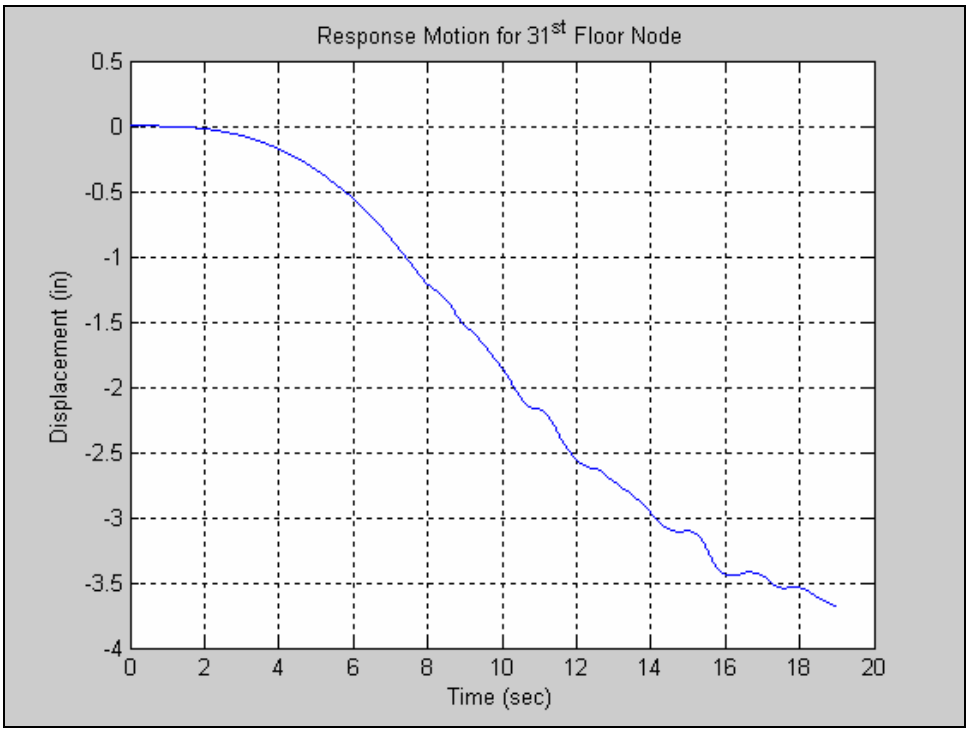

Figure 77. 30-Story Building: 31st Floor Lateral Displacement

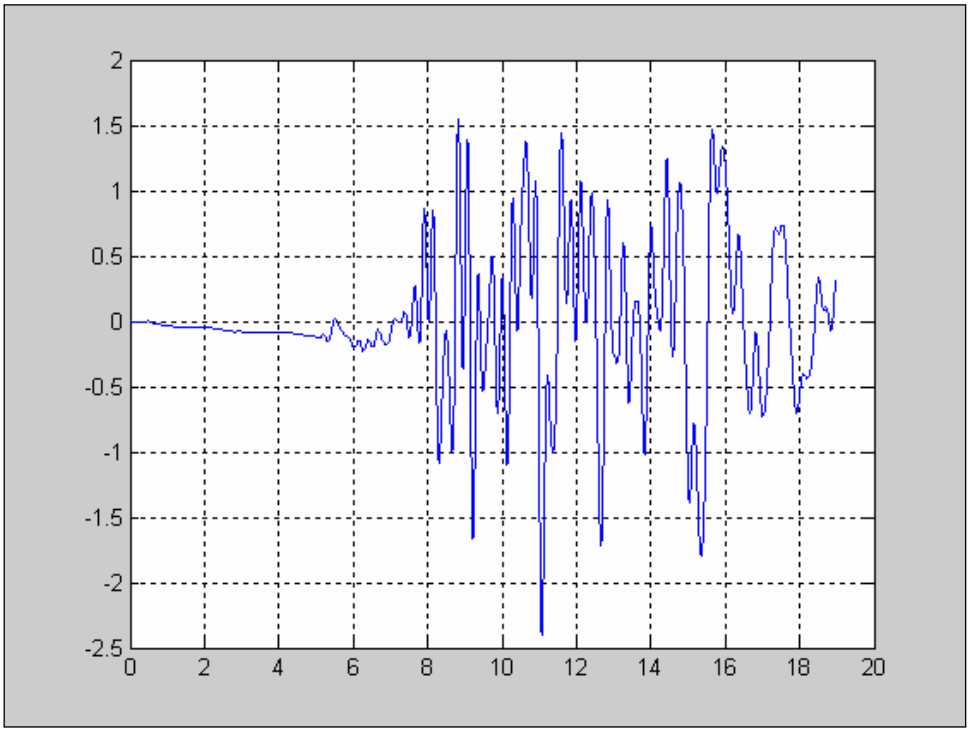

Figure 78. 30-Story Building: 31st Floor Acceleration
(Time (sec) vs. Acceleration (in/sec^2)

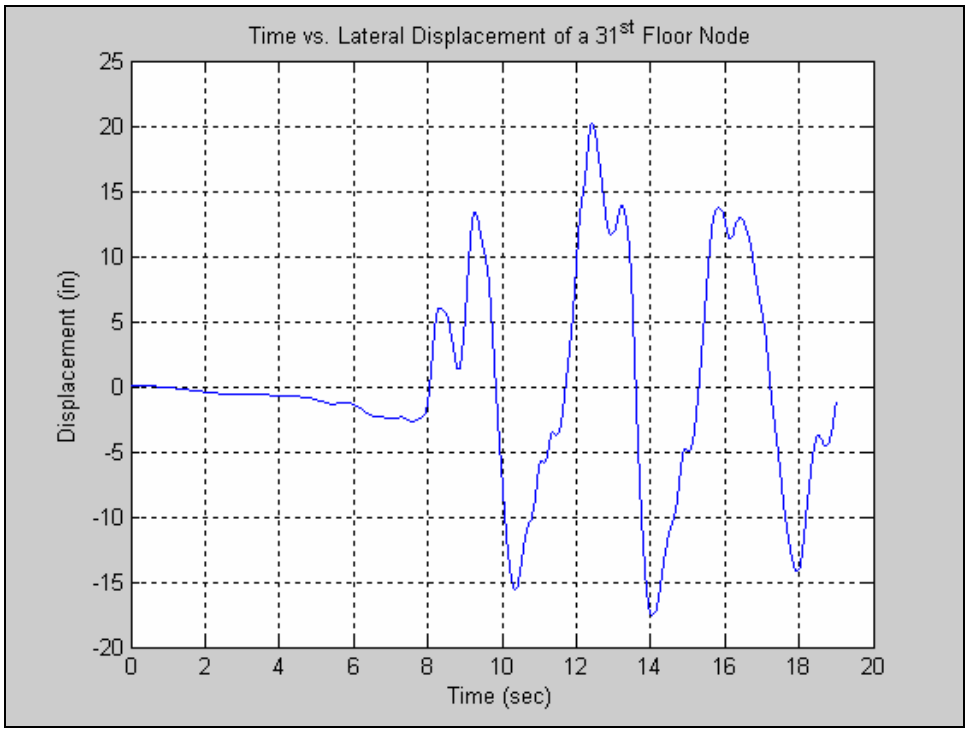

Figure 79. No Isolation: 31st Floor Lateral Displacement

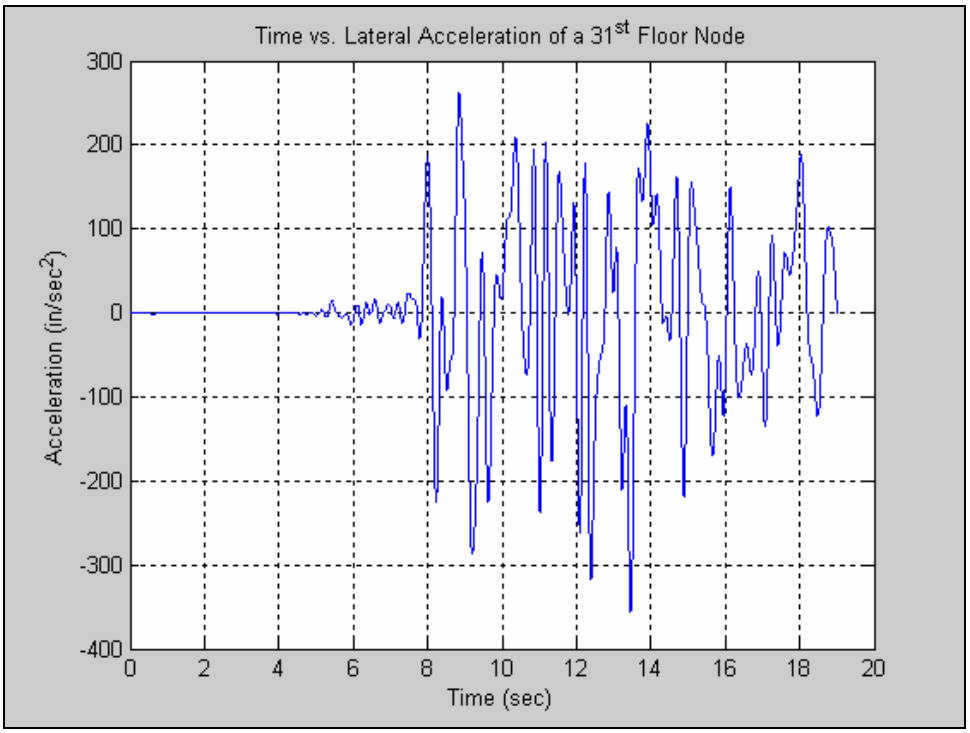

Figure 80. No Isolation: 31st Floor Lateral Acceleration

VI. CONCLUSION

MATLAB programs for Transient Structural Synthesis (TSS), Recursive Block-by-Block (RBB), and nonlinear numerical isolator models from [Ref. 8] were thoroughly investigated. As a result, numerous discrepancies in the isolator models were corrected, program logic was optimized, and a method that transforms MATLAB's rectangular-rule convolution into any integration rule with higher-order error was developed. This research also led to the development of three numerical models for sliding-friction isolators and a user-friendly Decision Support System (DSS) tool for transient response and analysis. OASIS (Optimization and Analysis of Structural Isolation Systems) is a DSS tool that gives a user the ability to quickly change isolator parameters for TSS / RBB, change types of base motions, optimize the isolator parameters, and post-synthesis / optimization analysis tools.

The program results were carefully validated with 2-DOF and 7-DOF systems in Working Model 2-D (WM2D). The results from OASIS and Working Model 2-D compared very well for short simulation times. For longer simulation times ($t > 15$ sec), small deviations in response were noted. This is due to Working Model's attempt to solve a "real world" system of blocks, springs, and dampers, instead of a lumped mass system. OASIS uses mass-normalized mode shapes in its calculation, which result in better solutions when compared to WM2D.

Several optimization scenarios were presented for comparison. Each example used different isolators with initial, lower-bound, and upper-bound parameters. The user also has the option to "fix" certain parameters with the use of nonlinear equality constraints. The objective function is the linear sum of either displacements, accelerations, or both. However, a future version will allow the optimization of nonlinear objective functions.

OASIS can also be used to analyze and optimize models of smaller scale. The program only needs the mode shapes and natural frequencies for the coupling nodes and the analysis nodes. TSS makes it possible to reduce a large DOF system into a small one that can be solved quickly. For example, the four story structure used in the optimization

examples has 20 nodes, each with six degrees of freedom. Only five nodes with lateral degrees of freedom are needed to find the lateral response of a node on the fifth floor – four coupling nodes and one fifth floor node. OASIS's ability to accept any size model, couple it with an isolator, and apply any base motion greatly extends its use for optimal engineering design.

VII. RECOMMENDATIONS

OASIS does not account for the uplift effects created by a structure's rocking during a base-motion event. To consider uplift in the structure's response, the vertical degrees of freedom need to be included for the impulse response function formulation. Reference [8] presents results of programs developed to account for uplift by modeling a linear spring. More information on past and current research on the effects of uplift and base isolation can be found in [Ref. 17].

THIS PAGE INTENTIONALLY LEFT BLANK

LIST OF REFERENCES

1. U.S. Geological Survey. [Online] Available. Internet: http://www.usgs.gov. June 2003.
2. Kelly, J. M. Earthquake-Resistant Design with Rubber. 2nd ed. London: Springer-Verlag, 1997.
3. Gordis, J.H. "Integral Equation Formulation for Transient Structural Synthesis." AIAA Journal 33 (1995): 320 – 324.
4. Institute for Crustal Studies. [Online] Available. Internet: http://www.crustal.ucsb.edu. July 2003.
5. The Franklin Institute Online. [Online] Available. Internet: http://www.fi.edu/earth/crust.html. May 2003.
6. How Stuff Works. [Online] Available. Internet: http://science.howstuffworks.com/earthquake.htm. August 2003.
7. "Seismic Isolation and Energy Dissipation." FEMA 356 — Prestandard and Commentary for the Seismic Rehabilitation of Buildings. 2001: 1 – 38.
8. Jarque, Al V. Recursive Block-by-Block Integral Equation Solution for Transient Dynamic Analysis with Memory-Type Elements. Monterey. Naval Postgraduate School. March 2001.
9. Radwick, and J. H. Gordis. "Efficient Transient Analysis for Large Locally Nonlinear Structures." Shock and Vibration 6 (1999): 1 – 9.
10. Ragsdale, Cliff T. Spreadsheet Modeling and Decision Analysis. 3rd ed. Cincinnati: South-Western, 2001.
11. Belegundu, and Tirupathi R. Chandrupatla. Optimization Concepts and Applications in Engineering. 1st ed. Prentice-Hall Inc., 1999.
12. "Constrained Optimization." [Online] Available. Internet: http://cnx.rice.edu/content/m11223/latest/. August 2003.
13. Constantinou, M. C., and I. G. Tadjbakhsh. "Hysteretic Dampers in Base Isolation: Random Approach," Journal of Structural Engineering. 111. (1985): 705 – 721.

14. Gordis, and Beny Neta. “Fast Transient Analysis for Locally Nonlinear Structures by Recursive Block Convolution.” Journal of Vibrations and Acoustics. 123. (2001): 545 – 547.

15. Wen, Y. K. “Method for Random Vibration of Hysteretic Systems." Journal of the Engineering Mechanics Division, EM2. (1976): 249 – 262.

16. Multidisciplinary Center for Earthquake Engineering Research. [Online] Available. Internet: http://mceer.buffalo.edu. March 2003

17. Lobo, Naeim, and G. C. Hart. “3D Nonlinear Analysis of Multistory Base Isolated Buildings with Significant Uplift.” Proceedings, 6th U.S. National Conference on Earthquake Engineering. (1985): 1 – 12.

18. Craig, R. R. Structural Dynamics: An Introduction to Computer Methods. New York: John Wiley & Sons, 1981.

19. Thomson, W. T. Theory of Vibration with Applications. Prentice Hall, 1993.

20. Gerald, and Patrick O. Wheatley. Applied Numerical Analysis. 6th ed. California: Addison-Wesley, 1999.

21. Rao, Singiresu S. Mechanical Vibrations. 3rd ed. California: Addison-Wesley, 1995.

22. Zwillinger, Daniel. Standard Mathematical Tables and Formulae. 31st ed. Boca Raton: Chapman and Hall / CRC, 2003.

23. Jerri, Abdul J. Introduction to Integral Equations with Applications. 2nd ed. New York: John Wiley and Sons Inc, 1999.

24. Paz, Mario. Structural Dynamics Theory and Computation. 4th ed. New York: Chapman and Hall, 1997.

25. Chen, W. F. The Civil Engineering Handbook. Boca Raton: CRC Press, 1995.

INITIAL DISTRIBUTION LIST

1. Defense Technical Information Center
   Ft. Belvoir, VA

2. Dudley Knox Library
   Naval Postgraduate School
   Monterey, CA

3. Commanding Officer (Code C35)
   Naval School, Civil Engineer Corps Officers
   Naval Construction Battalion Center
   Port Hueneme, CA

4. Information Systems Technology Program Office
   Naval Postgraduate School
   Monterey, CA

5. Professor Dan Boger, Code IS
   Naval Postgraduate School
   Monterey, CA

5. Engineering & Technology Program Office
   Naval Postgraduate School
   Monterey, CA

6. Professor Joshua H. Gordis, Code ME/Go
   Naval Postgraduate School
   Monterey, CA

7. Professor Young S. Shin, Code ME/Sg
   Naval Postgraduate School
   Monterey, CA

8. Professor Carlos F. Borges, Code MA/Bc
   Naval Postgraduate School
   Monterey, CA

9. LT Manuel A. Hernandez
   Commander, Naval Depot Jacksonville
   Jacksonville, FL